5-2009

The synthesis and spectroscopic studies of titanium-amido complexes as potential catalysts for small molecule activation and polymerization reactions

Andrew James Colvin
University of Tennessee

To the Graduate Council:

I am submitting herewith a dissertation written by Andrew James Colvin entitled "The synthesis and spectroscopic studies of titanium-amido complexes as potential catalysts for small molecule activation and polymerization reactions." I have examined the final electronic copy of this dissertation for form and content and recommend that it be accepted in partial fulfillment of the requirements for the degree of Doctor of Philosophy, with a major in Chemistry.

David C. Baker, Major Professor

We have read this dissertation and recommend its acceptance:

Accepted for the Council:

Carolyn R. Hodges

Vice Provost and Dean of the Graduate School

(Original signatures are on file with official student records.)

To the Graduate Council:

I am submitting herewith a dissertation written by Andrew James Colvin entitled "The synthesis and spectroscopic studies titanium-amido as potential catalysts for small molecule activation and polymerization reactions." I have examined the final electronic copy of this dissertation for form and content and recommend that it be accepted in partial fulfillment of the requirements for the degree of Doctor of Philosophy, with a major in Chemistry.

David C. Baker

Major Professor

We have read this dissertation
and recommend its acceptance:

Jamie L. Adcock

Fred M. Schell

Claudia J Rawn

.

Accepted for the Council:

Carolyn R. Hodges

Vice Provost and Dean of the
Graduate School

(Original signatures are on file with official student records)

The synthesis and spectroscopic studies of titanium-amido complexes as potential catalysts for small molecule activation and polymerization reactions.

A Dissertation
Presented for the
Doctor of Philosophy
Degree
The University of Tennessee, Knoxville

Andrew James Colvin
May 2009

Acknowledgement

I would like to take this opportunity to thank all that have contributed their personal and professional support to my work and have made this possible. In particular I would like to express my deepest gratitude to my committee members: Dr. David C. Baker, Dr. Fred M. Schell, Dr. Jamie L. Adcock and Dr. Claudia J. Rawn for their patience and professional contributions in completing this document. I would like to thank Dr. John F. C. Turner and Dr. Peter X. X. Zhang for their mentoring and guidance for my scientific development here in Tennessee. All research conducted for this dissertation was funded by John F. C. Turner's career award and NSF grant, which I am very grateful for.

A very special thank you to my peers and research fellows that assisted me throughout my studies: Ben Estes, Jamie Molaison, Cara Nygren, Sylvia Mclain, Michelle Dolgos, Megan Bragg, Micheal Blanchard, Ying Chen, Ming-Yung Lee, Guang-yao Gao, Robert Sacci and Brad O'Dell. I wish you all the best in whatever you choose to do.

To my family and loved ones, my mother and father, whose love and support helped through the more troubled times. To my wife Lina, I love you. Thank you for your support and love throughout. I look forward to starting a new and exciting chapter of our lives together.

Abstract

The last decade has seen what some have termed a 'renaissance' in amido–transition metal chemistry. In part, this has been due to a better appreciation of the amido moiety (R_2N) as a ligand. Moreover, it has been due to the dramatic reactivity that amido complexes have been shown to display, especially when the complex is low coordinate and high valent. This dissertation describes the utilization of dihydrodibenzoazepinyl and carbazolyl ligands to effectively stabilize titanium complexes. These two ligand sets vary in their electron contribution to the metal center due to reduced π-donation from the carbazolyl ligand, this in turn effects the structural properties of the system. These novel titanium–amido systems are potential catalysts for small molecule activation and polymerization reactions. Their synthesis and extensive characterization through X-ray and NMR spectroscopy techniques is described herein.

The synthesis of chelating amine ligands for the stabilization of metal centers can afford fascinating molecules. These compounds are fundamentally interesting due to the orientation of the four nitrogen lone pairs that are within close proximity to one another. The synthesis, reactivity and analysis of 1,2,3,4,5,6,7,8–octahydro-2a,4a,6a,8a-tetraazacyclopenta[*f,g*]acenaphthylene is reported.

Thesis Statement

The following document describes the synthesis of a variety of new titanium-amido ligand complexes that have excellent potential for small-molecule activation and polymerization reactions. These systems are designed using related ligand sets that have differing steric and electronic properties that influence the geometry and symmetry of the complex.

Chapter one covers some of the theoretical background that is relevant these kinds of systems alongside synthesis and demonstrated applications from notable work in this field.

Chapter two describes the synthesis and characterization of a range of novel titanium–dihydrodibenzoazepinyl complexes. Synthesis is described in detail with noted observations and reactivity. Characterization, primarily through in-depth NMR and single-crystal X-ray diffraction analysis is discussed in order to elucidate the structure and behavior of the complexes prepared.

Chapter three introduces the range of novel titanium–carbazolyl complexes prepared through the course of this work. The synthesis and characterization (primarily through various NMR experiments) is described herein, with comparison to observed features elucidated from titanium–dihydrodibenzoazepinyl complexes. This in turn will help illuminate the various electronic contributions from the amido ligand with respect to the nitrogen's involvement within an aromatic compared to a non-aromatic system when bound to a metal center.

Chapter four comprises of tetraamine synthesis and characterization that was intended for an X_2L_2 chelating ligand set for our titanium systems that developed into the discovery of a novel alkene molecule with extremely interesting properties. The synthesis and characterization is described in full, with particular emphasis on the reactivity and properties of the aforementioned tetraamine alkene molecule.

The final chapter of this document surmises the synthesis of all compounds discussed within the dissertation. Detailed synthetic procedures alongside bare-bone spectral details are presented.

Table of Contents

1 Introduction

1.1 Early Organometallic Compounds……...……...1

1.2 Bonding Fundamentals……3

1.3 Principles of MLX Theory.....7

1.4 Ziegler–Natta Polymerization……..8

1.5 Metallocenes in Olefin Polymerization……...12

1.6 Amido Ligand Systems in Polymerization Reactions…….19

1.7 Amido Ligand Systems for catalytic reduction of dinitrogen……..20

1.8 Early Transition Metals in Dinitrogen Reduction……27

2 Synthesis and Reactivity Studies of Arylamido Complexes of Titanium

2.1 Overview……..32

2.2 Introduction……..33

2.3 Results and Discussion……35

2.3.1 Synthesis of $(dda)_3TiCl$ and $(dda)_2TiCl_2$……..35

2.3.2 Spectroscopic studies of free ddaH……..37

2.3.4 Spectroscopic studies of $(dda)_3TiCl$…….41

2.3.5 Spectroscopic studies of $(dda)_2TiCl_2$……...51

2.3.6 Solid-state and molecular structure of $(dda)_3TiCl$……54

2.3.6.1 Solid-state structure of $(dda)_3TiCl$…….54

2.3.6.2 Molecular structure of $(dda)_3TiCl$……..57

2.3.7 Solid-state and molecular structure of $(dda)_2TiCl_2$…….63

2.3.7.1 Solid-state structure of $(dda)_2TiCl_2$…….63

2.3.7.2 Molecular structure of $(dda)_2TiCl_2$……..65

2.3.8 Metathetical reactivity of $(dda)_3TiCl$ and $(dda)_2TiCl_2$…….70

2.3.9 Synthesis of $(dda)_3TiBH_4$…….70

2.3.10 Spectroscopic studies of $(dda)_3TiBH_4$…….71

2.3.11 Solid-state and molecular structure of $(dda)_3TiBH_4$……74

2.3.12 Synthesis of $(dda)_3TiCH_2PMe_2$……76

2.3.13 Spectroscopic studies of $(dda)_3TiCH_2PMe_2$…….77

2.3.14 Synthesis of $(dda)_3TiMe$.....82

2.3.15 Spectroscopic studies of $(dda)_3TiMe$……...83

2.4 Discussion and future progress……87

3 Synthesis and Reactivity Studies of Carbazolyl Complexes of Titanium

3.1 Overview……..…89

3.2 Introduction……..…91

3.3 Results and Discussion……92

3.3.1 Synthesis and analysis of CbLi……92

3.3.2 Synthesis of $(Cb)_3TiCl.2THF$ and $(Cb)_2TiCl_2.2THF$……...94

3.3.3 Spectroscopic studies of $(Cb)_3TiCl.2THF$ and $(Cb)_2TiCl_2.2THF$……...96

3.3.4 Attempted synthesis of $(Cb)_3TiBH_4$……...103

3.3.5 Synthesis of $(Cb)_3TiMe$…….103

3.3.6 Spectroscopic studies of $(Cb)_3TiMe$……..103

3.3.7 Synthesis of $(Cb)_3TiCH_2PMe_2$……...104

4 Investigation of Tetraamines

4.1 Introduction……108

4.2 Synthesis and reactivity of tetraamines……..110

4.2.1 1,1'-Ethylenedi-2-imidazoline (9).....111

4.3.2 2,3,4,5,6,7,8,8c-Octahydro-1*H*-4a,6a,8a-triaza-2a-azoniacyclopent[*fg*]acenaphthylene bromide salt (10).....114

4.3.3 Decahydro-2a,4a,6a,8a-tetraazacyclo-pent[*fg*]acenaphthylene (11).....115

4.3.4 2,3,4,5,6,7,8,8c-Octahydro-1*H*-4a,6a,8a-triaaza-2a-azo-niacyclopent[*f,g*]acenaphthylene Bromide Salt.....118

4.3.5 1,2,3,4,5,6,7,8–Octahydro-2a,4a,6a,8a-tetraazacyclopenta[*f,g*]acenaphthylene (13).....120

4.3.6 Spectroscopic analysis and reactivity of 1,2,3,4,5,6,7,8–Octahydro-2a,4a,6a,8a-tetraazacyclopenta[*f,g*]acenaphthylene (13)……...121

4.3.6.1 Alkene oxidation reactivity……122

4.3.6.2 Investigation into the Magnetism of 1,2,3,4,5,6,7,8–Octahydro-2a,4a,6a,8a-tetraazacyclopenta[*f,g*]acenaphthylene……..……...126

4.3.7 1,4,7,10-Tetraaza-tricyclo[8.2.1.14,7]tetradecane-13,14-dione (14)…….130

4.4 Discussion and future work……...132

5 Experimental Section

5.1 General Considerations……..……133

5.2 Experimental methodology……136

5.2.1 Dihydrodibenzoazepinyl lithium……...136

5.2.2 *tris*(Dihydrodibenzoazepinyl)titanium chloride (1)……...137

5.2.3 *bis*(Dihydrodibenzoazepinyl)titanium dichloride (2)……138

5.2.4 *tris*(Dihydrodibenzoazepinyl)titanium borohydride (3)……139

5.2.5 *tris*(Dihydrodibenzoazepinyl)[(dimethylphosphino)-methyl]titanium (4)…139

5.2.6 *tris*(Dihydrodibenzoazepinyl)titanium methyl (5)…….140

5.2.7 Carbazolyl lithium…….141

5.2.8 *tris*(Carbazolyl)titanium chloride (6).....141

5.2.9 *bis*(Carbazolyl)titanium dichloride (7).....142

5.2.10 *tris*(Carbazolyl) titanium methyl (8).....143

5.2.11 1,1'-Ethylenedi-2-imidazoline (11).....144

5.2.12 2,3,4,5,6,7,8,8c-Octahydro-1*H*-4a,6a,8a-triaaza-2a-azo-niacyclopent[fg]acenaphthylene Bromide Salt (12).....144

5.2.13 Decahydro-2a,4a,6a,8a-tetraazacyclopent[*fg*]acenaphthylene (14).....145

5.2.14 1,2,3,4,5,6,7,8–Octahydro-2a,4a,6a,8a-tetraazacyclopenta[*f,g*]acenaphthylene (13).....145

5.2.15 Decahydro-2a,4a,6a,8a-tetraazacyclopent[*fg*]acenaphthylene Dibenzyl dibromide Salt (16).....146

5.2.16 1,4,7,10-Tetraaza-tricyclo[8.2.1.14,7]tetradecane-13,14-dione (17).....147

References.....148

Vita.....156

Tables:

Table 1: ^{1}H NMR resonances for ddaH ran in d_8-toluene, including coupling constants. 39

Table 2: ^{13}C NMR resonances for ddaH ran in d_8-toluene. 39

Table 3: ^{1}H resonances for ddaH compared to $(dda)_3TiCl$. 43

Table 4: ^{13}C resonances for ddaH compared to $(dda)_3TiCl$. 43

Table 5: ^{1}H NMR resonances for ddaH compared to $(dda)_2TiCl_2$. 52

Table 6: Lattice parameters for the crystal structure of $(dda)_3TiCl$. 54

Table 7: Important bond lengths in $(dda)_3TiCl$. 57

Table 8: Important bond angles in $(dda)_3TiCl$. 58

Table 9: Lattice parameters for the crystal structure of $(dda)_3TiCl$. 63

Table 10: Important bond angles in $(dda)_2TiCl_2$. 67

Table 11: Important bond angles in $(dda)_2TiCl_2$ 68

Table 12: ^{1}H NMR resonances for $(dda)_3TiBH_4$ compared to $(dda)_3TiCl$. 75

Table 13: ^{1}H NMR resonances for $(dda)_3TiBH_4$ compared to $(dda)_3TiCl$. 75

Table 14: ^{1}H NMR resonances for $(dda)_3TiCH_2PMe_2$ compared to $(dda)_3TiCl$. 81

Table 15: ^{1}H NMR resonances for $(dda)_3TiCH_2PMe_2$ compared to $(dda)_3TiCl$. 82

Table 16: ^{1}H NMR resonances for $(dda)_3TiMe$ compared to $(dda)_3TiCl$. 86

Table 17: ^{1}H NMR resonances for $(dda)_3TiMe$ compared to $(dda)_3TiCl$ 86

Table 18: A comparison of cyclic amine derivatives against simple "hard" amines. 89

Table 19: Tentative ^{1}H NMR spectral assignment for CbLi in d_8-THF. 93

Table 20: Tentative ^{13}C NMR spectral assignment for CbLi in d_8-THF 94

Table 21: ^{1}H NMR assignment for $TiCb_3Cl.2THF$ in benzene. 98

Table 22: ^{13}C NMR assignment for $TiCb_3Cl.2THF$ in benzene. 98

Table 23: The ^{1}H NMR assignment of 7 in benzene-d_6. 102

Table 24: The ^{13}C NMR assignment of 7 THF-d_8. 103

Table 25: ^{1}H NMR assignment of $(Cb)_3TiMe$ in benzene-d_6. 106

Table 26: Tentative ^{13}C NMR assignment of $(Cb)_3TiMe$ in benzene-d_6. 106

Table 27: ^{1}H and ^{13}C NMR assignment of 1,1'-Ethylenedi-2-imidazoline 113

Table 28: NMR Assignment of 9. 116

Table 29: Complete NMR Assignment of 11. 117

Table 30: NMR Assignment of 12. 119

Table 31: The ^{13}C NMR assignment for 13 123

Table 32: ^{1}H and ^{13}C NMR assignment for 14. 132

Table 33: The drying methods for various solvents. 133

Table 34: Various deuterated solvents used for analysis of compounds discussed within this document. 135

Figures:

Figure 1: Schematic representation Zeise's salt 1

Figure 2: Pauson's proposed Fe-cyclopentadienyl σ-bond with a canonical ionic formula. 2

Figure 3: The phases of the wavefunction for Cp 3

Figure 4: Atomic Orbitals of iron with matching symmetry to those of Cp 4

Figure 5: A qualitative MO diagram of ferrocene 6

Figure 6: i) terminal chloride moiety, X class. ii) bidentate sulfato ligand, X2 class. iii) bridging oxo-ligand, X-μ-X 8

Figure 7: i) tetrahydrofuran, L class. ii) bidentate bisphosphinato ligand, L2 class. iii) bridging oxo moiety, L-μ- L class ligand. 9

Figure 8: i) η2-acetate, LX class. ii) amido, class 9

Figure 9: i) MX6L3. ii) ML6. iii) When M = Cr, MX3L3 with three unpaired electrons (paramagnetic) and when M = W, MX6L3, M–M triple bond, diamagnetic species. 10

Figure 10: The Cossee mechanism for Ziegler–Natta polymerization. 11

Figure 11: Zirconocene polymerization catalyst precursors. 14

Figure 12: Brintzinger's experiment alkene insertion of trans-nBuCH=CHD. (In this experiment, erythro is favored by 1.3:1 showing that the C–H is favored and reinforcing the proposal of agostic interactions from Green and Rooney.) 16

Figure 13: Iron and cobalt catalytic systems with imino ligand set. 17

Figure 14: Brookhart's Anion. 18

Figure 15: Brookhart's nickel polymerization catalyst. 19

Figure 16: Amido ligands.are polyfunctional systems 20

Figure 17: The enzyme nitrogenase. 21

Figure 18: World population from 1750 to present. 24

Figure 19: Reduction of dinitrogen at a single metal center via the 'Chatt cycle'. ... 26

Figure 20: Yandulov and Schrock's [HIPTN$_3$N]Mo(N$_2$) complex. 26

Figure 21: Schrock's proposed intermediates in the reduction of dinitrogen at a [HIPTN$_3$N]Mo center through the stepwise addition of protons and electrons. 27

Figure 22: Chirik's titanium sandwich complex. 28

Figure 23: Schrock's NON-titanium dinitrogen complex. 29

Figure 24: Titanium-diazenido complex synthesized by Arnold et al. 30

Figure 25: Unique end-on, side-on bound dinitrogen in Fryzuk's tantalum complex. 30

Figure 26: A set of three electronically and sterically comparable amido ligands. .. 34

Figure 27: NMR labeling of ddaH and related Ti-dda complexes. 38

Figure 28: ^{1}H NMR spectrum of ddaH, illustrating equivalent protons at room temperature on the ethyl backbone of the molecule. 40

Figure 29: NOESY illustrating through-space coupling specifically between. protons: f to e and a through to b in ddaH. 42

Figure 30: The ^{1}H NMR spectrum for 1, you can clearly see the non-equivalent hydrogens between 2.0 and 3.0 ppm. 45

Figure 31: The 'rocking' of the backbone hydrogens which showing non-equivalency. 46

Figure 32: VT NMR depicting the coalescence temperature of $Ti(dda)_3Cl$. 47

Figure 33: Low temperature VT NMR of $Ti(dda)_3Cl$. 48

Figure 34: Showing the ethyl protons of the $Ti(dda)_3Cl$ looking down the C_3 rotational axis through the Ti to Cl bond. 49

Figure 35: NOESY spectrum of 1, clearly showing the correlation between aromatic protons and the alkyl region. 51

Figure 36: VT NMR expanding on the backbone hydrogens of complex 2. 53

Figure 37: The crystal and molecular structure of $(dda)_3TiCl$: (a) The bc plane of the unit cell of $(dda)_3TiCl$ (b) The molecular structure of $(dda)_3TiCl$, emphasizing the C_3 axis (c) A general view of $(dda)_3TiCl$. 56

Figure 38: The relationship between the N–Ti–X angle and the Ti–N bond length in $(dda)_3TiCl$ in comparison to other crystallographically characterized four coordinate e X–Ti–NR_2 complexes. 60

Figure 39: A comparison of $(dda)_3TiCl$ (a) and $((3,5,\text{-}Me_2Ph)(t\text{-}Bu)N)_3MoCl$ (b) with views along the molecular C_3 axis, containing the M–Cl bond. 61

Figure 40: (a) The structure of the reactive pocket in $(dda)_3TiCl$; the tetrahedron represents the N_3Cl centered on the Ti atom. (b) A comparison of the torsion angles between the N–CAr–M–Cl vector in $(dda)_3TiCl$ and $((3,5,\text{-}Me_2Ph)(t\text{-}Bu)N)_3MoCl$... 62

Figure 41: The molecular structure of $(dda)_2TiCl_2$: 64

Figure 42: The crystal and molecular structure of (dda)2TiCl2: (a) The general molecular structure of (dda)2TiCl2 (b) A view of the molecular structure emphasizing the pseudo C2 axis. 66

Figure 43: The relationship between the N–Ti–X angle and the Ti–N bond length in $(dda)_2TiCl_2$ (green point) in comparison to $(dda)_3TiCl$ (red point) and other crystallographically characterized four coordinate X–Ti–NR_2 complexes. 69

Figure 44: The ^1H NMR spectrum for $(dda)_3TiBH_4$. (Quinuclidine) in THF, focusing on the alkyl region. 72

Figure 45: A comparison between the precursor 1 to complex 3 (with bound THF), alongside the slight raise of the baseline around 1.5 ppm through to 0.0 ppm possibly due to the bound BH_4 moiety. 73

Figure *46: A VT NMR experiment in order to see the Ti–BH_4 moiety, free BH_4 is observed at 0.4 ppm.* 74

Figure 47: The X-Ray crystal structure of 3 viewed through the Ti-B bond to show the arrangement of the ligands. 76

Figure 48: The three possible binding modes of P,P-dimethylphosphinomethyl 77

Figure 49: The ^1H NMR spectrum for $(dda)_3TiCH_2PMe_2$ in d_8-toluene, the PMe_2 and CH_2–Ti can clearly be seen up field of the residual toluene methyl resonance. 78

Figure 50: NOESY experiment spectrum for 4. 80

Figure 51: ^1H NMR assignment in this species. 81

Figure 52: The ^1H NMR spectrum of $(dda)_3TiMe$ in d_8-toluene, clearly showing the integration of the methyl peak in relation to the other resonances. 84

Figure 53: The ^{13}C NMR spectrum of $(dda)_3TiMe$ in d_8-THF. 85

Figure 54: ^1H NMR assignment in this species. 85

Figure 55: A diagram showing the π-ligand and d-metal interaction, the π donating capacity of systems such as carbazolyl should be diminished. 91

Figure 56: Depicting the clear separation and splitting of the aromatic region of CbLi. 92

Figure 57: ^{1}H and ^{13}C NMR labeling system for Cb system discussed in this chapter. 93

Figure 58: The three possible isomers of compound 6. 95

Figure 59: Bound THF moiety in TiCb systems. 96

Figure 60: Depicting the ^{1}H NMR spectrum for $TiCb_3Cl \cdot 2THF$. 97

Figure 61: COSY showing H–H correlations in 6. 99

Figure 62: NOESY depicting H–H through-space correlations in 6. 101

Figure 63: The ^{1}H NMR spectrum of $Ti(Cb)_2Cl_2 \cdot 2THF$ in benzene-d_6, a small amount of residual toluene can also be seen. 102

Figure 64: ^{1}H NMR spectrum of $(Cb)_3TiMe$ with expansions of aromatic splitting. 104

Figure 65: Three related tetraamine species. 108

Figure 66: ^{1}H and ^{13}C NMR resonance labeling for 1,1'-Ethylenedi-2-imidazoline. 113

Figure 67: NMR labeling system for compound 10. 115

Figure 68: Depiction of decahydro-2a,4a,6a,8a-tetraaza-cyclopenta[fg]acenaphthylene (compound 11), the ^{13}C NMR spectrum for this species is particularly simple at room temperature with only five resonances (due to its high symmetry). 117

Figure 69: Side-view depiction of 12, the phenyl hydrogens have been omitted for clarity. 118

Figure 70: 1,2,3,4,5,6,7,8 –Octahydro-2a,4a,6a,8a-tetraazacyclopenta[f,g]acenaphthylene. 120

Figure 71: ^{1}H NMR spectrum of 13 in benzene, clearly showing the two singlets that correlate to the protons in the 5- and 6-membered rings within the molecule. 121

Figure 72: The ^{13}C NMR spectrum of 13 in benzene-d_6, clearly showing the two resonances that correlate to the carbons in the 5- and 6-membered rings within the molecule. 122

Figure 73: The tetraamine dication iodide. 124

Figure 74: Materials with different types of electron spin orientations; diamagnetic (A),paramagnetic (B), antiferromagnetic (C), ferrimagnetic (D), ferromagnetic (E). 127

Figure 75: The magnetic susceptibility of the alkene-C_{60} complex clearly showing the critical point where the magnetic susceptibility is theoretically infinite. 129

Figure 76: 1,4,7,10-Tetraaza-tricyclo[8.2.1.14,7]tetradecane-13,14-dione (13) 130

Figure 77: ^{1}H NMR spectrum of the diurea 14, with the expansion of the alkyl resonances superimposed. 131

1. Introduction

1.1 Early Organometallic Compounds

One of the oldest compounds belonging to the rapidly growing field of organometallic chemistry was prepared by W.C. Zeise in 1827; this was 40 years prior to the formulation of the Periodic Table of the Elements. He combined a solution of ethanol with a mixture of $PtCl_2$, $PtCl_4$ and KCl. This reaction yielded the compound $KPtCl_3(C_2H_4)\cdot H_2O$. Zeise's idea of ethylene being bound to platinum was disputed by many of the leading chemists of the time, notably Liebig, who severely attacked the notion of such a compound. Today, this compound has been fully characterized through modern structural techniques, and it has been revealed that platinum does indeed contain a bound ethylene moiety. Such bonding is now further understood and is termed a π-bond. The first metal-alkyl σ-bond was discovered by E. Frankland in 1849. [1]

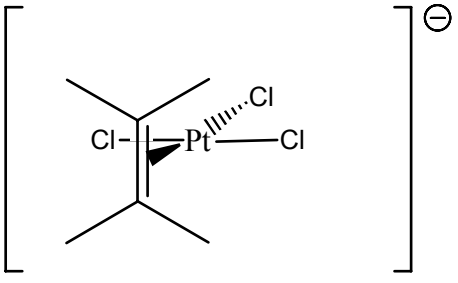

Figure 1: Schematic representation Zeise's salt

The milestone discovery of ferrocene by Kealy and Pauson[2] led to a heightened understanding of structure and bonding between organic moieties and transition metals. Pauson had first proposed the nature of the bonding between the two cyclopentadienyl rings and iron as depicted in Figure 2.

However, Wilkinson and Woodward[3] independently noted the inadequacy of this bonding model, used infrared and NMR spectroscopy to prove the existence of the "iron sandwich" with staggered and eclipsed configurations of ferrocene (or other $(\eta\text{-}C_5H_5)_2M$ species.

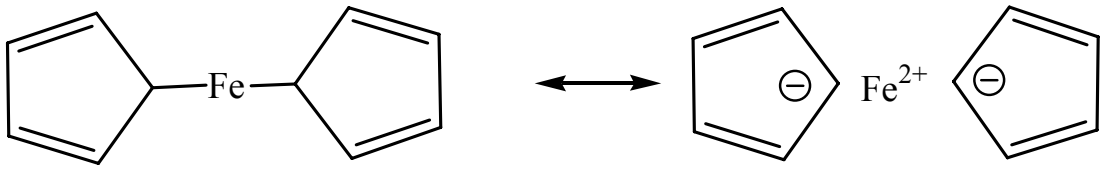

Figure 2: Pauson's proposed Fe-cyclopentadienyl σ-bond with a canonical ionic formula.

1.2 Bonding Fundamentals

The Cp-transition metal bonding interaction is of importance due to the ubiquity of this structural motif in transition metal chemistry. Moreover, it is a good example of the Dewar–Chatt–Duncanson model that describes the donor acceptor behavior of polyfunctional ligands. The interactions can be qualitatively described in terms of σ-, π- and δ-interactions. The symmetry adapted linear combinations of carbon *p*-functions, calculated in C_5, and these are shown below in Figure 3. They contain 0-node, 1-node and 2-node orbitals, the last pair often corresponding to *E* functions in the point group of the complex, where such functions are allowed.

When the metal orbitals are considered, then σ-, π- and δ-interactions are easily formulated on the basis of symmetry matching the frontier orbitals of the fragment and the metal. These interactions are shown, together with their classification, in Figure 4.

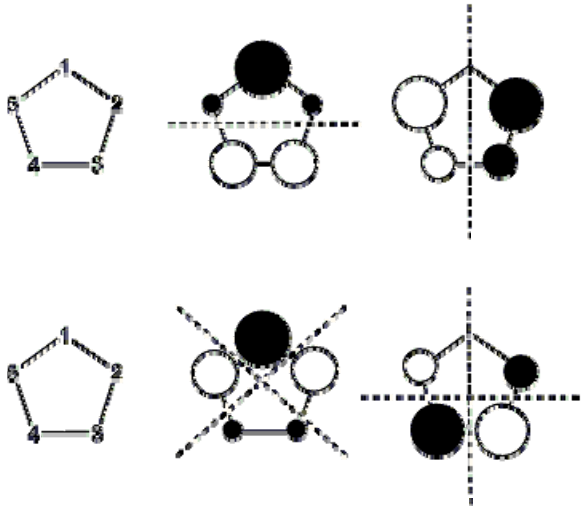

Figure 3: The phases of the wavefunction for Cp

$(n+1)s$ $(n+1)p_z$ nd_{z^2}

The interaction between the E_1 states and the E_1 ligand orbital will be π in character.

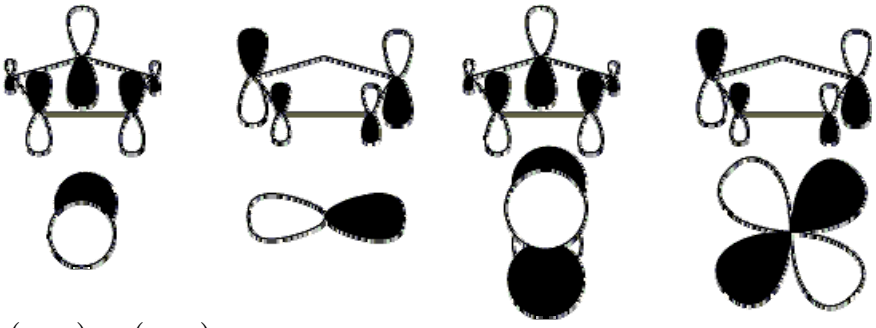

$(n+1)p_x, (n+1)p_y$ E_1

nd_{xz}, nd_{yz}

The interaction between the E_2 states and the E_2 ligand orbital will be δ in character.

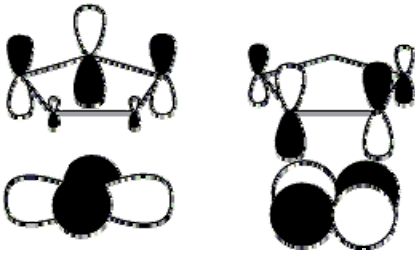

E_2

$nd_{x^2-y^2}, nd_{xy}$

Figure 4: Atomic Orbitals of iron with matching symmetry to those of Cp

The most important overlaps are between the E_1 states of the metal and the E_1 on the ligand. These make up the A_1, which is the lowest energy bonding MO in this system (the phases of the metal orbitals can be seen in Figure 4 with white lobes indicating a positive phase and the black lobe indicating a negative phase).

The interaction between the E_1 states and the E_1 ligand orbital will be π in character, and the interaction between the E_2 states and the E_2 ligand orbital will be δ in character.

Therefore, the combination of two sets of MOs of Cp with the atomic orbitals (AOs) of iron will produce the MO diagram for ferrocene, as shown in Figure 5. Iron is in a 2+ oxidation state, and it has six *d*-electrons. Combined with the twelve electrons from the two Cp ring systems, they occupy all MOs to the E_{2g} A_{1g} orbitals. This constitutes an 18-electron complex, and due to the large gap between E_{1g}* and E_{2g} levels caused from Cp being a strong field ligand, the Highest Occupied Molecular Orbital (HOMO) contains a pair of electrons; therefore, ferrocene is diamagnetic.

Ligand field strength can be illustrated by the spectrochemical ligand series which lists commonly used ligands in increasing value of Δ:

$$I^- < Br^- < Cl^- < F^- < H_2O < NH_3 < PPh_3 < CO$$

Scheme 1: The spectrochemical series of ligands

Iodide, which is at the far left of the spectrum, is a weak field ligand, low Δ and a π-donor, whilst carbon monoxide at the other end of the spectrum is a strong field ligand with a high Δ and is a strong σ-donor/ π-acceptor.

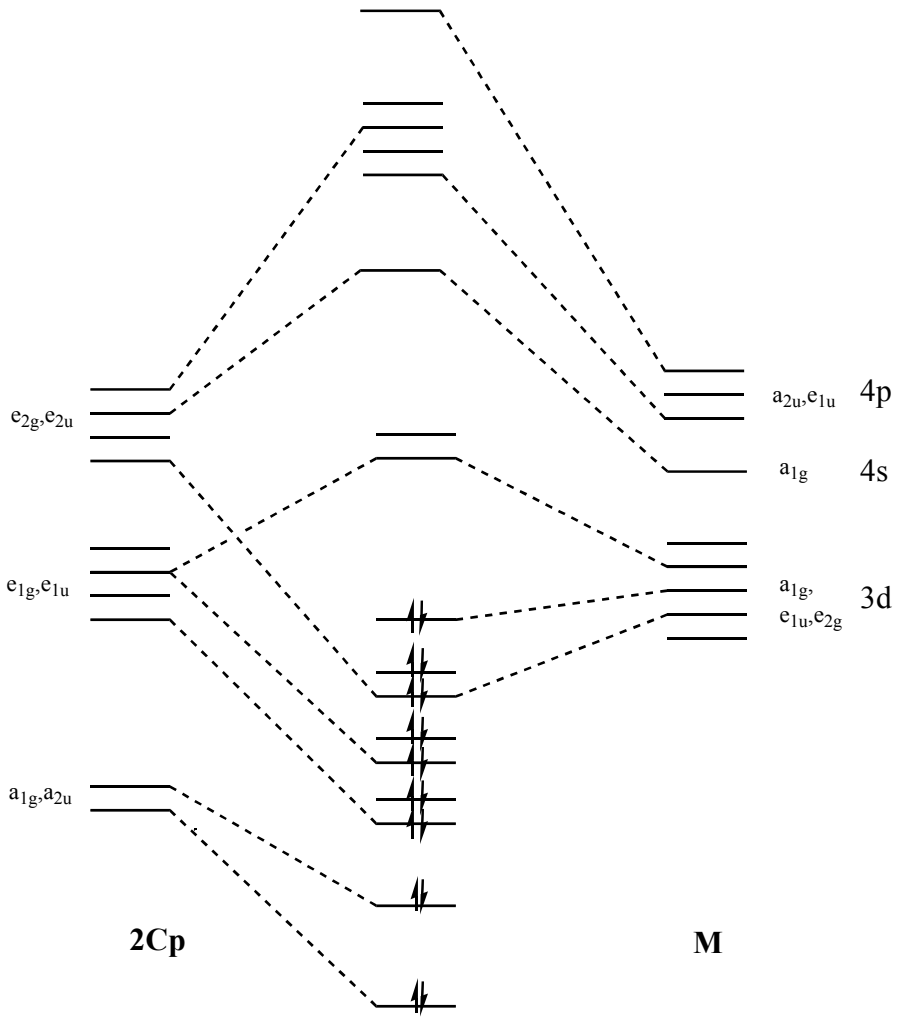

Figure 5: A qualitative MO diagram of ferrocene

The gap between the E_{2g} and the E^*_{2g} corresponds to the dπ – dσ energy gap (Δ). It is the absorption of light to these energy levels that often results in the characteristic colors of a variety of transition metal complexes. The value of Δ is a direct result of the crystal field strength of the ligands. So-called high field ligands such as phosphines and carbon monoxide give rise to a large Δ, while weak field ligands such as halides or water give a smaller value.

1.3 Principles of MLX Theory

The covalent bond classification has been reviewed by Green in 1995[4]. The MLX system outlines the exact contribution of different types of ligand *via* the amount of electrons donated to the metal center, M. Only the valence electrons from M are considered for the overall electron count of the system, therefore, in the case of titanium only four electrons are taken into account. Iron would be eight, and nickel ten, and so on. The actual oxidation state of the metal center in such covalently bound systems is a formality and is not useful for the classification of such compounds, as it bears very little resemblance to the actual charge upon the metal. Hoffman once stated that: "*Formalisms are convenient fictions which contain a piece of the truth, and it is so sad that people spend a lot of time arguing about the deductions they draw, often ingeniously and artfully, from formalisms, without worrying about their underlying assumptions*".

X-type ligands are one-electron, single covalent bonds, with a single electron occupying an orbital on the ligand that is overlapped with a singularly occupied

orbital upon the metal forming a bond. The local symmetry of the orbital is therefore σ, which is illustrated in Figure 6.

An L-type ligand is an interaction between a doubly occupied ligand orbital to a vacant orbital upon the metal, similar to that in a dative bond. Orbitals of both σ and π symmetry can contribute toward an L-type ligand interaction and is counted as a contribution of two electrons for obeying the eighteen electron rule.

Figure 7 depicts L-class ligand systems, alongside polyfunctional ligands shown in Figure 8, (a bar is drawn over the ligand class in order to draw attention to the polyfunctional nature of the ligating atom).

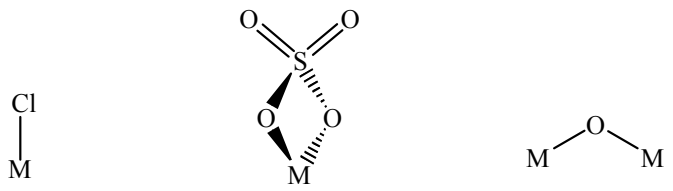

i) ii) iii)

Figure 6: i) terminal chloride moiety, X class. ii) bidentate sulfato ligand, X2 class. iii) bridging oxo-ligand, X-μ-X .

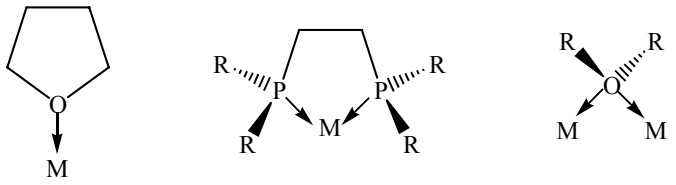

i) ii) iii)

Figure 7: i) tetrahydrofuran, L class. ii) bidentate bisphosphinato ligand, L2 class. iii) bridging oxo moiety, L-μ- L class ligand.

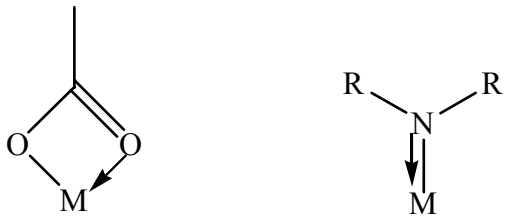

i) ii)

Figure 8: i) η2-acetate, LX class. ii) amido, class

The Z ligand is an electron-pair acceptor, basically a ligand that has an empty orbital that can accept an electron pair from the metal. Ligands that have a Z function are often rare, although the most common would be lewis acids such as BR_3, which has one Z function.

In order to assign a neutral covalent system, one only needs to look at the compound and assign its components $M_wL_xX_yZ_z$, where the subscripts w,x,y and z are simply the number of each type. For example in $Fe(CO)_5$ would be written ML_5 and ferrocene would be written as a ML_4X_2 system. A problem arises when we consider a non-innocent ligand system or where the degree of metal–metal bonding is unclear with respect to polyfunctional ligands. Such systems require information about the compound's electronic structure to unambiguously assign the ligands contribution. Such systems are illustrated in Figure 9, i) and ii) showing the problem occurring with non-innocent ligands and iii) detailing the ambiguity when not knowing the extent of M–M bonding within a system.

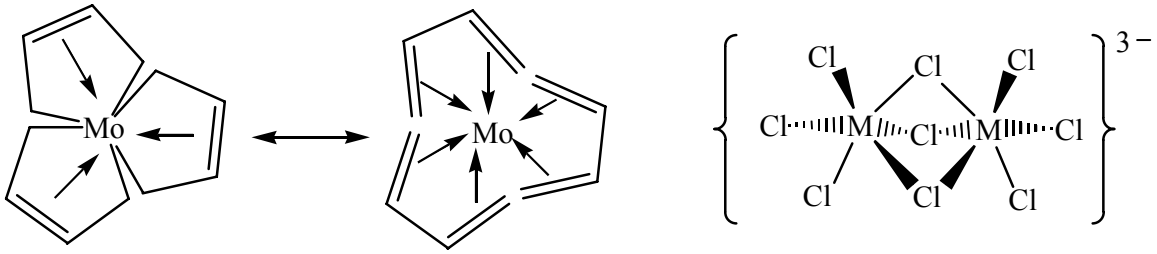

i) ii) iii)

Figure 9: i) MX6L3. ii) ML6. iii) When M = Cr, MX3L3 with three unpaired electrons (paramagnetic) and when M = W, MX6L3, M–M triple bond, diamagnetic species.

1.4 Ziegler–Natta Polymerization

In 1963 Karl Ziegler and Giulio Natta were awarded the Nobel Prize for the discovery and application of titanium-based polymerization catalysts. In the Ziegler–Natta polymerization process $TiCl_4$ is reduced by $AlEt_3$ to polymeric $TiCl_3$, which polymerizes ethylene at only 1 bar pressure and moderate temperatures to give high-density polyethylene (HDPE). Before this process, low-density polyethylene was produced in the absence of catalyst at high temperatures (~200 °C) and high pressure (1000–3000 bar) by a free-radical process, that in stark contrast to the Ziegler process, produces an extensively branched material consisting of chains of widely differing molecular weights and very different properties for the (compositionally identical) polymer obtained with metal catalysts. Today, this discovery accounts for the production of more than 15 million tons of polyethylene and polypropylene

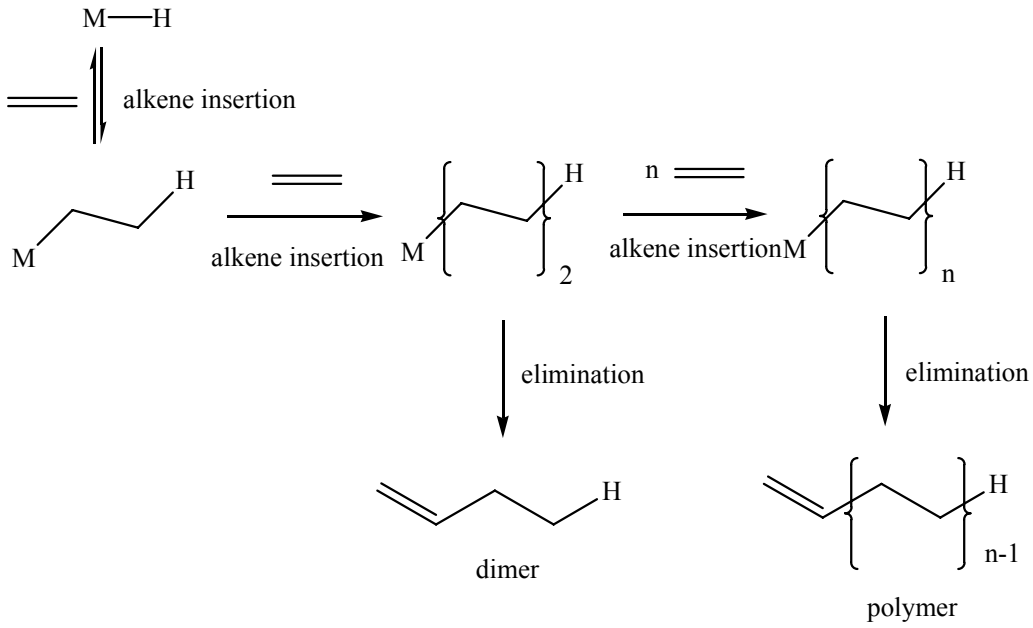

Figure 10: The Cossee mechanism for Ziegler–Natta polymerization.

annually. The mechanism of this process was outlined by Cossee, depicted in Figure 10.[5]

The relative rates between alkene insertion and β-hydride elimination determine the value of n, a slow rate of elimination and fast rate of insertion furnished a polymer of high molecular weight.

In the 1970s, the 'second generation' $MgCl_2$-supported Ziegler-Natta catalysts were discovered. These systems, which are highly active and stereospecific[6] consist of a $MgCl_2$/Lewis base/$TiCl_4$ ternary mixture as the catalyst component and aluminum alkyl/lewis base as cocatalysts. The $MgCl_2$-supported catalysts brought about a remarkable simplification of polymerization and work-up processes, and led to a revolutionary development for commercial production of linear polyethylene and isotactic polypropylene. The scientific and industrial aspects of both heterogeneous supported transition metal catalysts for olefin polymerization have been demonstrated.[7]

1.5 Metallocenes in Olefin Polymerization

The development of homogeneous catalysts for Ziegler–Natta polymerization is an important step for the rapidly growing field of olefin catalysis. The first homogenous Ziegler–Natta catalysts were independently discovered by Breslow and Newburg[8], and Natta *et al.*[9] in 1957. Cp_2TiCl_2 activated by an alkyl aluminum chloride exhibited low polymerization activity for ethylene; it was found later that adding small amounts of water increased the activity of the catalysts significantly. The reaction between alkyl aluminum chlorides and water produced aluminoxanes, which are now ubiquitous in polymerization reactions.[10]

Metallocenes such as Cp_2ZrCl_2 when activated with MAO (methylaluminoxane) form highly active polymerization catalysts. The active species in the case of Cp_2ZrCl_2 is thought to be $[Cp_2ZrMe]^+$, which is stabilized by the non-coordinating $[Me(MeAlO)_n]^-$ counterion. These metallocene catalysts produce polyethylene that is strictly linear, without any side branches, termed LLDPE (linear low density polyethylene). Modification of the ring systems of these metallocenes allow tailoring for specific performance on a variety of different polymerization reactions.

Metallocene catalysts, particularly *ansa*-metallocenes, have been found to be highly selective for the formation of isotactic and syndiotactic polypropylene. This is achieved through manipulation of the symmetry of the complex; in order to process isotactic polypropylene the catalyst needs to have a C_2 symmetry axis (see compound i in Figure 11), so that both binding sites upon the metal have the same chirality. Therefore each new propagating polymer chain binds in the same orientation giving an isotactic product.

In order to form syndiotactic polypropylene, a catalyst such as (ii) would need to be employed. In this system, each binding site has opposite chirality due to the symmetry plane through the entire molecule. Hence, binding propylene molecules enter with opposite chiralities and therefore form a chain of alternating chirality, which produces a syndiotactic product. Such highly syndiotactic polypropylene products are softer and tougher with excellent optical properties.[11]

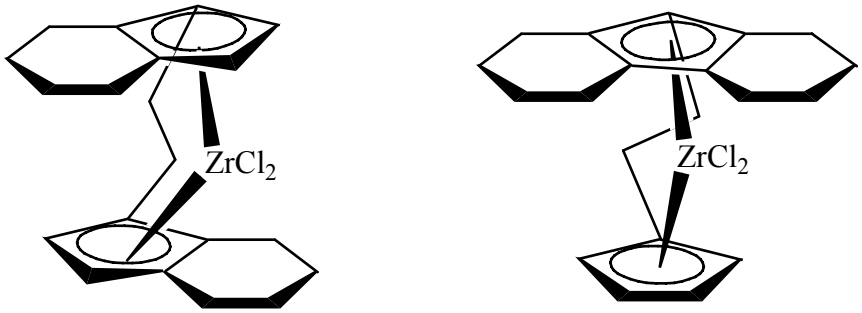

i) ii)

Figure 11: Zirconocene polymerization catalyst precursors.

These products are soon expected to replace other engineering plastics such as nylons, poly(ester)s and poly(carbonate)s Waymouth and Coates[12] have obtained novel and optically active polymers from cyclopolymerization of 1,5-hexadiene using $Et(Ind)_2ZrCl_2$ catalysts (Scheme 2).

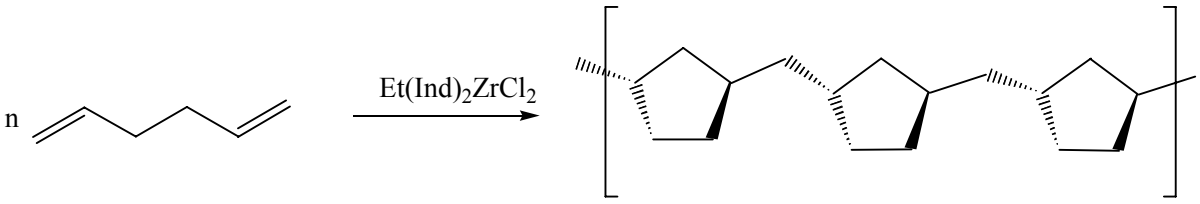

Scheme 2: Waymouth and Coates novel cyclopolymerization of 1,5-hexadiene.

The explanation for the efficiency of these homogeneous catalysts in olefin polymerization was explored by Green and Rooney.[13] They proposed that the reaction is greatly accelerated by the additional stability of the unsaturated intermediate (Figure 12) from the agostic alkyl group, which facilitates insertion.

Work from Brintzinger[14] and Bercaw[15] reinforced the initial proposals of Green and Rooney; they developed elegant mechanistic experiments to analyze the involvement of the agostic species. Figure 12 depicts the alkene insertion of *trans*-

*n*BuCH=CHD, in which the polymerization is halted with the insertion of H_2. Based on the pure Cosse mechanism, there should be an even distribution of erythro and threo isomers, although through the Green–Rooney mechanism the ratio will depend upon whether there is a preference between C–H and C–D being agostic. In this experiment, erythro is favored by 1.3:1, showing that the C–H is favored and reinforcing the proposal of agostic interactions from Green and Rooney.

It is evident from the contents of this chapter, that olefin polymerization is dominated by early transition metal catalytic systems. The electron deficiency of the metal is key to these systems being efficient catalysts, as it reduces the amount of electron donation to the σ* orbital of the β-H, therefore reducing the amount of β-H elimination product and promoting insertion and polymer propagation.

Late transition metal systems, however, are less electrophilic and exhibit a greater tendency to undergo β-H elimination, and therefore were better known for the oligermerization of olefins. However, recently late transition metal complexes containing neutral bis-imine ligands have been recognized as efficient polymerization catalysts. Bennett and Gibson[16] reported the first iron-based olefin polymerization catalysts (Figure 13), containing 2,6-bis(imino)pyridine ligands.

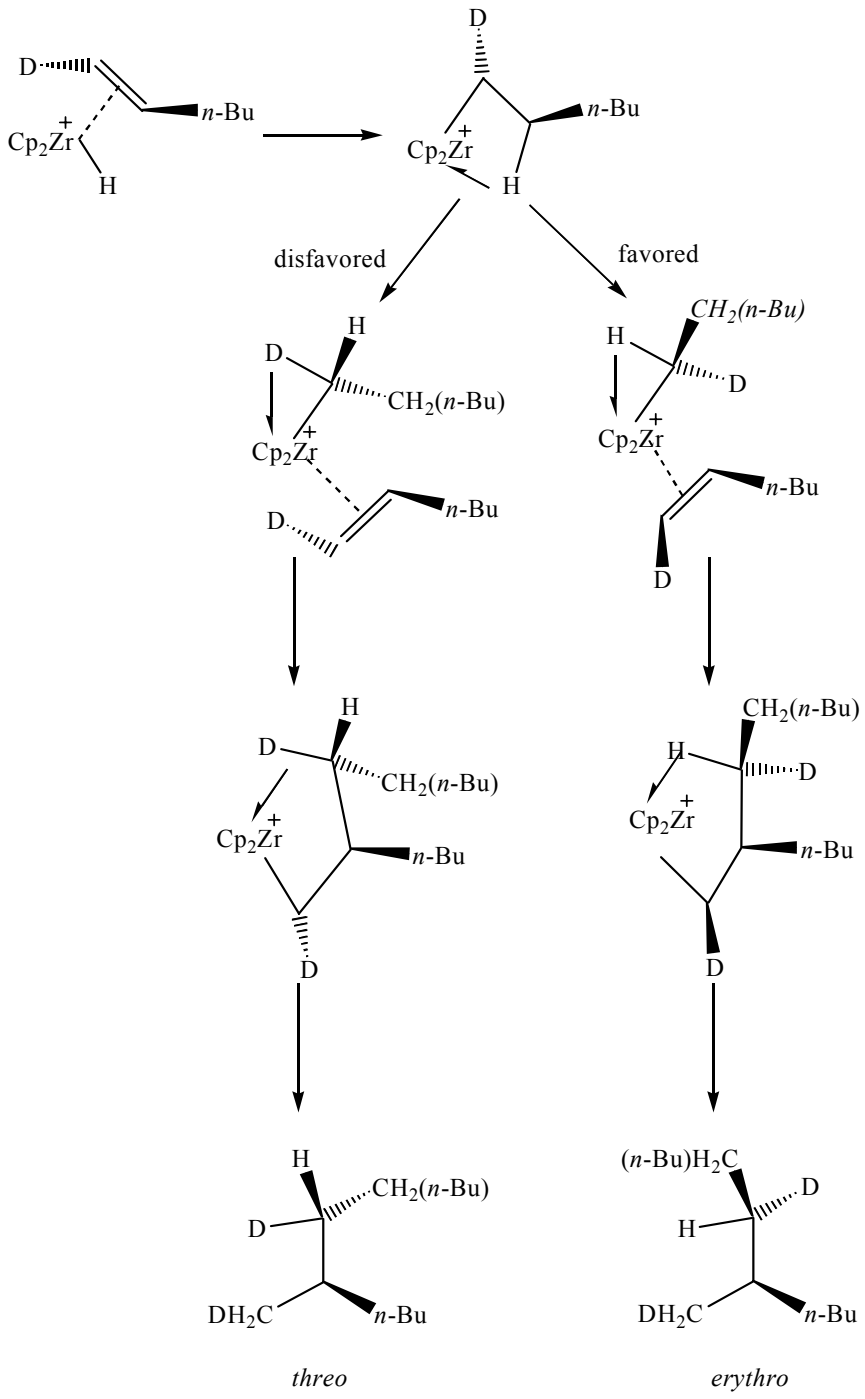

Figure 12: Brintzinger's experiment alkene insertion of trans-nBuCH=CHD. (In this experiment, erythro is favored by 1.3:1 showing that the C–H is favored and reinforcing the proposal of agostic interactions from Green and Rooney.)

These complexes when activated with MAO polymerize ethylene with exceptionally high activity, comparable to the most active Ziegler–Natta catalyst systems. These complexes have a pseudo square pyramidal geometry, with the aryl groups on the imine nitrogen being perpendicular to the square plane and the bulky ortho-substituents provide the necessary steric protection around the metal.[16]

Nickel(II) and palladium(II) systems were developed by Brookhart and coworkers.[17-19] Utilizing a square-planar diimine ligand set, they were able to produce high-molecular-weight polymers from longer chain olefins to ethylene. When treated with MAO, the nickel complexes demonstrate excellent activity, up to 11000 g mol^{-1} h^{-1} bar^{-1} due to the well-defined metal–alkyl cationic species, stabilized by Brookhart's anion (Figure 14), with the nickel system depicted in Figure 15.

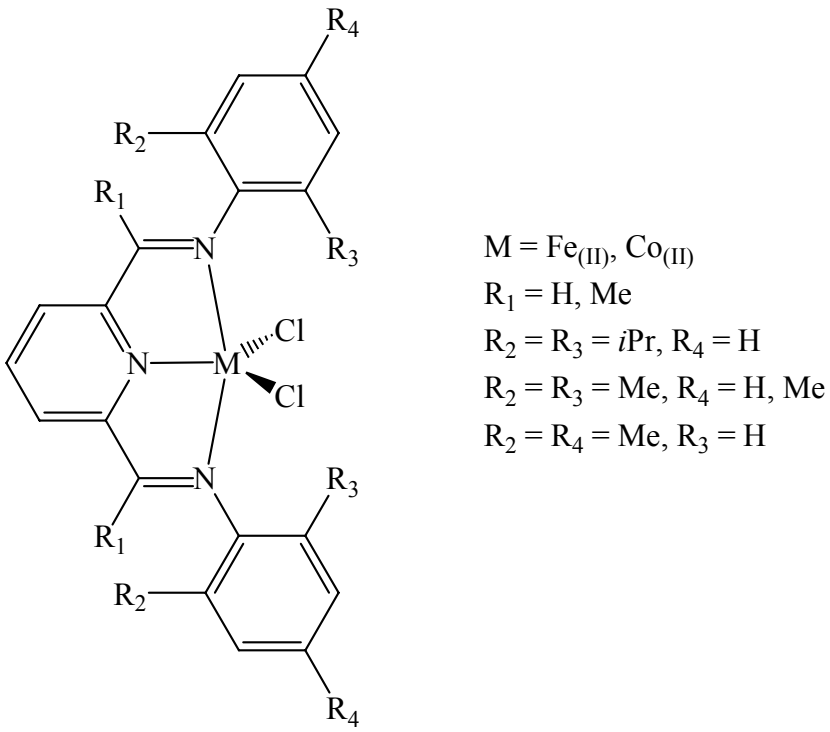

Figure 13: Iron and cobalt catalytic systems with imino ligand set.

β-Elimination from the growing polymer chain leads to chain branching or chain transfer. The formation of high-molecular-weight polymers is possible because of steric protection of the vacant axial coordination sites reduces the rate of associative displacement from β-eliminated olefin hydride complexes and thus reduces chain transfer rates.

Over the past 20 years there has been much progress in the evolution of Ziegler–Natta polymerization catalysts, leading to a variety of extremely efficient homogeneous systems. The explosion of interest in this area is a tribute to the combined efforts from both industry and academia, leading to many publications and patents for single-site polymerization catalysts. [20]

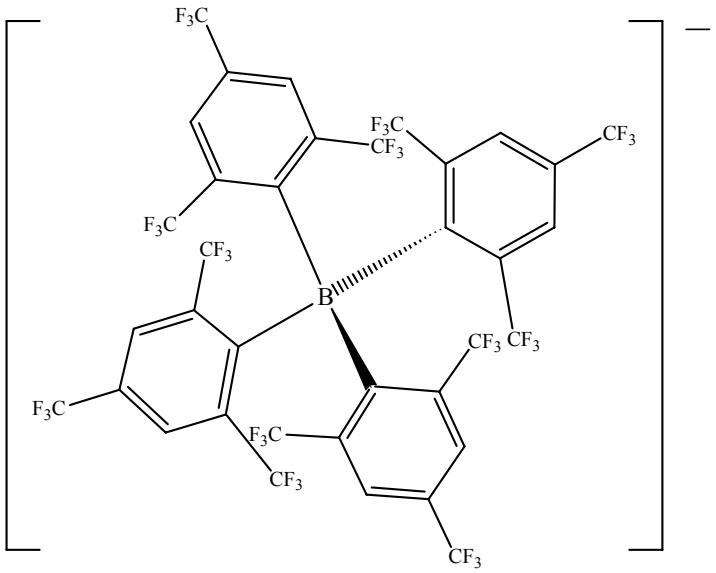

Figure 14: Brookhart's Anion.

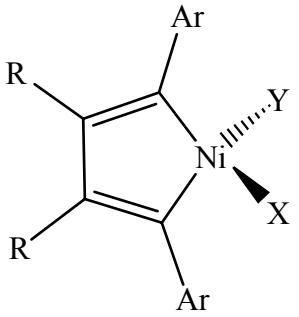

R = H, Me
X = Y = Br
X = B[3,5-$(CF_3)_2C_6H_3]_4$.Et_2O, Y = Me
Ar = 2,6-*i*$Pr_2C_6H_3$, 2,6-$Me_2C_6H_3$, 2-*t*BuC_6H_4

Figure 15: Brookhart's nickel polymerization catalyst.

1.6 Amido Ligand Systems in Polymerization Reactions.

The first amido–metal systems were developed in the 1960s and 1970s, by groups led by Bradley and Lappert.[21] The motivation for their research on amido–metal bonds was mainly focused with the comparison to metal–carbon bonds. From the middle of the 1970s to the late 1980s, interest in amido systems stagnated due to the huge interest in metallocenes. However, within the past two decades, many systems have used amido ligands to construct novel metal complexes with defined reactive centers. [22-25]

It is the realization of the amido donor function R_2N^- (Figure 16), which maybe placed in a great variety of structural environments that has ultimately led to the dramatic expansion of the area. The stabilization of coordination spheres in high valent, Lewis acidic early transition metals requires strong σ- and π-donor capabilities in order to adequately match the electronic demands of the metal center.

The chemistry of amido systems with Group IV metals has been successfully derived from the reactivity of metallocenes. Further development of olefin polymerization catalysts that are sterically demanding have the option of being

bis(amido) chelate ligands, whose dichlorotitanium complexes are accessible in good yields.

1.7 Amido Ligand Systems for Catalytic Reduction of Dinitrogen.

One of the most complex and fascinating transition metal-catalyzed reactions in nature is the reduction of dinitrogen to yield some 10^8 tons of ammonia per year. In 1930 it was discovered by Bortels,[26] that the fixation by leguminous plants required molybdenum, which is found in nitrogenase. Nitrogenases are found in all diazotrophs, which contain an iron–molybdenum protein. The iron protein is an Fe_4S_4 homodimer that transfers electrons, specifically to the MoFe protein that binds and

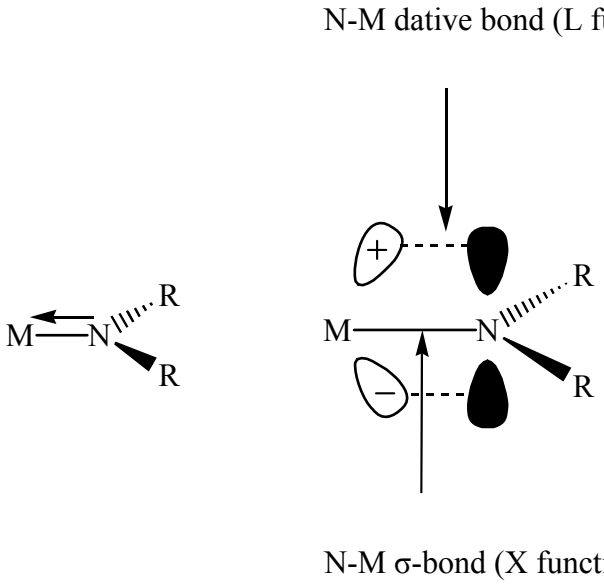

Figure 16: Amido ligands.are polyfunctional systems

reduces dinitrogen to form ammonia. Six electrons and six protons are consumed to produce two equivalents of ammonia per dinitrogen at 1 atmosphere of pressure and at ambient temperature, while two more electrons and two protons are consumed to make dihydrogen.

The structure of the $MoFe_7S_9$ cofactor that resides in a hydrophobic pocket within the protein that is depicted in Figure 17 is capable of reducing dinitrogen. This highly articulated structure, in particular the cavity that is created by the six iron atoms is believed by many to be the site of nitrogen reduction. However, no structure can prove the mechanism, no matter how accurately it is determined, and therefore to date, the exact "site" of N_2 fixation is yet to be determined.[27,28]

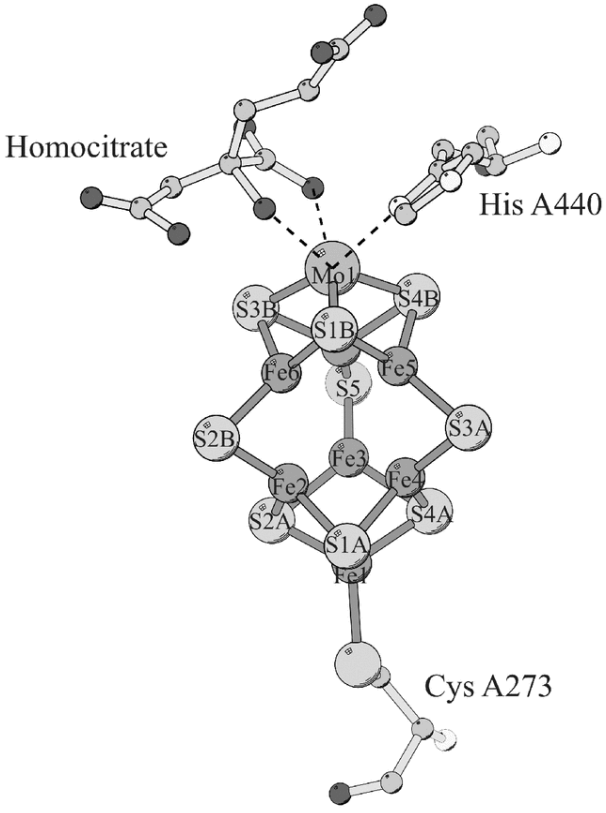

Figure 17: The enzyme nitrogenase.

The first dinitrogen complex of a transition metal, $[Ru(NH_3)_5(N_2)]^{2+}$, was discovered in 1965 by Allen and Senoff.[29] The implication of this finding was that perhaps other transition metal complexes could reduce dinitrogen into ammonia and was not limited to molybdenum or iron as the first structures of nitrogenase suggested. Of course a catalytic reduction of dinitrogen under ambient temperature and pressure would be extremely advantageous and would compete with the already well established Haber–Bosch process.

The Haber–Bosch process is the method of directly synthesizing ammonia from hydrogen and nitrogen, developed by the German physical chemist Fritz Haber. He received the Nobel Prize in 1918 for this method, which made the manufacture of ammonia economically feasible. The method was translated into a large-scale process using a catalyst and high-pressure methods by Carl Bosch, an industrial chemist who won a Nobel Prize in 1931 jointly with Friedrich Bergius for high-pressure studies.

$$N_2(g) + 3H_2(g) \rightleftharpoons 2NH_3(g) \quad +92kJ$$

The above equation shows the equilibrium of nitrogen and hydrogen to form ammonia; this is an endothermic reaction due to the stability of dinitrogen. Dinitrogen's stability is rationalized through the fact that it is a simple triply-bonded diatomic molecule that is very difficult to activate by its high ionization potential (15.058 eV), negative electron affinity (-1.8 eV) and high bond-dissociation enthalpy (945 kJ mol^{-1}). This inertness of dinitrogen is not just due to its strong triple bond. Carbon monoxide, which is isoelectronic with dinitrogen and undergoes a wide variety of chemical reactions, has an even greater bond dissociation enthalpy (1076 kJ mol^{-1}) that suggests other factors may be responsible. The orbital energies of

dinitrogen provide the rationale for this inertness. The low-energy HOMO (-15.6 eV) combined with the high energy LUMO (7.3 eV); disfavor electron transfer and Lewis acid–base reactions. At increased temperature to fulfill these high-energy requirements, equilibrium tends to shift towards reactants, although at increased pressure and with constant removal of ammonia, reasonable yields can be achieved. Today, pressures of up to 1000 atm are used, and the temperature is kept at about 500 ^{o}C. The catalyst used is a mixture of iron, potassium oxide, and aluminum oxide. Under these conditions, with the constant removal of the ammonia as it is formed and feeding in fresh supplies of nitrogen and hydrogen, the yields of ammonia can be 40% to 60%.

The Haber–Bosch process now supports some 40% of the world's population through the production of fertilizer for crops and has been one of the major contributors to the huge population increase over the past fifty years as illustrated in Figure 18.[30]

Currently, hundreds of dinitrogen complexes of all transition metals in Groups IV through IX are known. One of the mechanistically most elaborated systems that contained dinitrogen and reduced dinitrogen ligands had been the series of tungsten and molybdenum phosphine complexes studied initially by Chatt[31,32] and Hidai.[33] Chatt believed that dinitrogen could be reduced at a single metal center (either with molybdenum or tungsten) and was the first to show that up to two equivalents of ammonia per metal could be formed from a W(0) dinitrogen complex upon the addition of protons, with the six electrons being provided by tungsten.

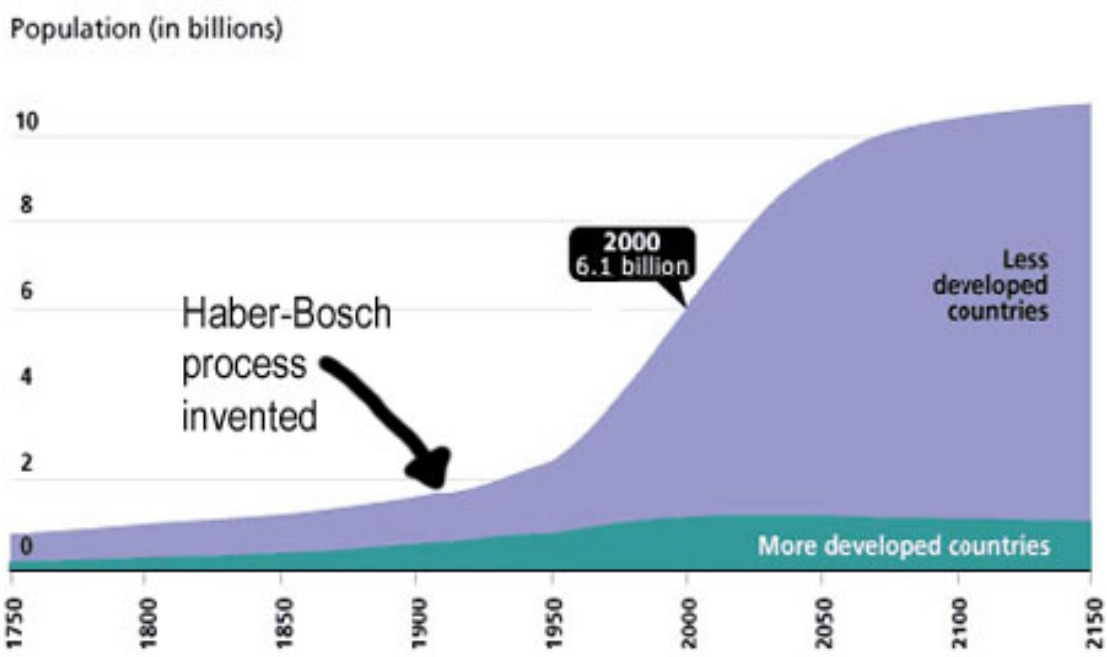

Figure 18: World population from 1750 to present.

If a distinct intermediate is formed after the addition of each proton and electron, then twelve intermediates can be imagined, or a total of fourteen if one includes the dinitrogen complex and a complex derived without any coordinated dinitrogen. This is known as the 'Chatt cycle' and is depicted in Figure 19, where L_x represents a set of ligands (that are not necessarily identical) and vary from compound to compound.

In 2001 Greco and Schrock produced a series of molybdenum complexes that contained the trisamidoamine ligand ($[ArNCH_2CH_2)N]^{3-}$), which is a sterically bulky ligand used to prevent the formation of the stable and unreactive complex of the molybdenum dimer.[34] A year later, Schrock and Yandulov[35] revealed that this molybdenum complex could bind dinitrogen and began replicating many of the steps in the Chatt cycle, which is depicted in Figure 20.

Figure 21 illustrates the replicated intermediates by Schrock at el.[36,37] starting with (HIPTN_3N)MoCl, which was reduced under dinitrogen to form the paramagnetic Mo(N_2) (1), (Figure 20), (2) is the diamagnetic [Mo(N_2)]$^-$, (3) the diamagnetic Mo-N=N-H, (4) the diamagnetic {Mo=B-NH_2}bro (where, Ar$'$ = 3,5-(CF_3)$_2$$C_6H_3$), (5) the diamagnetic Mo≡N, (6); which is also diamagnetic {Mo=NH}{BAr$'_4$}, (7) which is the paramagnetic {Mo(NH_3)} {BAr$'_4$} and (8) Mo(NH_3). Through extensive ^{15}N labeling experiments, NMR studies and X-ray structural analysis by Schrock and Yandulov, they revealed a trigonal pocket in which dinitrogen is reduced into ammonia through each intermediate with the three 2,4,6-*i*-$Pr_3C_6H_2$ rings surrounding and protecting this reactive site. This system's intermediates are analogous to those originally proposed by Chatt et al. in 1978 for the lower oxidation state molybdenum and tungsten phosphine complexes.

Schrock eludes to the importance of ligand protection around the reactive site, believing that it the reason why several of the more unusual species can be prepared.[38]

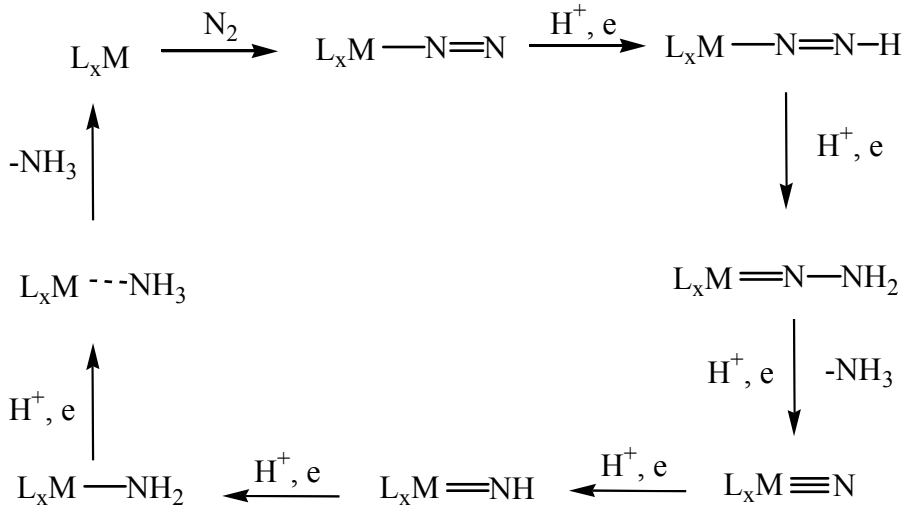

Figure 19: Reduction of dinitrogen at a single metal center via the 'Chatt cycle'.

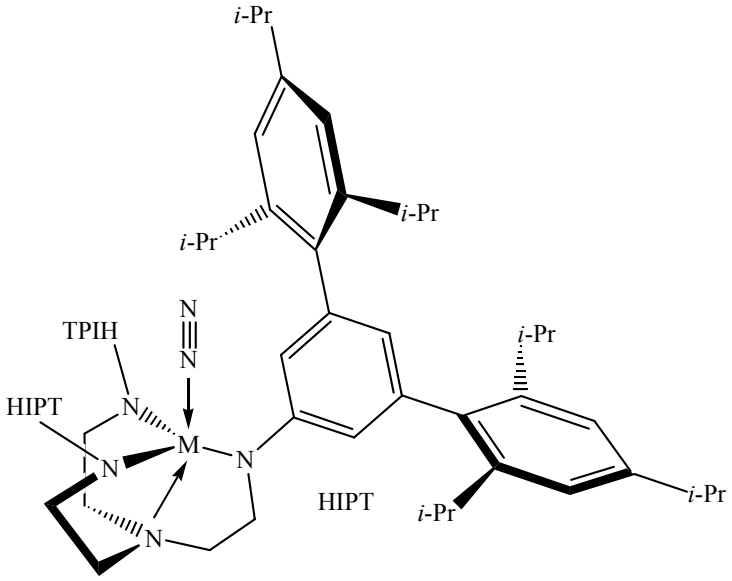

Figure 20: Yandulov and Schrock's [HIPTN$_3$N]Mo(N$_2$) complex.

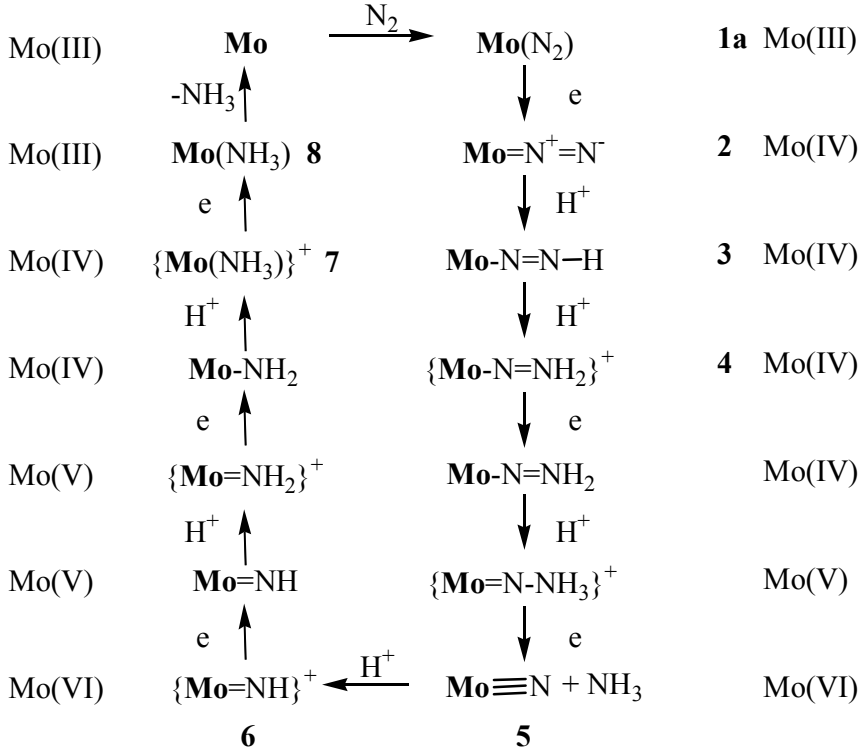

Figure 21: Schrock's proposed intermediates in the reduction of dinitrogen at a [HIPTN$_3$N]Mo center through the stepwise addition of protons and electrons.

It can be concluded that the reduction of dinitrogen at room temperature using Schrock's proposed mechanism is indeed a very difficult catalytic reaction, involving no less than fourteen steps, although the scope of this reaction is not strictly limited to molybdenum and iron metal as used in *vivo*.

1.8 Early Transition Metals in Dinitrogen Reduction.

The very first report of dinitrogen reduction by a Group IV metal was by Vol'pin and Shur in 1966.[39] They produced ammonia though the protonolysis of dinitrogen using a $(C_5H_5)_2TiCl_2$/alkyllithium mixture, although, any mechanistic detail on how this process occurred was unknown, work by Chirik *et al*., however,

reported the molecular structure of a *bis*(dinitrogen)titanocene complex depicted in Figure 22.[40]

In a related system, Chirik describes a side-on bound zirconocene dinitrogen complex that undergoes addition of two equivalents of dihydrogen to furnish a hydrido zirconocene hydrazido complex. This unusual reactivity is explained by the "imido-like" ground state of the zirconocene dinitrogen complex, arising from the overlap of the out-of-plane $1a_1$ molecular orbitals of the zirconocene with the dinitrogen π^* orbitals.[41]

The decomposition of [*i*Pr-NON]Ti(CH_2CHMe)$_2$ in the presence of PMe_3 under dinitrogen affords the bridging dinitrogen complex {[*i*-Pr-NON]Ti(PMe_3)$_2$(μ-N_2)}, which is illustrated in Figure 23. This complex is similar to other titanium dinitrogen complexes, in which the N_2 unit is formally reduced to a hydrazido moiety.[42]

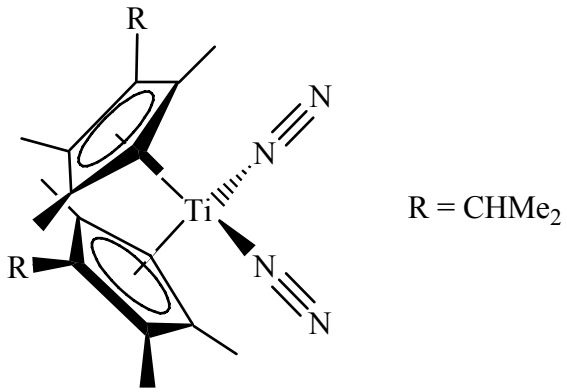

Figure 22: Chirik's titanium sandwich complex.

Figure 24 depicts a similar titanium complex that is supported by guanidinate ligands. The complex is synthesized through reduction of the dichloride precursor, $[(Me_2N)C(N\textit{i}Pr)_2]TiCl_2$, under an atmosphere of dinitrogen. In this case, the N–N bond length and paramagnetism of the complex support the existence of the diazenido unit. The dinitrogen ligand is still somewhat labile and readily reacts with phenyl azide to give a titanium–amido complex. Reaction with pyridine *N*-oxide gives the bridging oxo complex, and propylene sulfide affords the bridging sulfide titanium dimer, all *via* loss of the N_2 moiety.[43]

While all the compounds discussed in this section have shown either side-on or end-on bound dinitrogen, there is a third type of coordination that combines the two and is illustrated in Figure 25. This tantalum complex reacts with dinitrogen without the use of any strong reducing agents. Rather, the electrons from the reductive elimination of dihydrogen and the Ta–Ta bond present provide the reducing power to activate dinitrogen in a unique manner.

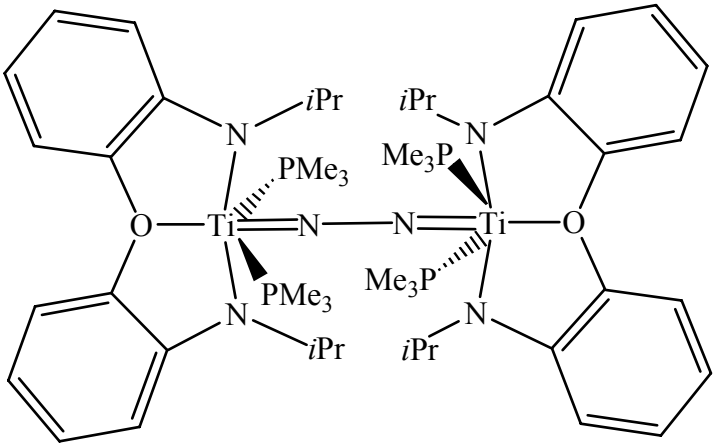

Figure 23: Schrock's NON-titanium dinitrogen complex.

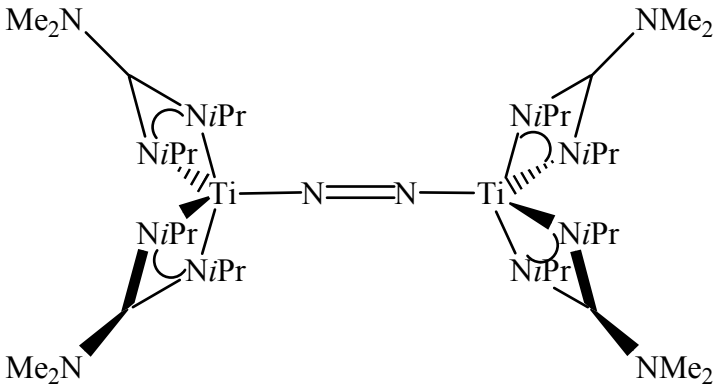

Figure 24: Titanium-diazenido complex synthesized by Arnold et al.

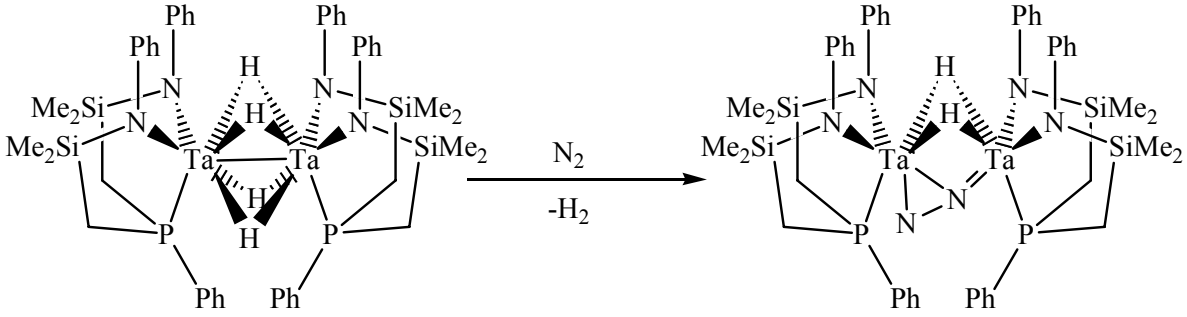

Figure 25: Unique end-on, side-on bound dinitrogen in Fryzuk's tantalum complex.

While end-on binding of dinitrogen is favorable in related Group V systems, it is thought that the bridging hydrides make the asymmetric bonding mode more energetically and sterically favorable. Fryzuk supports this by reacting the bridging nitrogen complex with propene to form the propyl tantalum species $\{[NPN]Ta(CH_2CH_2CH_3)\}_2(\mu\text{-}\eta^1\text{:}\ \eta^1\text{-}N_2)$ with symmetrically end-on bound nitrogen.[44]

With the increasing number of publications in this area, not only does it suggest that dinitrogen activation is clearly undergoing a renaissance, but the reactivities exhibited by transition metal complexes are reaching greater levels of sophistication. The development of a catalytic system that can efficiently reduce dinitrogen into ammonia under mild conditions is the long-standing task facing many chemists. Despite all this exciting progression, there are still few processes whereby the use of dinitrogen as a feedstock is applicable to industrial processes. The preparation of many of these complexes needs the use of strong reducing agents, which are unstable for large-scale production.

Although the use of dinitrogen has not been realized for an industrial feedstock, it is being realized by more and more researchers that dinitrogen could very well be an important synthon in their experiments. The hope is that one day a catalytic cycle in which the use of a dinitrogen feedstock to synthesize a variety of high-value organonitrogen compounds, could finally by accomplished.

2. Synthesis and Reactivity Studies of Arylamido Complexes of Titanium

2.1 Overview

The last decade has seen what some have termed a 'renaissance' in amido–transition metal chemistry. Impetus in the field had waned after the pioneering work of the 1960s and 1970s, and the field has grown dramatically recently. In part, this has been due to a better appreciation of the amido moiety (R_2N) as a ligand. Moreover, it has been due to the dramatic reactivity that amido complexes have been shown to display, especially when the complex is low coordinate and high valent. Perhaps the most important demonstrations have been seen in the reduction of dinitrogen to ammonia by Yandulov and Schrock following on from the splitting of dinitrogen at room temperature by Cummins *et al.* [52] Other examples include the trapping and activation of methane at a Zr center by Wolczanski *et al.* [46] This area has been extensively reviewed recently.[35,36,45-49]

The stabilization or protection of the coordination sphere of high-valent Lewis acidic early transition metals may be achieved by considering several important aspects. Firstly, ligands should be chosen to be non-reactive after installation within the coordination sphere of the metal, thus acting as *spectator* or *ancillary* ligands, while providing the electronic environment to promote the desired reactivity at the metal center. For the systems discussed within this chapter, the utilization of strong σ- and π-donors are required to effectively stabilize titanium due to its Lewis acidity. The very nature of amido systems as "hard" σ- and π-donors allows them to

effectively stabilize d^0 titanium systems, a functionality that was once dominated by the ubiquitous cyclopentadienyl ligand.

Secondly, the ancillary ligands must obviously have significantly different bonding and reactive properties in comparison to the more transiently bound and therefore reactive substrates, so that the ligands do not undergo transformations at reactive sites. Thirdly, the distribution of donor functions over the protected sector of the coordination sphere should be well balanced, leaving room for a catalytic pocket and providing steric protection against unwanted kinetic transformations. This latter point is one of the major advantages of cyclopentadienyl ligand derivatives and is currently being challenged by amido complex chemistry.

2.2 Introduction

Figure 26 depicts the three amido ligand systems that possess a set of structural and electronic properties that are clearly related. dihydrodibenzoazepinyl (**A**) is a hard σ- and π-donor, LX ligand, contributing three electrons to the metal center. It is directly comparable to diphenylamide (**B**) for the electronic contribution from the ligand; however, the phenyl rings are tethered to each other by an ethyl bridge, thus constraining the steric profile of the ligand and providing a more rigid comparison to carbazolyl (**C**). The carbazolyl system structurally should be very similar to **A**; however, it is a non-innocent system, not in the Gray sense,[50] but rather because the L_π orbital on nitrogen can either engage with other ligand orbitals, forming pyrrole-like aromatic interaction, or it can act as a donor to the metal center. This possibility of interaction implies that there may be a strong interaction between the *d*-derived molecular orbitals on the metal center and the ligand orbitals. **A** and **B**

are classic hard amido systems, although (**C**) is predicted to be chemically softer in comparison to the hard amine ligand sets and therefore should mimic some of the softer ligands that are found in nature.

This chapter presents the synthesis and initial reactivity studies of dihydrodibenzoazepinyl titanium complexes, with **d**ihydro**d**ibenzo**a**zepinyl being written as **dda** for brevity. ddaH is commercially available from Sigma–Aldrich; deprotonation is carried out using *tert*-butyllithium at low temperature, producing the lithium salt, ddaLi, in high yields. Synthetic details are presented in the experimental section for this and all other new compounds in this chapter.

ddaLi is extremely air sensitive and will readily undergo oxidation at dioxygen concentrations below 50 ppm, The fine, white powder will discolor to green upon oxidation, further darkening to blue and then charring black with sufficient exposure. Such colorful degradation allows visual checking on the status of stored starting materials. Any discoloration of the dihydrodibenzoazepinyl lithium salt has catastrophic effects to the yields of subsequently synthesized metal complexes.

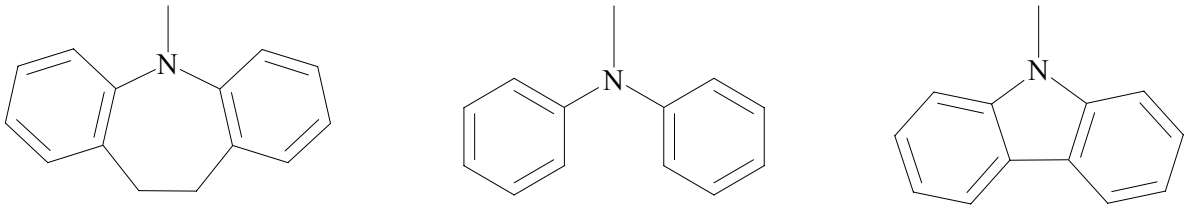

A **B** **C**

Figure 26: A set of three electronically and sterically comparable amido ligands.

2.3 Results and Discussion

2.3.1 Synthesis of $(dda)_3TiCl$ and $(dda)_2TiCl_2$

Treatment of ddaH with *tert*-butyllithium affords ddaLi in good yields (82%), the reaction proceeding smoothly in toluene at room temperature. Although ddaLi shows some solubility in toluene, a small volume of hexanes, when added to the solution, will reduce the solubility of the salt. Filtration yields the pure lithiated salt without any trace of impurities; residual toluene can be removed by washing the salt with hexanes and pentane, filtering and drying under reduced pressure.

Reaction of three molar equivalents of ddaLi with one molar equivalent of $TiCl_4 \cdot 2THF$ affords $(dda)_3TiCl$ (**1**). The metathesis was carried out in toluene and upon addition of the lithium salt to the titanium-containing solution, the color darkens to almost black. As more of the salt is added, the solution starts to become redder in appearance until it is unmistakably blood red. These sequences of color changes may indicate that the metatheses are sequential, in part or in full, albeit very rapid as reaction times do not exceed an hour even at -78 °C. Filtration of the solution from a precipitate, presumed to be lithium chloride, followed by evaporation of the solvent under reduced pressure, yields crude $(dda)_3TiCl$. Recrystallization of the crude product from a toluene/hexane solution at low temperature affords bright orange crystals from the dark solution.

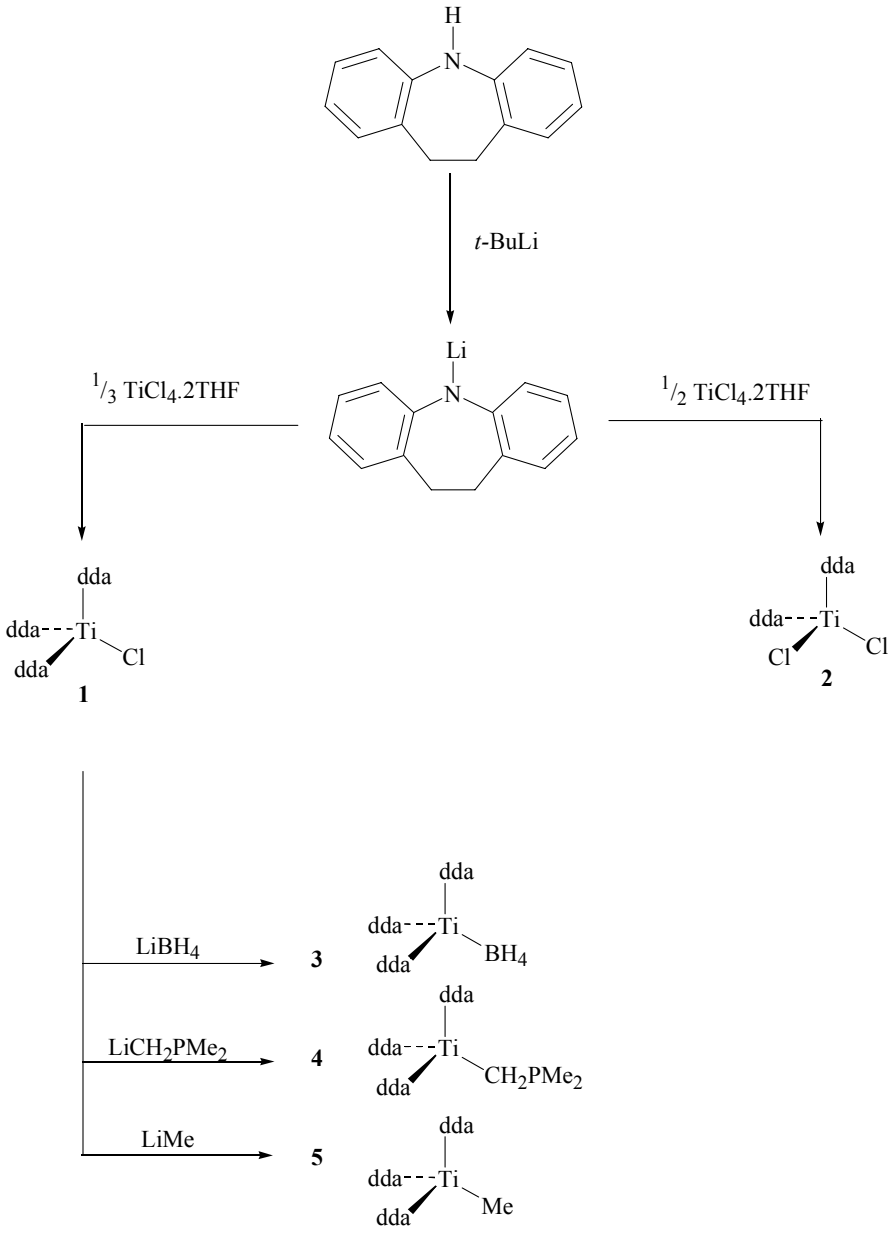

Scheme 3: Reaction scheme for the formation of dihydrodibenzoazepinyl complexes of titanium.

Metathesis reactions in THF resulted in much lower yields. One possible reason for this is that in THF, the efficiency and extent of the amido-chloride substitution is limited, perhaps by saturating the titanium coordination sphere after initial replacement or by forming titanates of the form $[(dda)_{3-x}TiCl_{4-x}(THF)_y]^{(3-x)-}$, ($x$

+ y = 6). Published work from this laboratory has shown that retention of the alkali metal or formation of the metalate anion does occur.[51] The use of diethyl ether was also explored, due to the tedious time span of the removal of such high-boiling-point solvents such as toluene, although the solubility of ddaLi and indeed the product is exceedingly poor in diethyl ether, and consequently, the reaction time is prolonged, which results in very low yields (~20%).

Complex **1** is a fourteen-electron, *pseudo*-tetrahedral complex, assuming all three amido ligands are acting as LX donors. The complex shows reasonable resistance to ligand oxidation and hydrolysis in the solid-state; slow hydrolysis in ambient atmosphere releases ddaH. Formation of $(dda)_2TiCl_2$ **2** proceeded in an analogous manner to that of **1**. Reaction of two molar equivalents of ddaLi with $TiCl_4$·2THF results in metathetical replacement of two chlorides; yields of this compound were particularly low (60%), and the material is highly air and moisture sensitive, readily degrading to a charred black material upon exposure to the air. The absence of a third amido ligand (in comparison to **1**) makes this system far more open and reactive.

2.3.2 Spectroscopic studies of free ddaH

The description of dda systems within this chapter will adhere to the labeling system depicted in Figure 32. ^{1}H and ^{13}C NMR analysis was conducted on the ddaH, and although the system can be assigned, 2D (NOESY, COSY and TOCSY) and variable temperature (VT) experiments were conducted to provide a base comparison to other systems discussed in this chapter. Tables 1 and 2 display the NMR assignment for the free ddaH.

The ^{1}H NMR spectrum for ddaH can be observed in Figure 33, where the sharp singlet at 2.815 ppm relates to the four backbone hydrogens of the molecule. It is this signal that drastically changes once the ligand has been coordinated to the metal center, which provided an excellent handle in the analysis of these systems. In the free ddaH these protons are *pseudo* equivalent in the sense that any energy barriers between axial and equatorial interconversion are low and the rate of interchange between these positions is fast on the NMR timescale.

A VT experiment was carried out upon the ddaH in order to cool the system down so that the rate of interconversion could be observed within the NMR experiment's time frame. The experiment was cooled down as far as 188 K (-90 °C) in d_8-toluene, and no such non-equivalency was observed. The signal of the free ddaH alkyl hydrogens remains a sharp singlet.

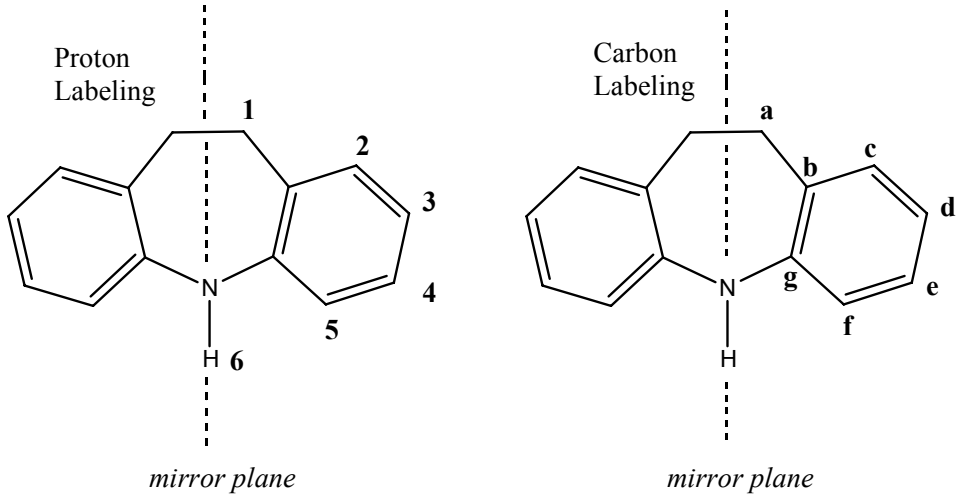

Figure 27: NMR labeling of ddaH and related Ti-dda complexes.

Table 1: ^{1}H NMR resonances for ddaH ran in d_8-toluene, including coupling constants.

Proton label	Signal (ppm)	Multiplicity	Coupling Constants
1	2.815	s	N/A
2	6.863	d	J = 6.9 Hz
3	6.972	d of d	J = 8.1 Hz, J = 7.2 Hz
4	6.698	t	J = 8.1 Hz, J = 7.2 Hz
5	6.253	d	J = 7.2 Hz
6	5.397	s	N/A

Table 2: ^{13}C NMR resonances for ddaH ran in d_8-toluene.

Carbon label	Signal (ppm)
A	35.278
B	142.843
C	118.324
D	119.663
E	126.9
F	130.919
G	128.839

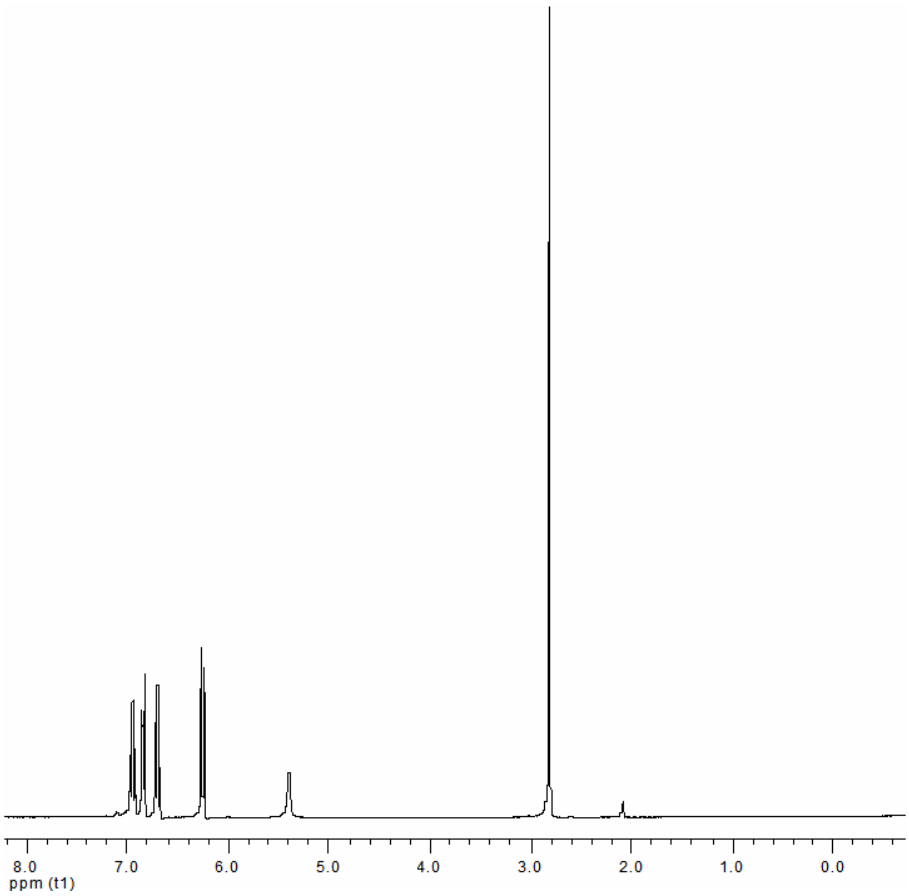

Figure 28: ^{1}H NMR spectrum of ddaH, illustrating equivalent protons at room temperature on the ethyl backbone of the molecule.

2D NMR analysis of the ddaH was conducted in a very concentrated solution of toluene- d_8, although toluene is generally a poor choice of NMR solvent for these types of systems due to the complication of the aromatic regions. However, it is a necessary evil in order to obtain a good temperature range in VT NMR analysis, preparing highly concentrated samples help minimize interpretation impediment due to the solvent. The 2D spectra on this compound are very clear. From the TOCSY experiment; perfect correlations between: H-5 and C-f, H-4 and C-e, H-3 and C-d, H-2 and C-c and H-1 with C-a can be seen. The NOESY experiment displayed in Figure 37 clearly reveals the through-space coupling of the backbone hydrogens to the adjacent aromatic hydrogens. Likewise, coupling from the N-H (**6**) to (**f**) can unambiguously be correlated this key factors allowed ddaH to be easily assigned.

2.3.4 Spectroscopic studies of $(dda)_3TiCl$

The NMR spectroscopy for **1** was carried out in d_8-toluene in an NMR tube fitted with a Young's tap. The d_8-toluene was dried over Na_3K amalgam and was transferred into the sample tube *via* vacuum transfer on a high-vac Schlenk line. Table 37 and 38 reports the ^1H and ^{13}C NMR resonances (respectively) for $(dda)_3TiCl$ as a comparison to the free ddaH.

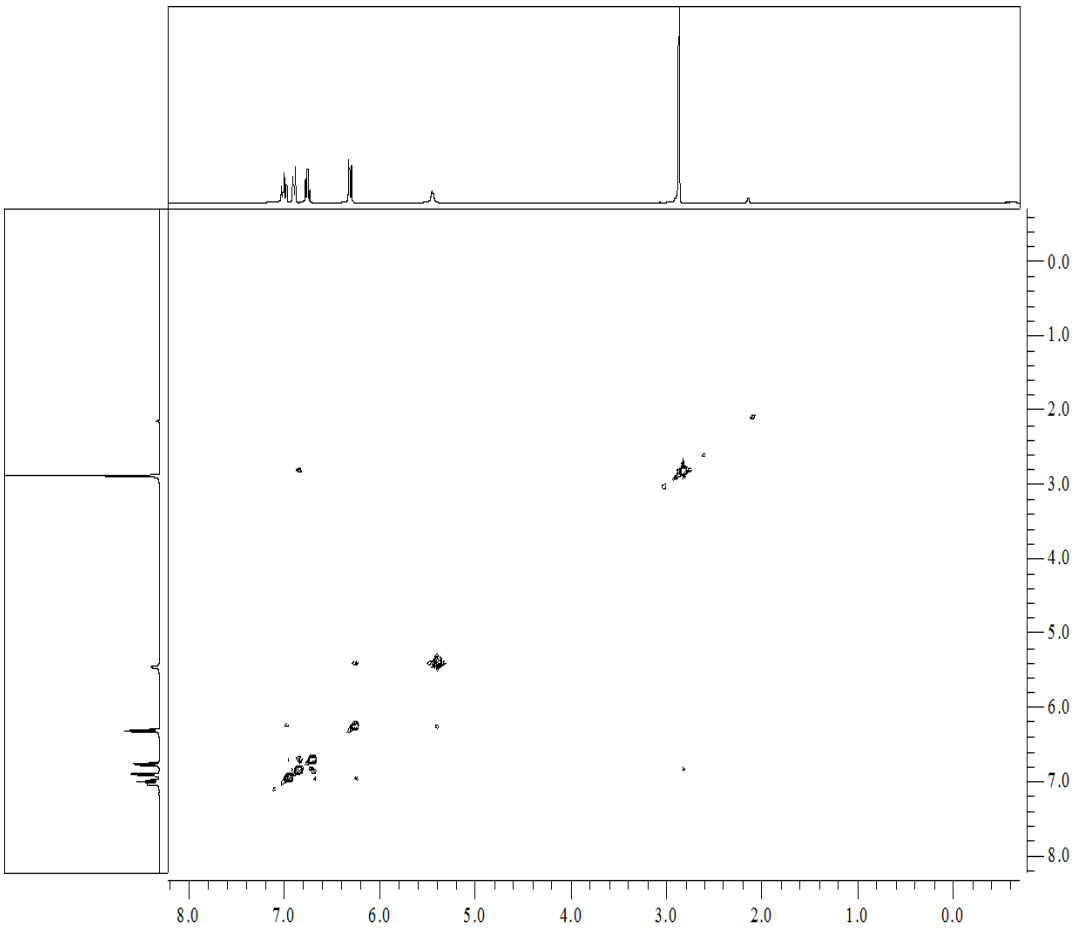

Figure 29: NOESY illustrating through-space coupling specifically between. protons: f to e and a through to b in ddaH.

Table 3: ^{1}H resonances for ddaH compared to $(dda)_3TiCl$.

Proton label	1 Signal (ppm)	ddaH Signal (ppm)	Multiplicity	Coupling Constants
1a	2.266	2.815	s	N/A
1b	2.872	N/A	s	
2	6.727	6.863	d of d	J = 4.5 Hz, J = 5.7 Hz
3	6.812	6.972	m	N/A
4	6.812	6.698	m	N/A
5	7.305	6.253	d of d	J = 4.2 Hz, J = 4.8 Hz
6	N/A	5.397	s	N/A

Table 4: ^{13}C resonances for ddaH compared to $(dda)_3TiCl$.

ddaH (ppm)	Complex 1 (ppm)	Carbon label
35.278	31.547	a
142.843	151.04	b
118.324	125.981	c
119.663	126.227	d
126.9	126.734	e
130.919	130.543	f
128.839	132.743	g

^{1}H NMR spectroscopic analysis of **1** shows marked differences from ddaH. The most obvious difference is the resonance of the backbone hydrogens. This is due to the lowering of symmetry in the system as well as a change in the energetics of fluxionality, due to hindered rotation about the M–N bond (making axial and equatorial protons non-equivalent and therefore two distinct signals).

The aromatic region of the ddaH shows a distinctive ^{1}H shift once it has been deprotonated and coordinated to the titanium center. Figure 30 shows the ^{1}H NMR spectrum for **1**. From this comparison we can observe a shift towards low field by 0.5 ppm by the *ortho* aromatic protons of the coordinated dda. This can be rationalized through an inductive effect, via the σ-donation of electron density from the nitrogen to the metal center. Complex **1** has a more disordered spectrum due to the overlapping of two aromatic proton signals.

At ambient temperatures the hydrogens can be observed undergoing interconversion between axial and equatorial positions in the NMR timescale. This "rocking" effect is illustrated in Figure 34 *via* a Newman projection. Although as the temperature is increased above 310 K, the two signals become broader until the coalescence temperature is reached at 330 K (Figure 35); thereafter the signal becomes increasingly sharp. This sharpness that was observed at all temperatures in the free ddaH system is due to the system gaining more energy, which allows backbone hydrogens to interchange between axial and equatorial positions too quickly on the NMR timescale.

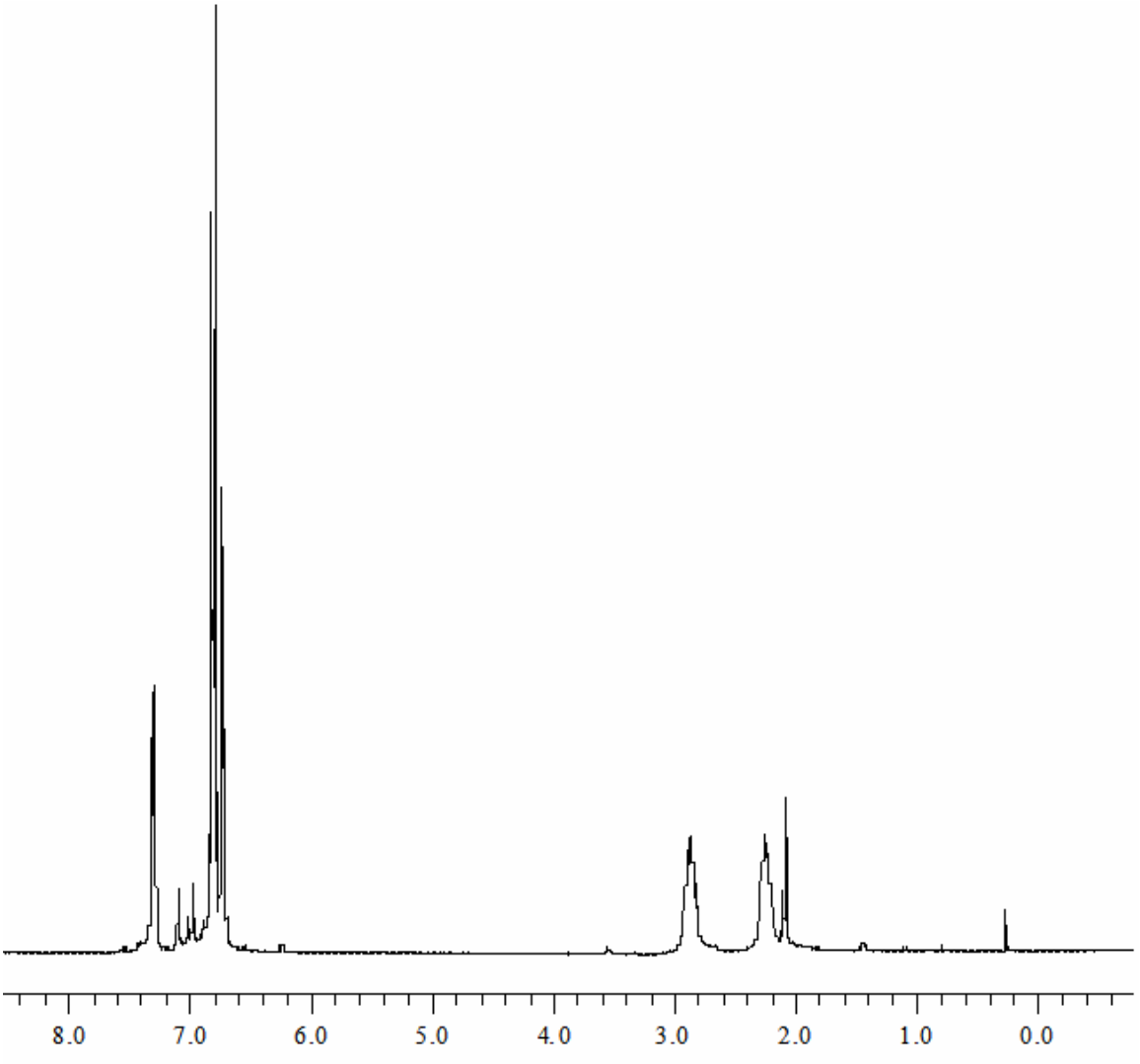

*Figure 30: The ^{1}H NMR spectrum for **1**, you can clearly see the non-equivalent hydrogens between 2.0 and 3.0 ppm.*

A low-temperature experiment was conducted and can be seen in Figure 36. This experiment alludes to a second process that is revealed at low temperature. The integration of the protons on the backbone change from 6H: 6H at 298 K to 1H: 1H: 4H: 6H at 208 K. This infers that the C_3 rotational symmetry of the molecule has been broken. This can be explained by the shortening of one of the Ti-amido ligand bonds, although this contradicts the solid-state structure of the molecule that describes them as being equal. Figure 37 illustrates the view down the C_3 axis of the molecule, assuming that two of the bond lengths are longer than the other.

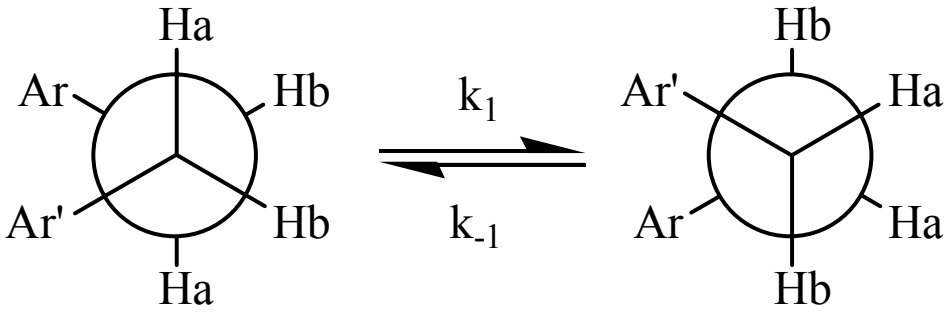

Figure 31: The 'rocking' of the backbone hydrogens which showing non-equivalency.

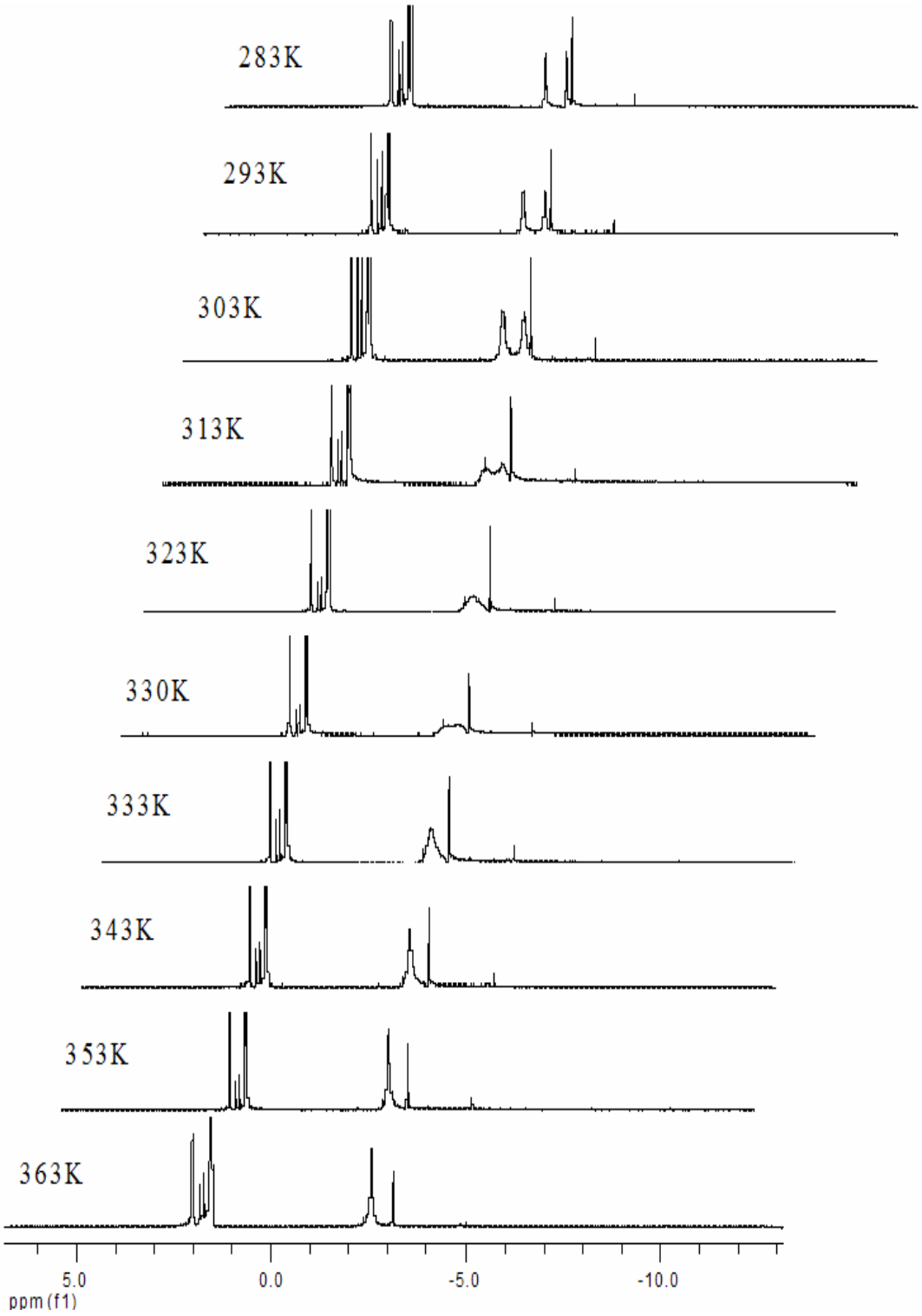

Figure 32: VT NMR depicting the coalescence temperature of $Ti(dda)_3Cl$.

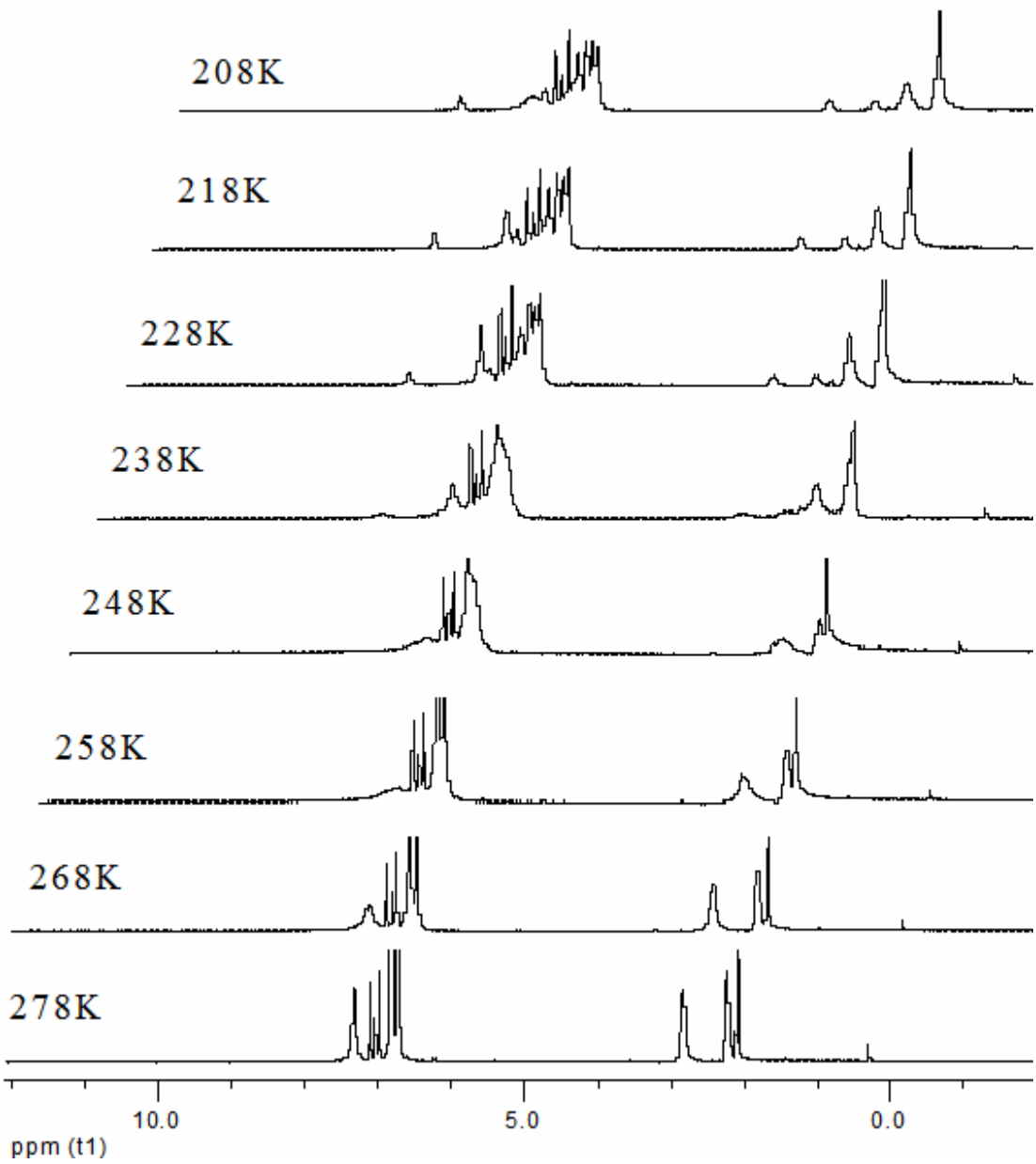

Figure 33: Low temperature VT NMR of $Ti(dda)_3Cl$.

Hb' is the equatorial proton that points in towards the titanium center, while Hb is the axial proton that points away. Ha is the axial proton that points along the axis and out of the page, while Ha' is the axial proton that points down and away from the titanium. This would give a splitting of 1:1:2:2:3:3 considering all Ha and Hb to

be equivalent as they are nearly in the same environment. The protons closest to the titanium are the ones that would have the biggest shift; therefore, protons Hb' (short bond) will have the greatest shift, which I propose to be the proton at lowest field (3.557 ppm), and the Ha (short bond) therefore to be the other resonance at 2.955ppm. The corresponding protons of the longer bonds at this temperature, overlap, although given a lower temperature, I believe this broad singlet, too, would spit into two distinct signals. I predict the same with the Ha and Hb protons. They currently show an integration of 6, although I expect them to split into two signals should this be run at a lower temperature. Although at this temperature in toluene we already are seeing some dissolution.

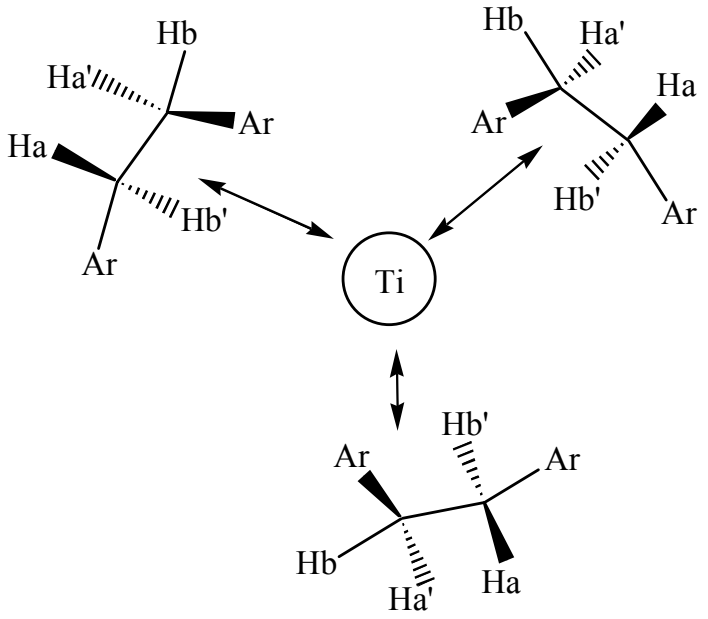

Figure 34: Showing the ethyl protons of the Ti(dda)$_3$Cl looking down the C_3 rotational axis through the Ti to Cl bond.

*2*D NMR analysis of **1** revealed some differences to the free ddaH. The most major was through the NOESY experiment on each species, the spectrum of which can be seen in Figure 38. NOESY revealed through-space correlation between the high-field protons of the aromatic region and the N–H, which corresponded to the ortho aromatic hydrogens being closest to the amine. Although in **1** the aromatic protons that were of highest field were those of the adjacent to the ethyl backbone. This signifies a shift of 1.2 ppm downfield for the ortho protons to the titanium–nitrogen bond, which can be explained via a σ-effect donating electron density of the ring system to the titanium.

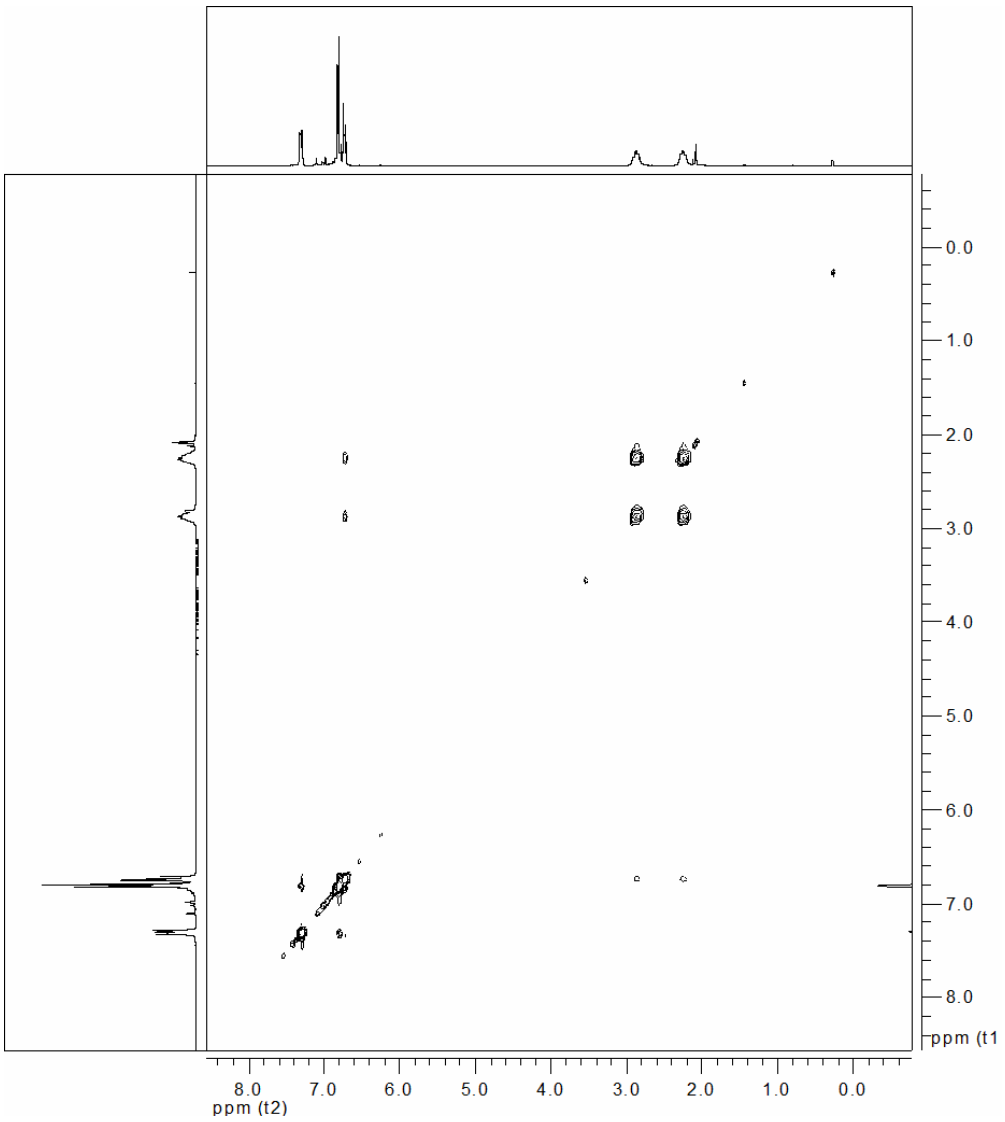

*Figure 35: NOESY spectrum of **1**, clearly showing the correlation between aromatic protons and the alkyl region.*

2.3.5 Spectroscopic studies of $(dda)_2TiCl_2$

This compound has a *pseudo* C_2 rotational axis. This, coupled with the loss of the steric constraint between the ring systems, causes the NMR of this species to show a more fluxional proton resonance for the backbone hydrogens. Assuming each amido ligand to be considered as an LX type ligand, this is a 12-electron system and

would be predicted to be more reactive than **1**. The ^{1}H NMR assignment for this species is given in Table 5 with a comparison to the ddaH starting material. There is a significant shift downfield for all protons which would indicate that the hydrogens of the bound dda moiety are more deshielded. Figure 36 depicts the VT NMR experiment carried out upon **2**, which reveal backbone hydrogens upon the ligand in this system to be a broad singlet at room temperature. This singlet at 2.99 ppm in THF-d_8 confirms that the alkyl hydrogens in this system are indeed less restricted than in the case of compound **1**. As the temperature is reduced, a coalescence temperature was observed at 258 K, where the alkyl hydrogen singlet separates into two distinct signals, clearly represented at the lowest recorded temperature. This low-temperature spectrum is similar to the room temperature spectrum of compound **1**.

Table 5: ^{1}H NMR resonances for ddaH compared to $(dda)_2TiCl_2$.

Proton label	2 Signal (ppm)	ddaH Signal (ppm)	Multiplicity	Coupling Constants
1	2.986	2.815	S	N/A
2	7.422	6.863	D	J = 6.0 Hz
3	7.149	6.972	M	N/A
4	7.045	6.698	M	N/A
5	7.045	6.253	M	N/A
6	N/A	5.397	S	N/A

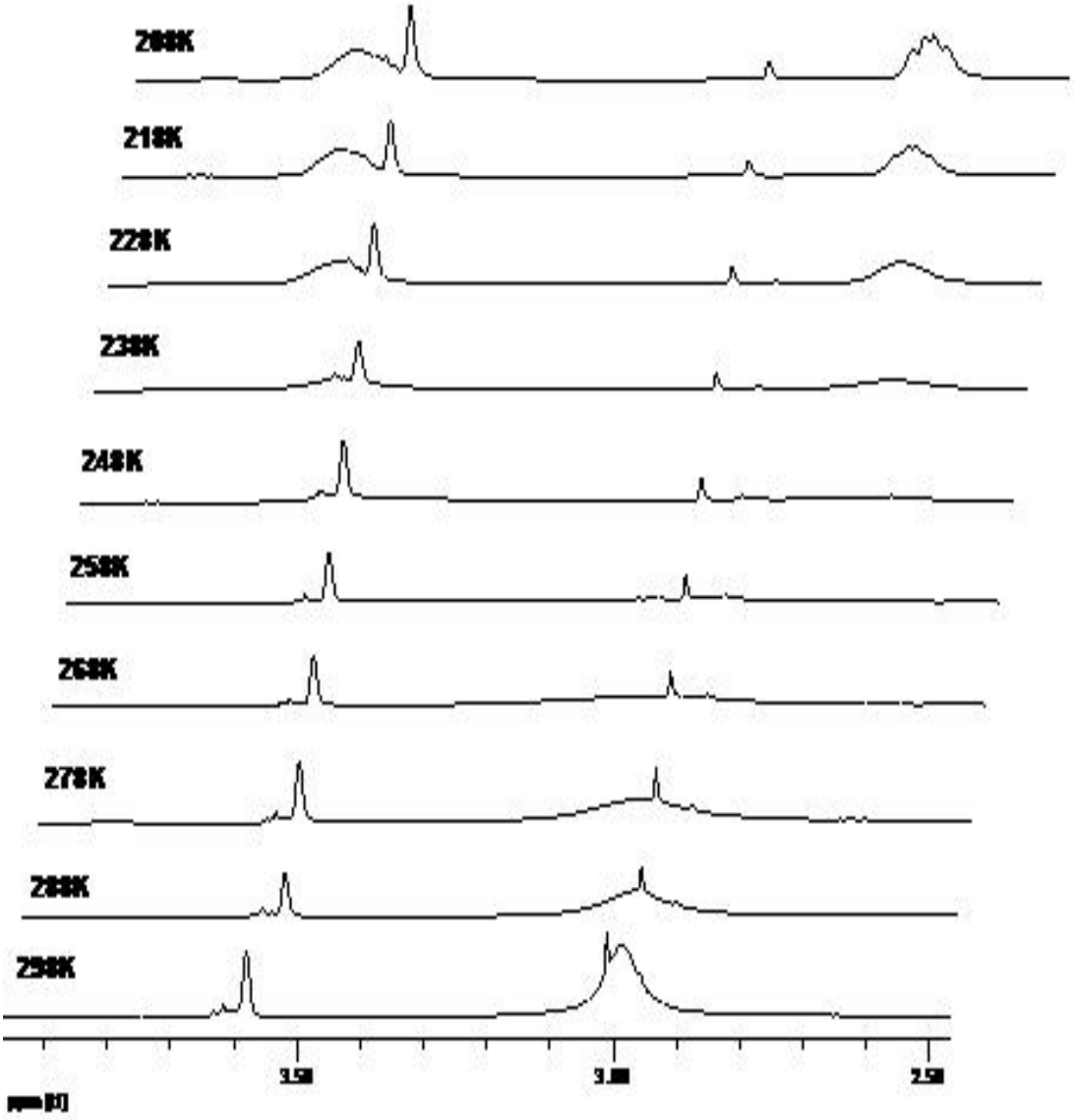

Figure 36: VT NMR expanding on the backbone hydrogens of complex **2**.

2.3.6 Solid-state and molecular structure of $(dda)_3TiCl$

X-Ray quality crystals of **1** were grown from a toluene solution layered with hexanes which was cooled to -78 ºC. Crystals were observed growing at the interface around the sides of the recrystallization vessel, and they were subsequently filtered, dried under reduced pressure, and isolated. The crystals were then placed on a microscope slide within the glove box and covered with Paratone oil to protect them during the crystal mounting process. They were then carefully mounted upon a cryoloop and centered in the beam. After the collection, the data reduction and spherical atom analyses were carried out using Saint. A multi-scan absorption correction was made using SADABS. The spherical atom structures were solved by direct methods (SHELXTL), refined by the full-matrix least squares method and completed by a series of difference Fourier syntheses. All non-hydrogen atoms were refined anisotropically, with hydrogen atoms being introduced at idealized positions and refined using a riding model. Crystal mounting, data collection and structure solution were performed by Dr. C. L. Nygren.

2.3.6.1 Solid-state structure of $(dda)_3TiCl$

Salient structural parameters for $(dda)_3TiCl$ are given in table 6.

Table 6: Lattice parameters for the crystal structure of $(dda)_3TiCl$.

a		9.745(2) Å	
b		18.377(5) Å	
c		18.487(5 Å	
Space group: $P2_12_12_1$	□ = □ = □ = 90º	V_{cell} = 3310.8(14) Å^3	*Z* = 4

$(dda)_3TiCl$ crystallizes in the space group $P2_12_12_1$ (No. 19). The asymmetric unit contains the entire molecule, and there is no imposed crystallographic symmetry. Given that $Z = 4$, the structure is complex; the best visualization is given in Figure 37a, which depicts the unit cell for **1** in the solid-state, viewing the *bc* plane; Figure 37b and 37c show two views of the molecular structure, emphasizing the C_3 axis present in the molecule in 37b. Intermolecular contacts between molecules in the lattice divide into two types. In the lower hemisphere of the molecule, which contains the ethyl groups of dda ligand, the ethyl hydrogens are in close contacts with the aromatic carbon atoms of the neighboring molecules, presumably acting as weak acceptors. The upper hemisphere, containing the Cl atom and the upper aromatic dda rings, form weak donor interactions with the ethyl groups of the nearest neighbor. Surprisingly, there are few multipole interactions between the aromatic rings, which may be due to the curvature of the ligated dda moiety presenting steric interactions that overwhelm the possible multipole interactions. The range of Ti–Ti vector lengths span 10.77–22.21 Å, and so dipolar interactions between the Ti–Cl vectors are unlikely to play a major role in the lattice, given that the dipole–dipole interaction scales with r^{-6}.

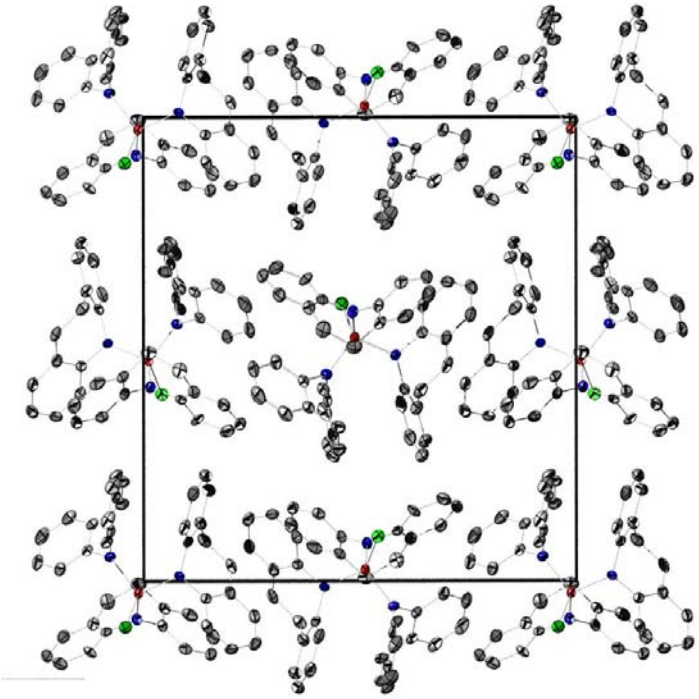

(a)

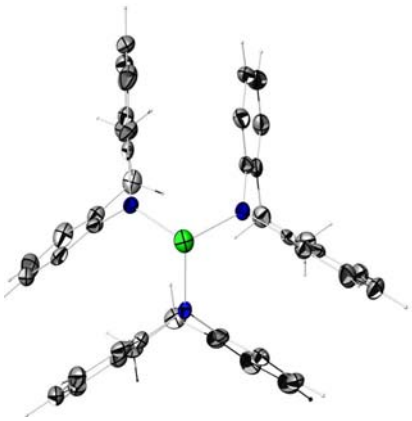

(b)

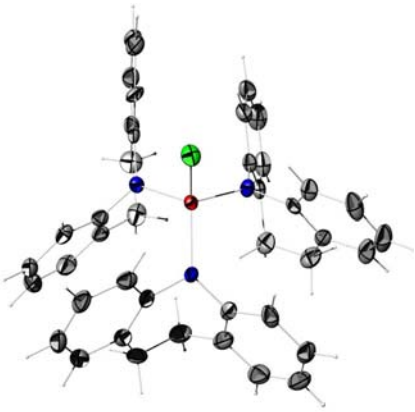

(c)

Figure 37: The crystal and molecular structure of $(dda)_3TiCl$: (a) The bc plane of the unit cell of $(dda)_3TiCl$ (b) The molecular structure of $(dda)_3TiCl$, emphasizing the C_3 axis (c) A general view of $(dda)_3TiCl$.

2.3.6.2 Molecular structure of $(dda)_3TiCl$

$(dda)_3TiCl$ is a *pseudo*-tetrahedral molecule with C_3 symmetry. The titanium center is four coordinate and is ligated by the three dda fragments and the single chlorine atom. Important molecular bond lengths and angles are collected in Tables 7 and 8.

Table 7: Important bond lengths in $(dda)_3TiCl$.

Atom vector		r_{iJ} / Å	$\Delta r = r_{ij} - r_{av}$ / Å
i	*J*		
Ti1	N1	1.896(4)	-0.005
	N2	1.893(4)	-0.008
	N3	1.914(4)	0.013
	Cl1	2.3022(15)	-
N1	C1	1.449(6)	0.0045
	C14	1.439(6)	-0.0055
N2	C28	1.428(6)	-0.0165
	C15	1.450(6)	0.0055
N3	C42	1.440(6)	-0.0045
	C29	1.461(7)	0.0165

Table 8: Important bond angles in $(dda)_3TiCl$.

Interatomic angle			θ_{ijk} / °	$\Delta\theta = \theta_{ijk} - \theta_{Tet}$ / °
i	*J*	*k*		
N1		N2	107.61(17)	-1.86
N1		N3	110.53(18)	1.06
N2	Ti1	N3	111.38(18)	1.91
N1		Cl1	109.29(13)	-0.18
N2		Cl1	108.33(12)	-1.14
N3		Cl1	109.63(13)	0.16
Interatomic angle			θ_{ijk} / °	$\sum\theta_{ijk}$ / °
i	*J*	*k*		
C42		C29	114.7(4)	
C42	N3	Ti1	126.5(3)	359.8
C29		Ti1	118.6(3)	
C1		C14	113.8(4)	
C1	N1	Ti1	119.3(3)	359.9
C14		Ti1	126.8(3)	
C28		C15	113.3(4)	
C28	N2	Ti1	128.1(3)	359.8
C15		Ti1	118.4(3)	

A search of the CCSD reveals that Ti–NR_2 bond lengths in four-coordinate Ti systems typically lie in the range 1.83–-2.05 Å, albeit with a very asymmetric distribution, the mean for which lies at 1.916 Å. In this respect, the Ti–N bond lengths in $(dda)_3TiCl$ are unexceptional. The variation in the bond lengths from the average Ti–N bond length in $(dda)_3TiCl$ is also sufficiently small that no firm

conclusions with respect to the electronic structure can be made from these data. A similar review of Ti–Cl bond lengths shows that a range of 2.16–2.37 Å encompasses all crystallographically characterized four coordinate Ti–Cl bonds, with a mean at 2.226 Å; again, the observed length for this bond in $(dda)_3TiCl$ is unexceptional. Table 4 shows that the N–Ti–Cl bond angles are almost perfectly tetrahedral, with the tetrahedral angle being given as $\theta_{\mathrm{Tet}} = 109.47^{\circ}$. The N_i–Ti–N_J deviate more strongly, but the sum of the deviations from the tetrahedral angle is very nearly zero $\sum \Delta\theta = \sum \theta_{ijk} - \theta_{Tet} = -0.05^{\circ}$, showing that there is very little angular deviation from *pseudo*-tetrahedral geometry at the Ti center.

The bond lengths and angles at nitrogen show that there is little difference between the N–C bond lengths and that the N atoms are essentially planar, which is consistent with the involvement of the L_{π} function on the N atom in the bonding of the complex. Figure 38 shows the relationship between the average bond length and angles for $(dda)_3TiCl$ in relation to other crystallographically characterized four-coordinate X–Ti–NR_2 complexes.

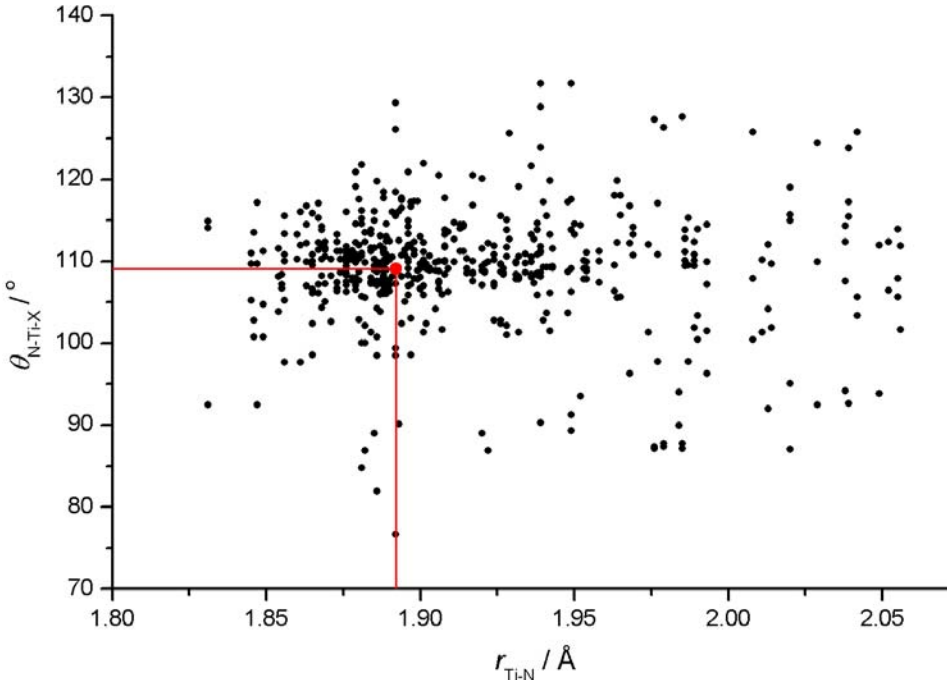

Figure 38: The relationship between the N–Ti–X angle and the Ti–N bond length in $(dda)_3TiCl$ in comparison to other crystallographically characterized four coordinate e X–Ti–NR_2 complexes.

The molecular structure of $(dda)_3TiCl$ displays some very interesting features that contrast with the structures of other arylamido systems, particularly the molybdenum *tris*anilides of Cummins *et al.*[52] These species, which were first used to cleave dinitrogen at sub-ambient temperature, are well known to present a specifically engineered reactive pocket, occupied by Cl in the precursor complex $((3,5,\text{-}Me_2Ph)(t\text{-}Bu)N)_3MoCl$. A comparison of the effects of 'secondary interactions' in the coordination sphere in both $((3,5,\text{-}Me_2Ph)(t\text{-}Bu)N)_3MoCl$ and $(dda)_3TiCl$ are shown in Figure 39.

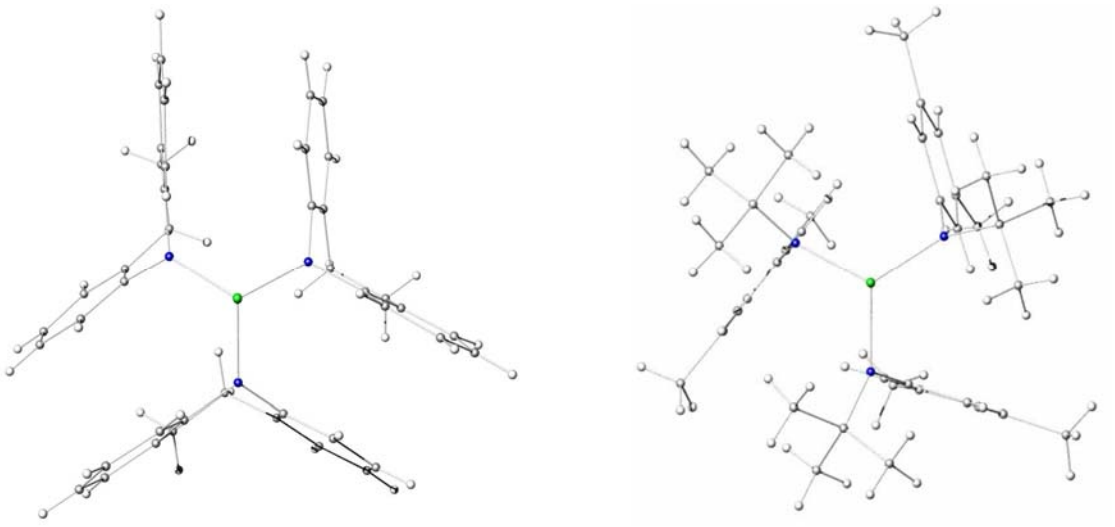

(a) (b)

Figure 39: A comparison of $(dda)_3TiCl$ (a) and $((3,5,\text{-}Me_2Ph)(t\text{-}Bu)N)_3MoCl$ (b) with views along the molecular C_3 axis, containing the M–Cl bond.

Figure 39(a) amplifies the structure of the structure around the upper hemisphere of $(dda)_3TiCl$. The tetrahedron represents the N_3Cl coordination sphere around the Ti atom, which is not shown. Although the coordination spheres for both systems are qualitatively similar, the torsion between the $N–C_{Ar}–M–Cl$ vectors is significantly different; the value for $(dda)_3TiCl$ being $\tau_{\text{N-C}_{Ar}-\text{M-Cl}}(\text{Ti}) = -114.5^{\circ}$, whereas for $((3,5,\text{-}Me_2Ph)(t\text{-}Bu)N)_3MoCl$, , $\tau_{\text{N-C}_{Ar}-\text{M-Cl}}(\text{Mo}) = -142.03^{\circ}$.

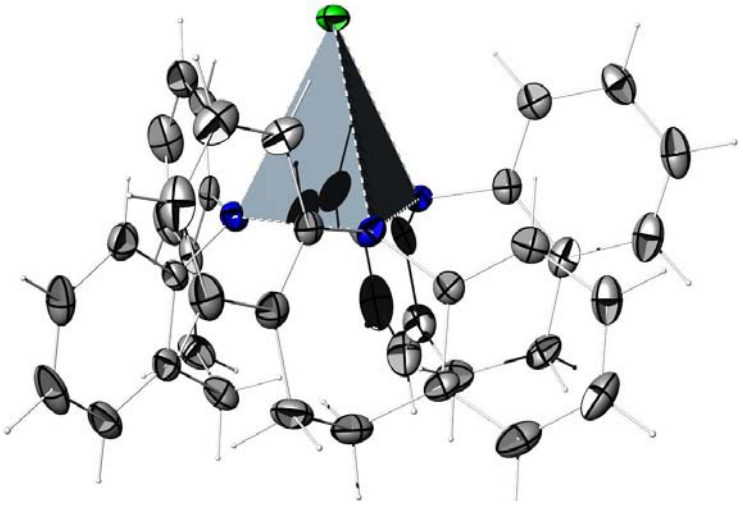

(a)

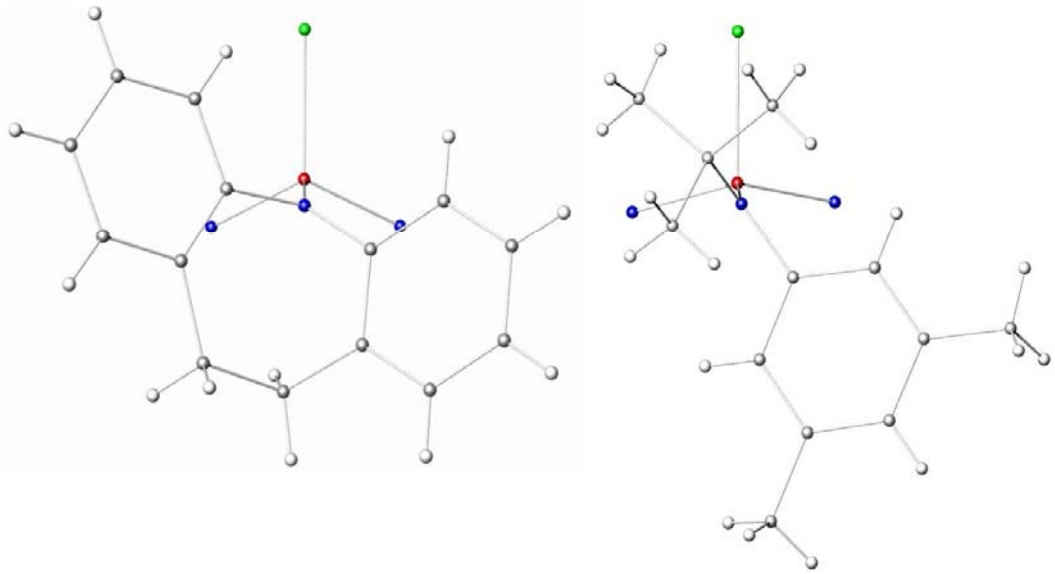

(b)

Figure 40: (a) The structure of the reactive pocket in $(dda)_3TiCl$; the tetrahedron represents the N_3Cl centered on the Ti atom. (b) A comparison of the torsion angles between the N–CAr–M–Cl vector in $(dda)_3TiCl$ and $((3,5,\text{-}Me_2Ph)(t\text{-}Bu)N)_3MoCl$.

2.3.7 Solid-state and molecular structure of $(dda)_2TiCl_2$

2.3.7.1 Solid-state structure of $(dda)_2TiCl_2$

Salient structural parameters for $(dda)_2TiCl_2$ are given in Table 9. $(dda)_2TiCl_2$ crystallizes in the space group $P2_12_12_1$ (No. 19). The asymmetric unit contains the entire molecule, and there is no imposed crystallographic symmetry on the molecule. The crystal structure is shown in Figure 41.

The structure of $(dda)_2TiCl_2$ is less ordered than that of $(dda)_3TiCl$, but contains four molecular units. The less efficient packing of the molecules results in a lower crystallographic density; the density of $(dda)_3TiCl$ is $\rho_{crystal}\left((dda)_3TiCl\right) = 1.682\ g\ cm^{-3}$, whereas that for $(dda)_2TiCl_2$ is $\rho_{crsytal}\left((dda)_2TiCl_2\right) = 1.403\ g\ cm^{-3}$.

Intermolecular contacts in the structure are again confined to two types: a $C_{aryl}–H_{Ethyl}$ interaction, in which the H atom is acting presumably as a weak acceptor and a $Cl–H_{Aryl}$ interaction, in which it is assumed that the H atom is acting similarly. The two Cl atoms participate close contacts with two other molecules, whereas the $C_{aryl}–H_{Ethyl}$ interaction is strictly on a pairwise intermolecular basis.

Table 9: Lattice parameters for the crystal structure of $(dda)_3TiCl$.

a		7.791(3) Å	
b		16.695(6) Å	
c		18.458(6) Å	
Space group: $P2_12_12_1$	□ = □ = □ = 90º	V_{cell} = 2401.0(14) Å^3	*Z* = 4

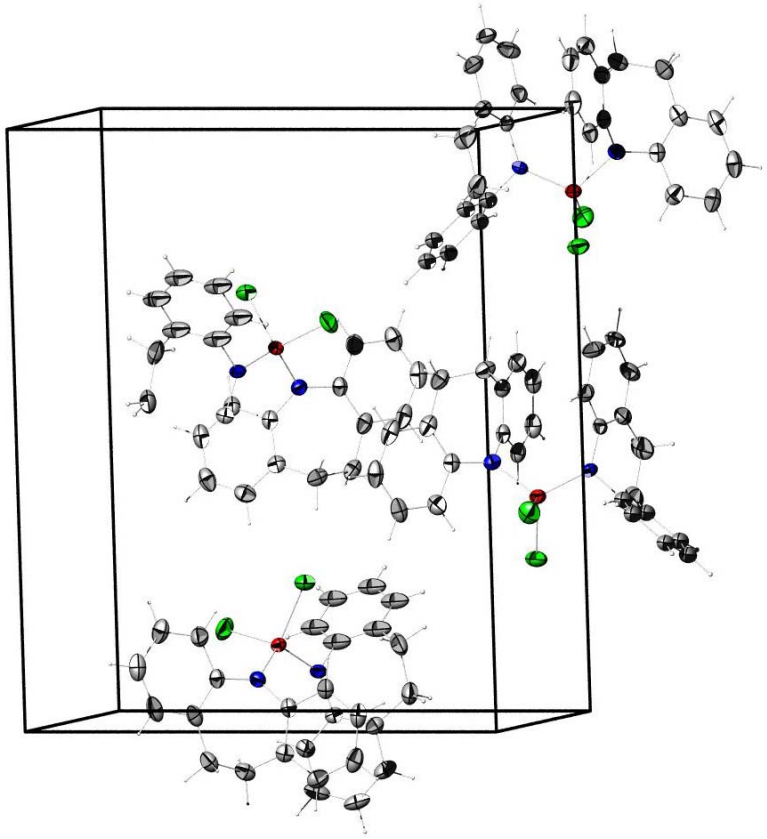

Figure 41: The molecular structure of $(dda)_2TiCl_2$*:*

Given the lack of symmetry of the molecule, the directionality of these interactions is much more dispersed than in the more ordered crystal structure of $(dda)_3TiCl$, and there is no suggestion of any other interaction that acts as a structure director.

2.3.7.2 Molecular structure of $(dda)_2TiCl_2$

$(dda)_2TiCl_2$ is a *pseudo*-tetrahedral molecule with no overall symmetry, though an approximate C_2 axis is present. The titanium center is four coordinate and is ligated by the two dda fragments and two chlorine atoms. Important molecular bond lengths and angles are collected in Tables 2 and 3. Figure 39 show two views of the molecular structure. The crystallographic mean of Ti–NR_2 bond lengths in four-coordinate Ti systems is 1.916 Å, with an asymmetric distribution over the range 1.83 -2.05 Å; in comparison, the Ti–N bond lengths in $(dda)_2TiCl_2$ are shorter than the average, but do not lie outside the range. The average bond length in $(dda)_2TiCl_2$, $r_{av}^{\text{Ti-N}}\left(\left(\text{dda}\right)_2\text{TiCl}_2\right) = 1.879\,\text{Å}$, is shorter than the average in $(dda)_3TiCl$, for which $r_{av}^{\text{Ti-N}}\left(\left(\text{dda}\right)_3\text{TiCl}\right) = 1.901\,\text{Å}$. Similarly, the Ti–Cl bond length in $(dda)_3TiCl$, $r^{\text{Ti-Cl}}\left(\left(\text{dda}\right)_3\text{TiCl}\right) = 2.302\,\text{Å}$, exceeds the average Ti–Cl bond length in $(dda)_2TiCl_2$, for which $r_{av}^{\text{Ti-Cl}}\left(\left(\text{dda}\right)_2\text{TiCl}_s\right) = 2.253\,\text{Å}$. Given that $(dda)_2TiCl_2$ is formally a 12-electron system, counting each amide as LX, then the decreased formal electron density at the Ti center may force a shorter bond length in the complex overall. Although the interligand angles show a wide variation in magnitude, the average angle subtended by the ligands at the Ti center is equal to the tetrahedral angle within the e.s.d's of the measurement. The sum of the angles subtended at the nitrogen atoms is 360°, which is structurally consistent with the LX assignment.

Figure 43 shows the placement of the average structural parameters with respect to other four-coordinate titanium amido species. Although the change in angular parameter is small, the change in Ti–N bond length is very clear.

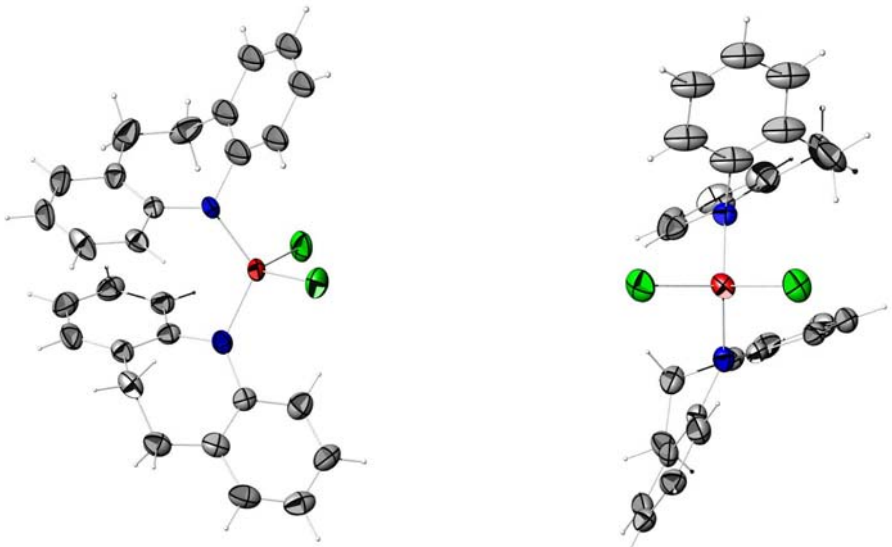

(b) (c)

Figure 42: The crystal and molecular structure of (dda)2TiCl2: (a) The general molecular structure of (dda)2TiCl2 (b) A view of the molecular structure emphasizing the pseudo C2 axis.

Table 10: Important bond angles in $(dda)_2TiCl_2$.

Atom vector		r_{iJ} / Å	$\Delta r = r_{ij} - r_{av}$ / Å
i	*J*		
Ti	N1	1.875(3)	-0.0035
	N2	1.882(3)	-0.0035
	Cl1	2.2425(15)	-0.0109
	Cl2	2.2643(14)	0.0109
N1	C1	1.413(5)	-0.016
	C10	1.443(5)	0.014
N2	C15	1.429(5)	0
	C28	1.432(6)	0.003

Table 11: Important bond angles in $(dda)_2TiCl_2$

Interatomic angle			θ_{ijk} / °	$\Delta\theta = \theta_{ijk} - \theta_{Tet}$ / °
i	*J*	*k*		
N1		N2	116.45(14)	6.98
N1		Cl1	108.68(11)	-0.79
N1	Ti	Cl2	105.44(11)	-4.03
N2		Cl1	109.31(11)	-0.16
N2		Cl2	107.06(12)	-2.41
Cl1		Cl2	109.71(6)	0.24
Interatomic angle			θ_{ijk} / °	$\sum\theta_{ijk}$ / °
i	*J*	*k*		
C1		C10	122.5(3)	
C1	N1	Ti	109.4(3)	360
C10		Ti	128.1(3)	
C15		C28	116.6(3)	
C15	N2	Ti	129.7(3)	360
C28		Ti	113.7(3)	

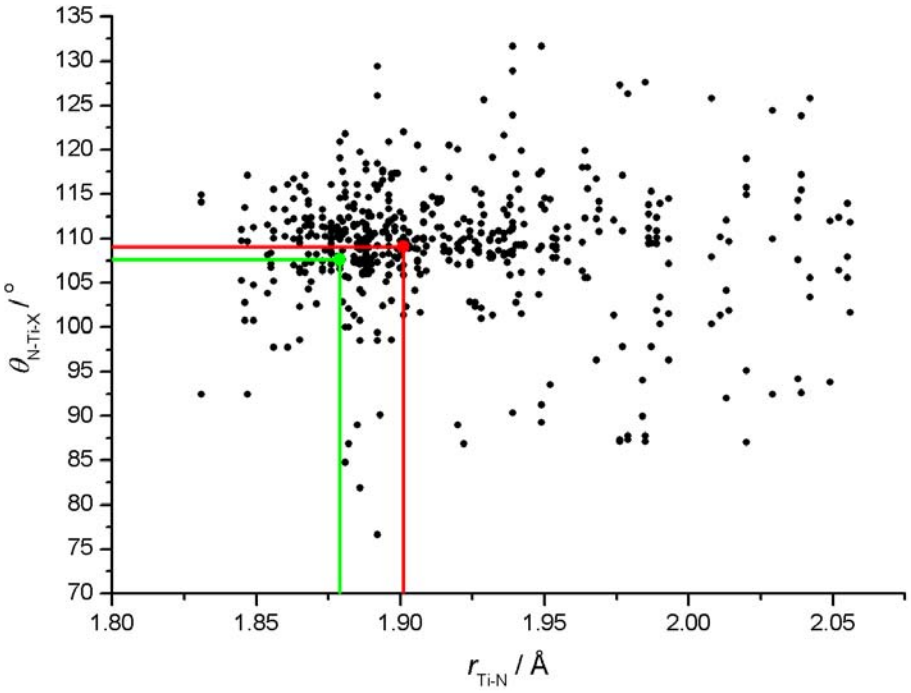

Figure 43: The relationship between the N–Ti–X angle and the Ti–N bond length in $(dda)_2TiCl_2$ (green point) in comparison to $(dda)_3TiCl$ (red point) and other crystallographically characterized four coordinate X–Ti–NR_2 complexes.

2.3.8 Metathetical reactivity of $(dda)_3TiCl$ and $(dda)_2TiCl_2$

Successful preparation of $(dda)_3TiCl$ and $(dda)_2TiCl_2$ provided an entrance into further elaboration of the coordination sphere with overall synthetic targets including $[(dda)_xTiH_y]$, $[(dda)_xTiR_y]$ (R = hydrocarbyl) and $[(dda)_xTiNX_y]$; the last species is a generic formulation for species on the Chatt cycle for the reduction of dinitrogen to ammonia, as well as possible species involved in nitrate–ammonia redox.

2.3.9 Synthesis of $(dda)_3TiBH_4$

Reactions using KBH_4 to produce $(dda)_3TiBH_4$ (**3**) showed no reactivity to **1**, even in a THF reaction medium, in order to increase solubility of the salt. Reaction of 1 molar equivalent of complex **1** with 1.2 molar equivalents of $LiBH_4$ yields **3**. The metathesis was carried out in toluene at low temperature (-40 °C) with the $LiBH_4$ dissolved in a minimal amount of THF. The $LiBH_4$ is then added dropwise over a period of a couple of minutes, and the resulting solution is allowed to react for 24 hours, over which time no real visible color change is observed, except a slight cloudiness to the solution as LiCl is evolved. Complete solvation of the $LiBH_4$ in THF is vital for good yields. Simply using a toluene slurry results in very poor yields (<50%), which proves difficult to purify from **1** as they have very similar solubility in most solvents. Workup involved filtering the reaction solution through a fine frit, which was washed with toluene, leaving a white precipitate, presumably LiCl and unreacted $LiBH_4$. Making the $Ti(dda)_3BH_4{\cdot}THF$ adduct allows easier recrystallization and purification from residual starting materials. The $Ti(dda)_3BH_4$ is

yellow in color (recrystallized from toluene/hexanes), although the THF adduct is orange (recrystallized from THF:hexanes (50/50) and is very similar in appearance to **1**. Initial studies for the reactivity of this species were conducted with the goal of removing the BH_3 and preparing the $(dda)_3TiH$. Complex **3** was reacted with one equivalent of quinuclidine in order to form the BH_3–quinuclidine adduct and freeing up (dda)TiH. NMR spectroscopy revealed the quinuclidine binding to the complex as depicted in Figure 44. A clear shift downfield for the quinuclidine protons labeled (a) can be observed by ~.5 ppm. It is not clear if the quinuclidine is in fact coordinated to the BH_4 moiety or simply bound to the titanium. When the reaction was carried out with excess quinuclidine (3 molar equivalents), the resulting complex quickly discolored from a red solution to colorless and a black precipitate formed, presumably titanium black.

2.3.10 Spectroscopic studies of $(dda)_3TiBH_4$.

The first thing that is noticed in the ^1H NMR spectrum of **3** is the sharpening of the splitting that correlates to the protons on the backbone of the dda ligand, along with a noticeable shift downfield. This would infer that these protons are in a more static and different chemical environment. Figure 45 shows a nice comparison of **3** superimposed above the starting material **1** for the alkyl region. This part of the spectrum is very interesting. With no signs of the BH_4 moiety, one can only assume that the scrambling of the protons off and on the titanium center is too fast for the NMR time scale and is only causing a slight broadness from 1.5 ppm to just past 0.0 ppm (Free $LiBH_4$ shows up a sharp quartet at room temperature at around 0.4 ppm). A VT experiment was conducted whereupon the sample was

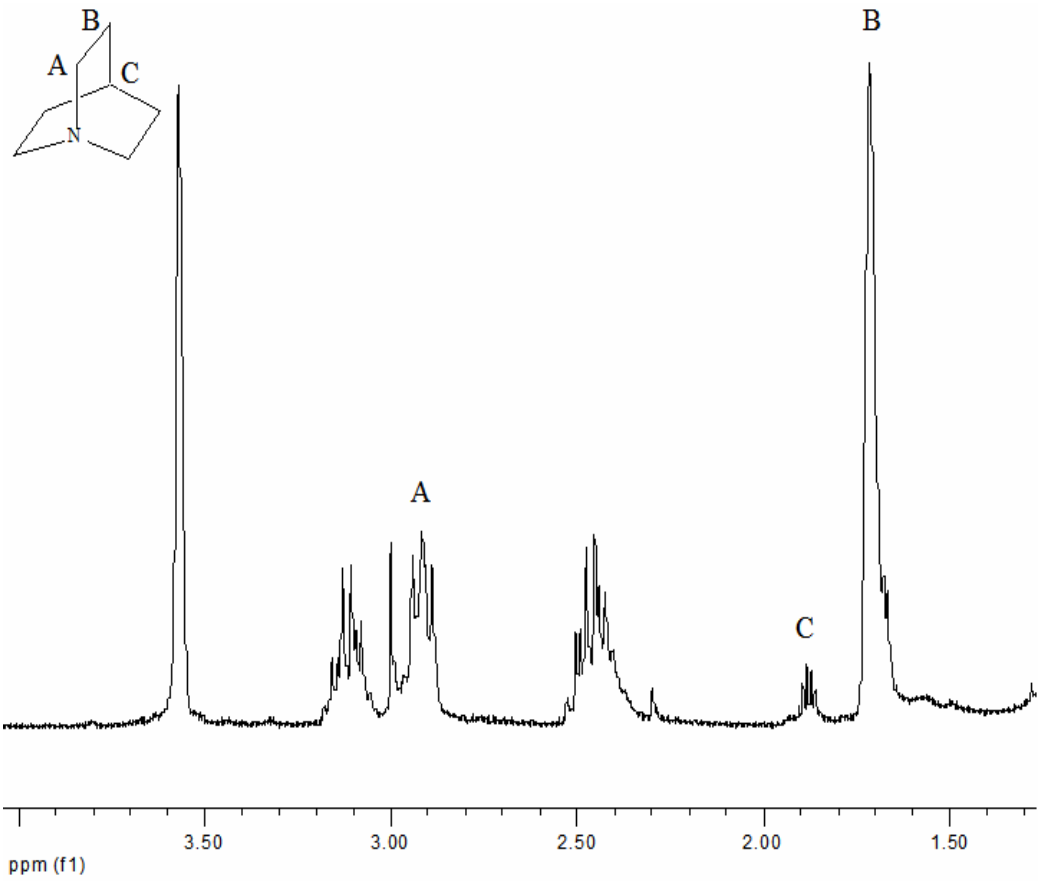

Figure 44: The ^{1}H NMR spectrum for $(dda)_3TiBH_4$. (Quinuclidine) in THF, focusing on the alkyl region.

cooled down to 198 K in order to see the BH_4 moiety; the results are shown in Figure 46. Although no such signal was observed, although the same low temperature processes that are observed in complex **1** are also observed in this case.

2.3.11 Solid-state and molecular structure of $(dda)_3TiBH_4$

Compound **3** is one of the few examples of amido-supported titanium borohydride complexes. X-Ray quality crystals for **3** were grown a from THF/hexane solution, they were filtered, dried under reduced pressure and harvested as pale-orange cubic blocks. From the solid-state structure it may be noted that the borohydride is displayed binding in an $^3\eta$ fashion to the titanium with the Ti–B distance being 2.215 Å. The Ti–N bond lengths are comparable to the $Ti(dda)_3Cl$ of 1.932 Å. The N–Ti–N bond angle is 110.27º and N–T–B bond angles are an average of 109.31º.

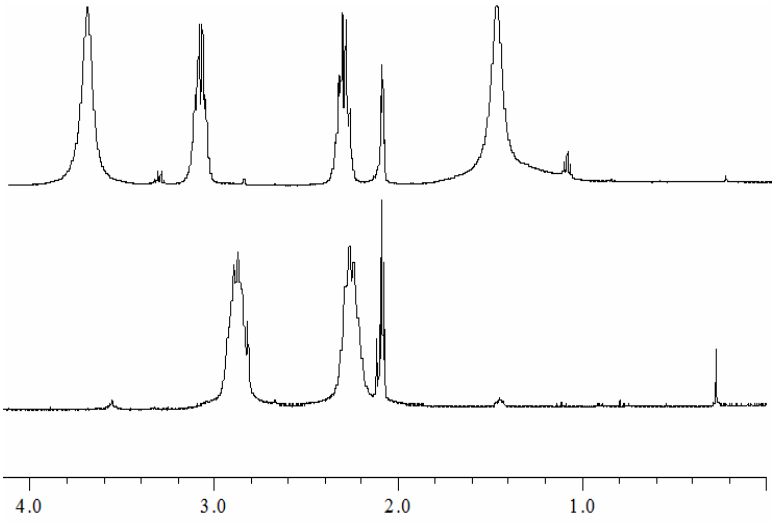

Figure 45: A comparison between the precursor 1 to complex 3 (with bound THF), alongside the slight raise of the baseline around 1.5 ppm through to 0.0 ppm possibly due to the bound BH_4 moiety.

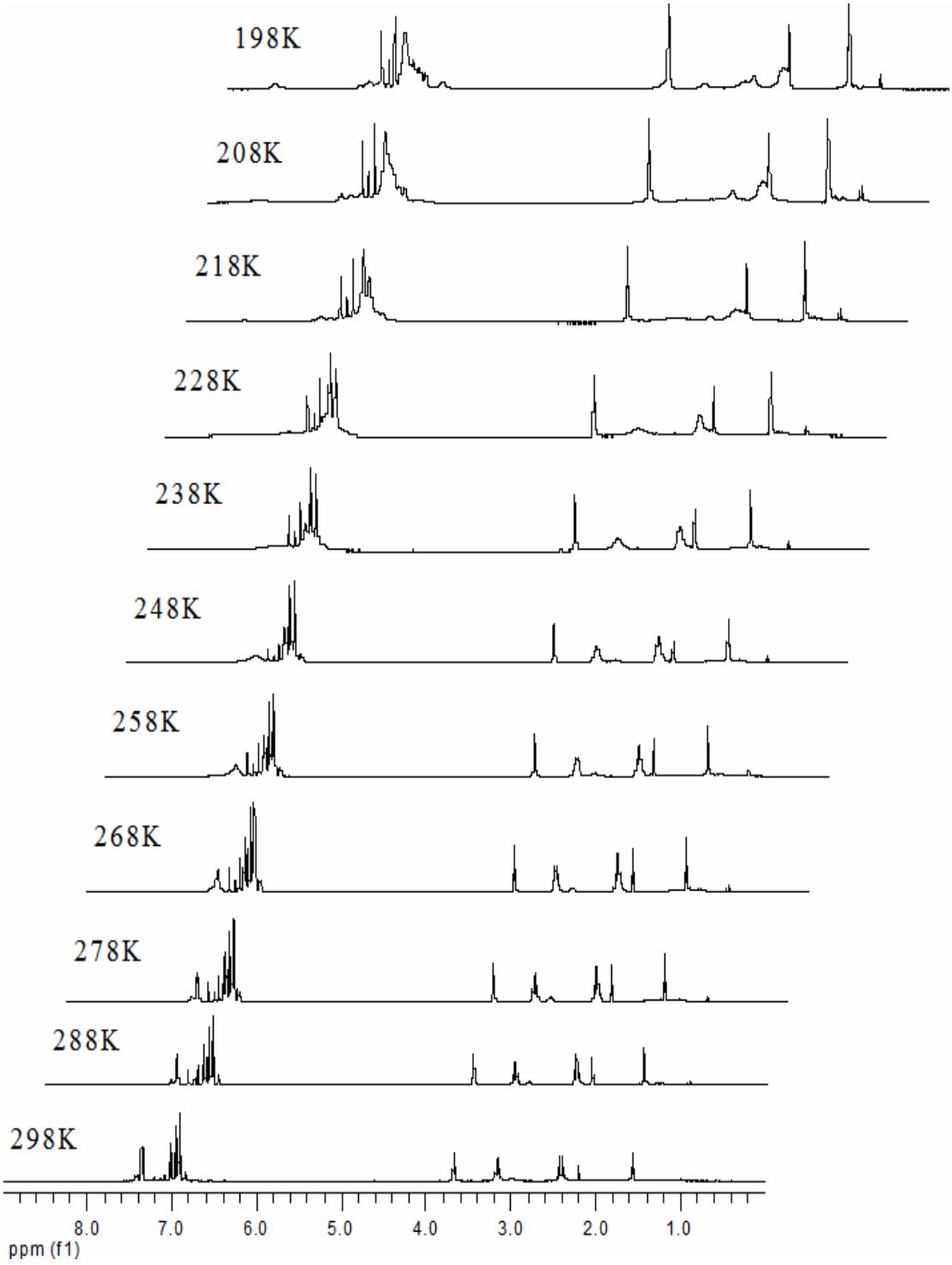

Figure *46: A VT NMR experiment in order to see the Ti–BH_4 moiety, free BH_4 is observed at 0.4 ppm.*

Table 12: ^{1}H NMR resonances for $(dda)_3TiBH_4$ compared to $(dda)_3TiCl$.

Proton label	Complex 1 (ppm)	Complex 3 (ppm)	Multiplicity	Coupling Constants
1a	2.266	2.293	d of d	J = 11.7 Hz, J = 6.3 Hz
1b	2.872	3.054	d of d	J = 11.5 Hz, J = 6.3 Hz
2	6.727	6.8	D	J = 5.4 Hz
3	6.812	6.843	T	J = 5.7 Hz
4	6.812	6.905	t of d	J = 5.4 Hz, J = 1.2Hz
5	7.305	7.24	D	J = 5.7 Hz

Table 13: ^{1}H NMR resonances for $(dda)_3TiBH_4$ compared to $(dda)_3TiCl$.

Complex 1 (ppm)	Complex 3 (ppm)	Carbon label
31.547	32.04	a
151.04	126.42	b
125.981	126.88	c
126.227	127.08	d
126.734	131.17	e
130.543	133.5	f
132.743	151.64	g

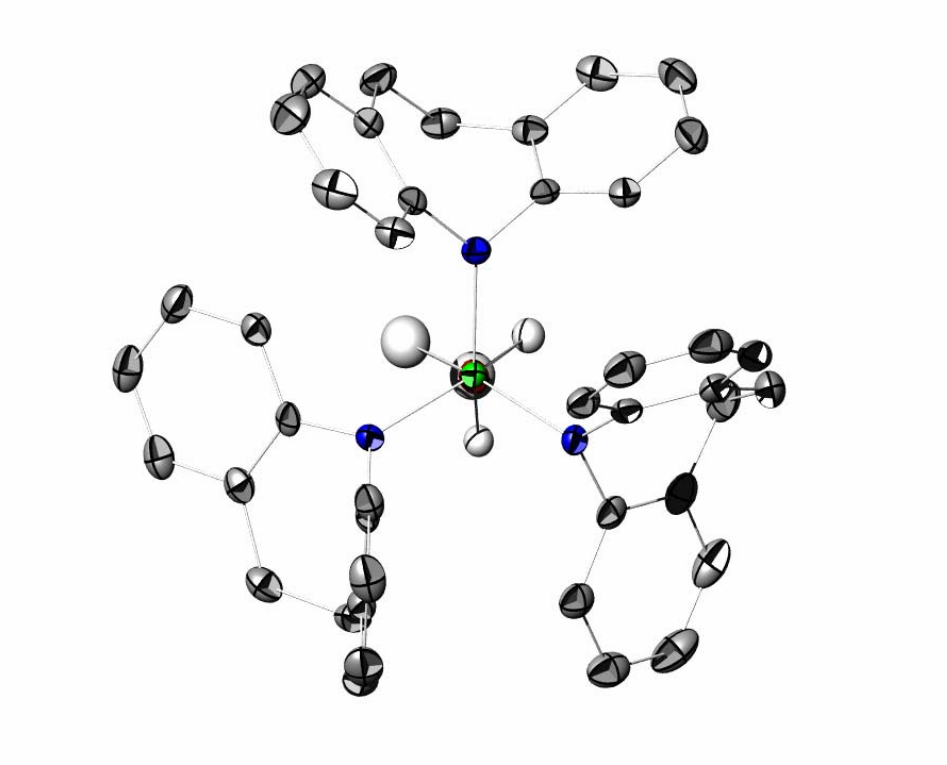

Figure 47: The X-Ray crystal structure of 3 viewed through the Ti-B bond to show the arrangement of the ligands.

The solid-state structure of **3** differs greatly from that of **1** as the rings are no longer facing each other. This change in geometry can only be accounted by the additional bond order for the bound BH_4 moiety. The solid-state structure of the unique unit is depicted in Figure 47.

2.3.12 Synthesis of $(dda)_3TiCH_2PMe_2$

Formation of $(dda)_3TiCH_2PMe_2$ **4** proceeded in an analogous manner to that of **3**. Reaction of 1.2 molar equivalents of *P*,*P*-dimethylphosphinomethyl lithium with **1** results in metathetical replacement of the chloride to bind the CH_2PMe_2 moiety; yields of this compound were very good (91%). Unlike **3**, reaction times for

the formation of **4** are much faster, and the reaction is complete within an hour. The complex can be recrystallized from toluene/hexanes to yield an orange powder, although recrystallization from THF/hexanes yields cherry red crystals. Complex **4** is very reactive upon exposure to air and rapidly degrades to a white powder with O_2 concentrations as low as 20 ppm. By heating this complex in toluene at 100 °C for 48 hours under 1 atm of dihydrogen gas, it was hoped to give another route to the titanium hydride. However, the ^{1}H NMR spectrum after the reaction showed no change to **4** at all.

2.3.13 Spectroscopic studies of $(dda)_3TiCH_2PMe_2$

The CH_2PMe_2 moiety is of particular interest due to its functionality as both an X and L donor, with a classic X-type alkyl function alongside the ability to donate the lone pair from the phosphorus. In this system it has a possibility to bind in one of three modes (illustrated in Figure 48):

1) X only, with the phosphorus not having enough space to bind to the titanium.

2) XL donor, with the phosphorus bound to the titanium center.

3) XL donor, with the phosphorus binding to another titanium center to form a dimer.

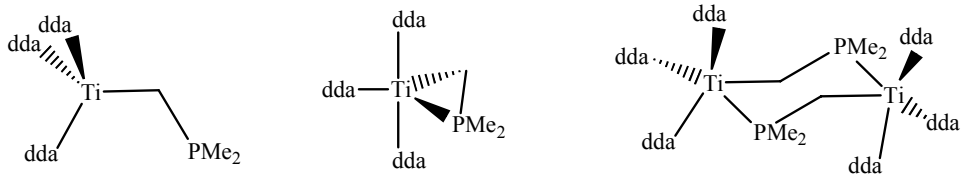

1 **2** **3**

Figure 48: The three possible binding modes of P,P-dimethylphosphinomethyl

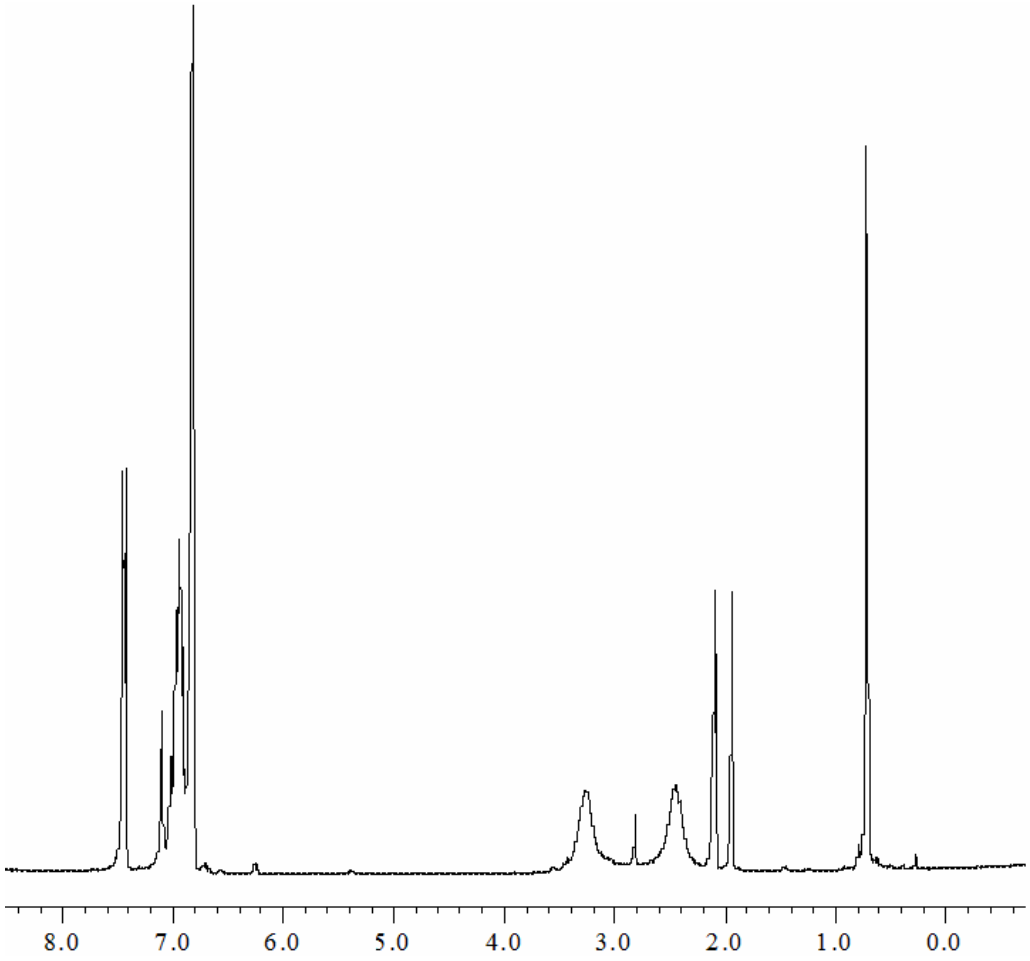

Figure 49: The ^{1}H NMR spectrum for $(dda)_3TiCH_2PMe_2$ in d_8-toluene, the PMe_2 and CH_2–Ti can clearly be seen up field of the residual toluene methyl resonance.

The ^{1}H NMR spectrum for this compound infers a lot of freedom within the molecule, with a sharp signal in the alkyl region, forming a clear doublet relating to the two methyl groups (0.72 ppm, 6H) upon the phosphorus and a broad singlet at 1.94 corresponding to the CH_2 between the phosphorus and the titanium. One would expect to see some splitting from the CH_2 especially being bound to phosphorus; therefore, a NOESY experiment was conducted in order to see through-space coupling between the methyl groups and the presumed CH_2 on the phosphorus. Figure 50 clearly shows that this is indeed the case, that which was wonderful about this experiment was the clear correlation between the protons on the CH_2 matching up with the aromatic protons that are in close proximity. This all points to the idea that the CH_2PMe_2 moiety is in fact $^{1}\eta$ bound to the titanium due to the steric restraints of the dda ligand set.

The ^{31}P NMR spectrum is indicative that there is only one type of phosphorus in the system, which is that of the CH_2PMe_2 moiety. The spectrum shows two peaks, one for the standard (D_3PO_4 which was set at 0 ppm) and the other being the phosphorous of the Ti–CH_2PMe_2, which is displayed at -33.1 ppm (a shift of 7.2 ppm upfield from the lithiated starting material).

Assigning the ^{13}C for complex **4** was made very straightforward with the use of a TOCSY experiment, using the ^{1}H data already assigned from COSY and NOESY experiments, one was able to correlate most of the carbons in the molecule to their corresponding proton. Tables 14 and 15 show the complete assignment for the ^{1}H and ^{13}C NMR spectra for this species.

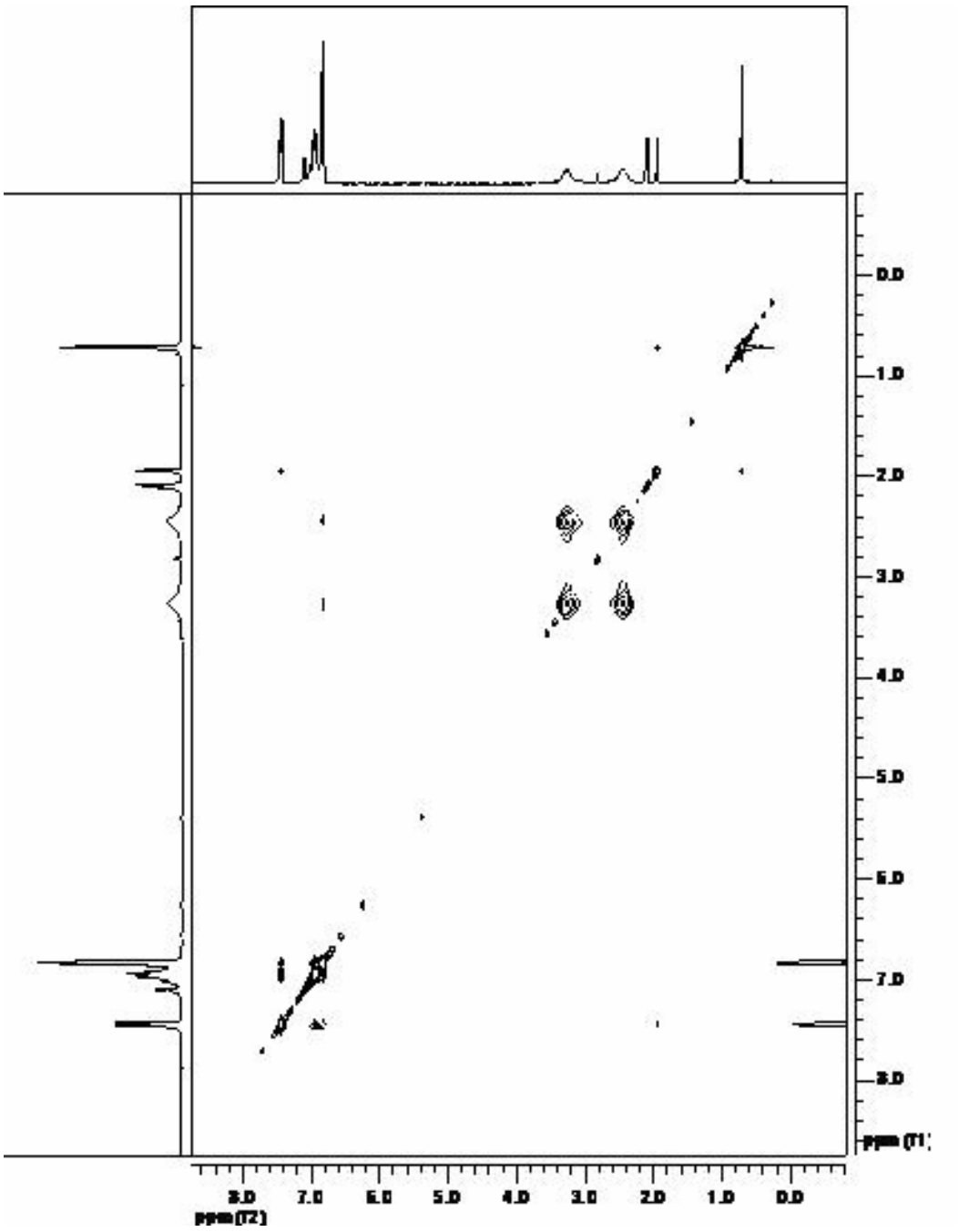

Figure 50: NOESY experiment spectrum for ***4****.*

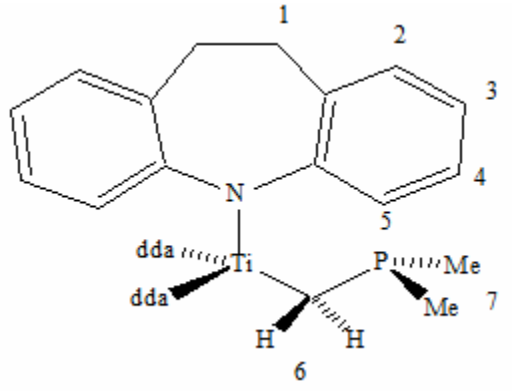

Figure 51: ^{1}H NMR assignment in this species.

Table 14: ^{1}H NMR resonances for $(dda)_3TiCH_2PMe_2$ compared to $(dda)_3TiCl$.

Proton label	Complex 1 (ppm)	Complex 4 (ppm)	Multiplicity	Coupling Constants
1a	2.266	2.449	S	N/A
1b	2.872	3.269	S	N/A
2	6.727	6.83	M	N/A
3	6.812	6.83	M	N/A
4	6.812	6.939	M	N/A
5	7.305	7.429	D	$J = 7.5$ Hz
6	N/A	1.941	S	N/A
7	N/A	0.715	D	$J = 3.3$ Hz

Complex 1 (ppm)	Complex 4 (ppm)	Carbon label
31.547	31.547	a
151.04	133.426	b
125.981	125.418	c
126.227	126.583	d
126.734	127.926	e
130.543	130.815	f
132.743	150.842	g
N/A	83.842	h
N/A	19.297	i

Table 15: ^{1}H NMR resonances for $(dda)_3TiCH_2PMe_2$ compared to $(dda)_3TiCl$.

2.3.14 Synthesis of $(dda)_3TiMe$

Complex **5** is the $(dda)_3TiMe$ and was synthesized after many failed attempts of trying to create the other classic alkyl derivative $(dda)_3TiBz$ through reaction of **1** with $Mg(Bz)_2$. Trying to stabilize Ti–Et through the metathesis of **1** with $Mg(Et)_2$ also proved unfruitful as neither was ever isolated. Again, this species was formed in an analogous manner to that of **3**, although the importance of dissolving the LiMe in THF before the reaction is necessary in order to get the reaction to proceed. Reaction of LiMe and **1** in toluene yielded complete recovery of **1** with no visible methylation after 48 hours. Dissolving 1.2 equivalents of LiMe in THF and adding dropwise with stirring a solution of **1** in toluene at -40 °C over 2 minutes causes a change in the solution's appearance after 5 minutes. The reaction is quick and complete within an hour. Using a large excess of LiMe or other methylating agents such as $AlMe_3$ causes the metal to be reduced to titanium black and fall out of solution. Workup involves

filtering the reaction solution through a fine frit, washing with toluene in order to remove the white precipitate of the LiCl, recrystallization from toluene/hexanes. This produced cubic yellow crystals of **5** in good yield (89%).

2.3.15 Spectroscopic studies of $(dda)_3TiMe$

The ^1H NMR spectrum for this compound is very similar to that of compound **4** in relation to ^1H resonances especially in the aromatic region. Of course in the case of **5** there are only three resonances in the alkyl region that relate to this species. Again, as with all the other bound dda systems, we see the tell-tale splitting of the hydrogens upon the backbone of the ligand sets. There is a marginal shift from the precursor by 0.2 ppm downfield for the alkyl protons on the ligand set. The major difference is obviously the CH_3 which appears at 0.556 ppm in d_8-toluene and integrates to a total of three protons in ratio to the other signals in the system. Figure 52 shows the ^1H NMR spectrum for **4,** complete with integrations.

The ^{13}C NMR spectrum of 5 in toluene proved to be difficult to identify the carbon that corresponded to the methyl from the baseline. Therefore a highly concentrated sample in d_8-THF was prepared and can be seen in Figure 53. The methyl peak clearly visible at 60.909 ppm, with the other carbon resonances being very reasonable for the dda ligand set.

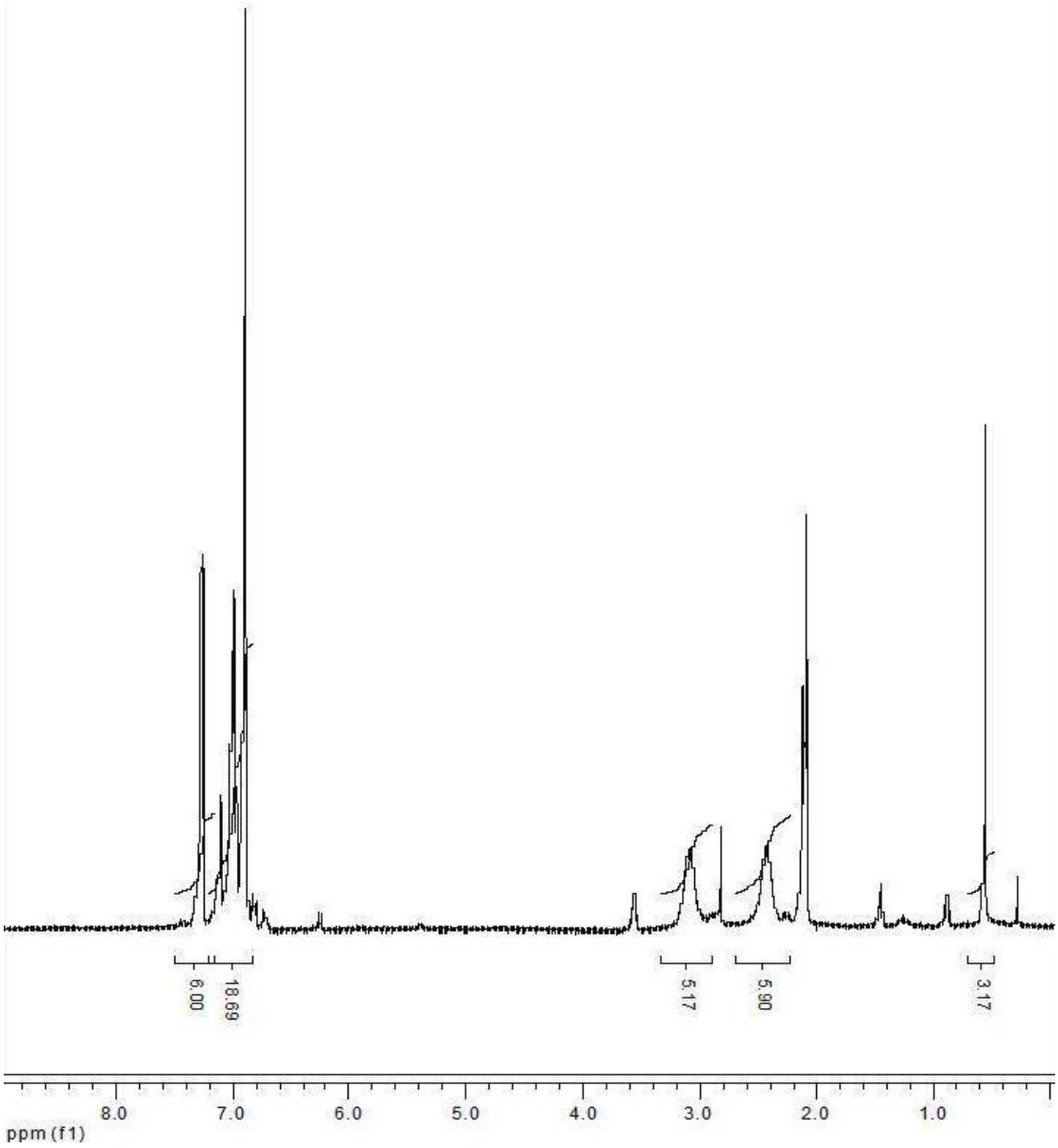

Figure 52: The ^{1}H NMR spectrum of $(dda)_3TiMe$ in d_8-toluene, clearly showing the integration of the methyl peak in relation to the other resonances.

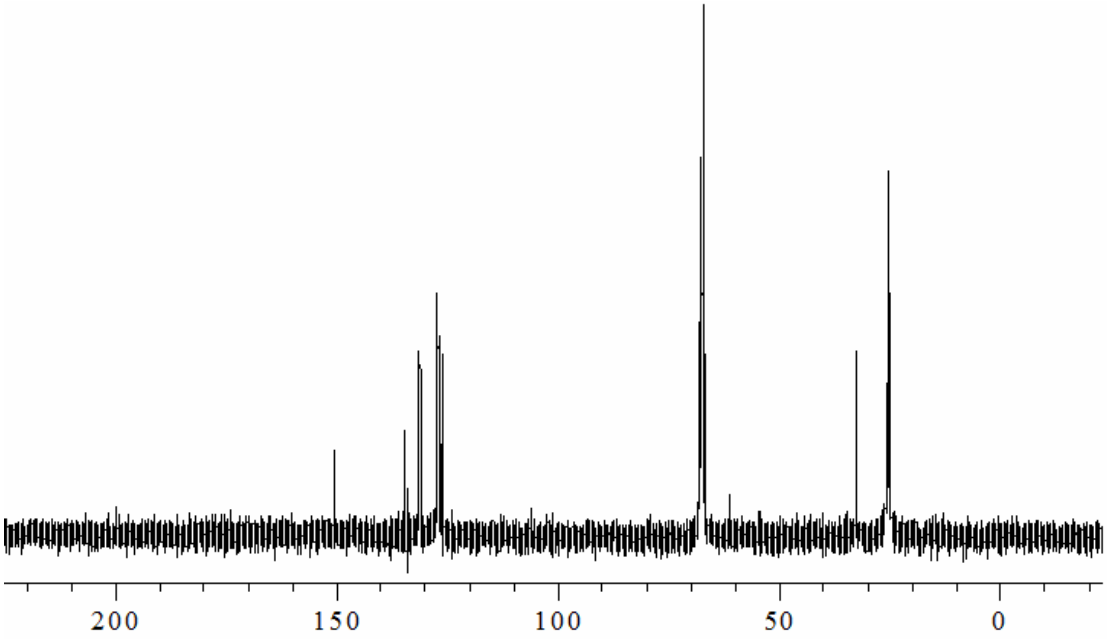

Figure 53: The ^{13}C NMR spectrum of $(dda)_3TiMe$ in d_8-THF.

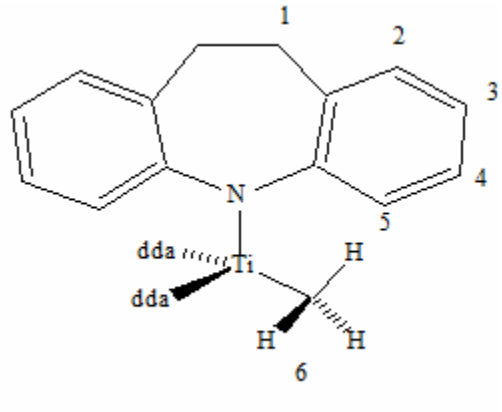

Figure 54: ^{1}H NMR assignment in this species.

Table 16: ^{1}H NMR resonances for $(dda)_3TiMe$ compared to $(dda)_3TiCl$.

Proton label	Complex 1 (ppm)	Complex 5 (ppm)	Multiplicity	Coupling Constants
1a	2.266	2.43	S	N/A
1b	2.872	3.083	S	N/A
2	6.727	6.898	M	N/A
3	6.812	6.898	M	N/A
4	6.812	6.999	M	N/A
5	7.305	7.258	D	J = 5.4 Hz
6	N/A	0.555	S	N/A

Table 17: ^{1}H NMR resonances for $(dda)_3TiMe$ compared to $(dda)_3TiCl$

Complex 1 (ppm)	Complex 5 (ppm)	Carbon label
31.547	32.667	a
151.04	150.740	b
125.981	126.156	c
126.227	127.067	d
126.734	127.166	e
130.543	131.246	f
132.743	134.523	g
N/A	61.113	$Ti–CH_3$

.

2.4 Conclusions and future progress

This chapter has detailed the synthesis and characterization of a range of titanium complexes supported with the dda amido ligand set. These ligands provide excellent electronic contribution to the metal center, alongside a fair amount of steric protection (most notably with the complex being in a tetrahedral symmetry with three bound dda ligands). These properties coupled with the molecular similarities to known complexes[52] that have shown progress in the binding and splitting of dinitogen led us to pursue dinitrogen activation reactions with $(dda)_3TiCl$.

Preliminary studies resulted in the reductive–elimination of bound dda moieties to form the bisdihydrodibenzoazepinyl dimer, which was observed in the NMR after the reaction work up and analysis. The aggressive approach used to remove the halide, at low temperature (-78 ºC) using strong reducing agents such as NaK or potassium–graphite intercalation was probably too harsh and caused the reduction of titanium. A milder reaction using sodium amalgam and over an extended period of time might be a more advantageous route to avoid further reduction of the metal center.

Initial polymerization reactions were carried out with the assistance of M. Blanchard. In a reaction consisting of a toluene solution of $Ti(dda)_3Cl$ with MAO, propylene was added to be effectively polymerized into polypropylene. These results were very unexceptional compared to other systems being researched in our laboratory. Reaction of $Ti(dda)_3Cl$ with $KB(C_6F_5)_4$ would be predicted to give the Brookhart-type[17] metal cation countered with a highly charge dispersed counter

anion. This complex would be an excellent point to further pursue exploration of polymerization reactions.

Future work would involve the optimization of conditions for the binding of dinitrogen to the titanium center in the $Ti(dda)_3Cl$ system. Once the dinitrogen–titanium adduct is formed: single hydrogenation to form the diazenido species followed by further hydrogenation to form the $Ti–NH_2$ moiety, which would then be carried through to free NH_3. Completing Schrock's proposed Mo cycle[38] with our titanium system, with the steps understood, devising an efficient catalytic system for the production of ammonia from ambient nitrogen could be developed.

3. Synthesis and Reactivity Studies of Carbazolyl Complexes of Titanium

3.1 Overview

The carbazolyl moiety (Cb for brevity) structurally should be very similar to dda; however, it is a non-innocent system, meaning the L_π orbital on nitrogen can either engage with other ligand orbitals, forming pyrrole-like aromatic interaction, or it can act as a donor to the metal center. Recent studies have confirmed that aromatic cyclic counterparts to Cb, such as pyrrolyl and indolyl, exhibit a reduced π-donor capability as a result of the nitrogen π-orbital being involved in the aromatic π - system of the ligand.[53-55]

A clear indication of the delocalization of the electron density on nitrogen, which may have a strong effect on the electron-donating properties of such ligands, is illustrated by the p*K*a's of some aromatic cyclic amine derivatives that are significantly lower than those of simple amines. These are compared in Table 18.

Table 18: A comparison of cyclic amine derivatives against simple "hard" amines.

cyclic amine	**pKa**	**Amine**	**pKa**
pyrrole	17.5	Pri_2NH	35.7
indole	17	$(Me_3Si)_2NH$	29.5
carbazole	16.5	Ph_2–NH	22.4

Such ligands have been utilized before; Pauson and Qazi[56] demonstrated how such cyclic amines could be used as ligands by complexing them to $Fe(Cp)(CO)_2$. Further studies were carried out by Rothwell *et al.*[57] They utilized the carbazolyl moiety for the formation of several metal complexes including niobium, tantalum, zirconium and titanium. The synthetic route for their systems was though metal benzyl derivatives with the free carbazole eliminating toluene and forming the metal carbazolyl system. With an investigation into mixed ligand systems, using carbazolyl, cyclopentadiene and 2,6-dimethylphenylisocyanide (which formed the alkylidene bridging dimer).

It has already been demonstrated by groups such as Cummings and Schrock that the use of hard amido ligands can effectively been used to stabilize molybdenum metal centers to a binding dinitrogen moiety.[52] These complexes are important intermediates in the Chatt cycle for the catalytic reduction of dinitrogen to ammonia and other amines.[36] In nature, for many catalytic transformations ligands found in systems such as cysteine found in proteins (disulfide ligation), and heme units for oxygen transportation in red blood cells (porphyrin ligation), use "soft" ligand sets. These soft ligand sets have strong π-interactions. The use of carbazole as a ligand mimics these properties due to the obvious strong π-interaction within the aromatic ring system. This is depicted in Figure 55.

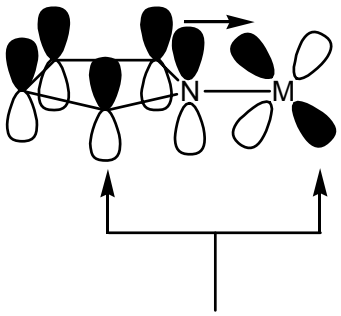

Lπ-d

Figure 55: A diagram showing the π-ligand and d-metal interaction, the π donating capacity of systems such as carbazolyl should be diminished.

It was therefore our goal to synthesize carbazolyl titanium species that could be applied to current advances in catalytic dinitrogen reduction at a metal center.

3.2 Introduction

This chapter presents the synthesis and initial reactivity studies of Cb titanium complexes as a direct comparison to the dda systems covered earlier. Carbazole is commercially available from Sigma–Aldrich; deprotonation is carried out using *tert*-butyllithium at low temperature, producing the lithium salt, CbLi, in high yields. Synthetic details are presented in the experimental section for this and all other new compounds in this chapter.

CbLi is air sensitive and will readily undergo oxidation upon exposure to the air. The fine, white powder will discolor to pale green upon oxidation and then char black with sufficient exposure. The pale-green discoloration is quite subtle, although it does allow a visual estimation of the status of stored CbLi.

3.3 Results and Discussion

3.3.1 Synthesis and analysis of CbLi

Treatment of carbazole with *tert*-butyllithium affords CbLi (CbLi for brevity) in excellent yields (93%), the reaction proceeding smoothly in toluene at -40 °C. Both carbazole (CbH) and *tert*-butyllithium show good solubility in toluene, while CbLi is insoluble; therefore, filtration and several washings of hexane/pentane (to remove trace *tert*-butyllithium), followed by drying under reduced pressure, yields the pure lithiated salt. This was confirmed by ^{1}H and ^{13}C NMR spectroscopy. The ^{1}H spectrum is depicted in Figure 56 to illustrate the clear and sharp splitting observed in CbLi. The ^{1}H and ^{13}C NMR assignments are given in Tables 19 and 20 respectively, with Figure 57 showing the labeling scheme.

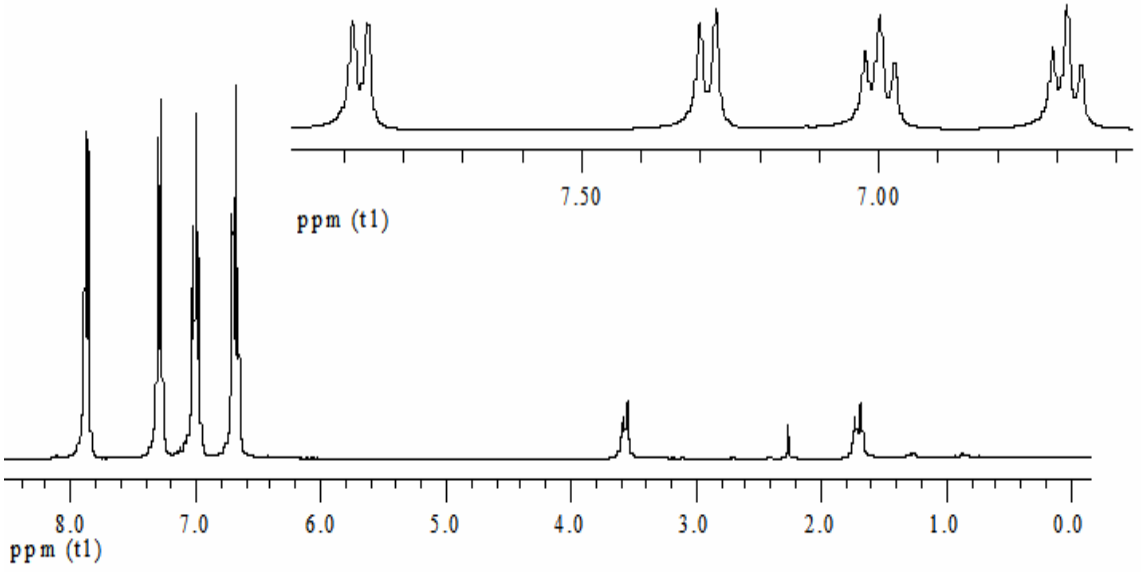

Figure 56: Depicting the clear separation and splitting of the aromatic region of CbLi.

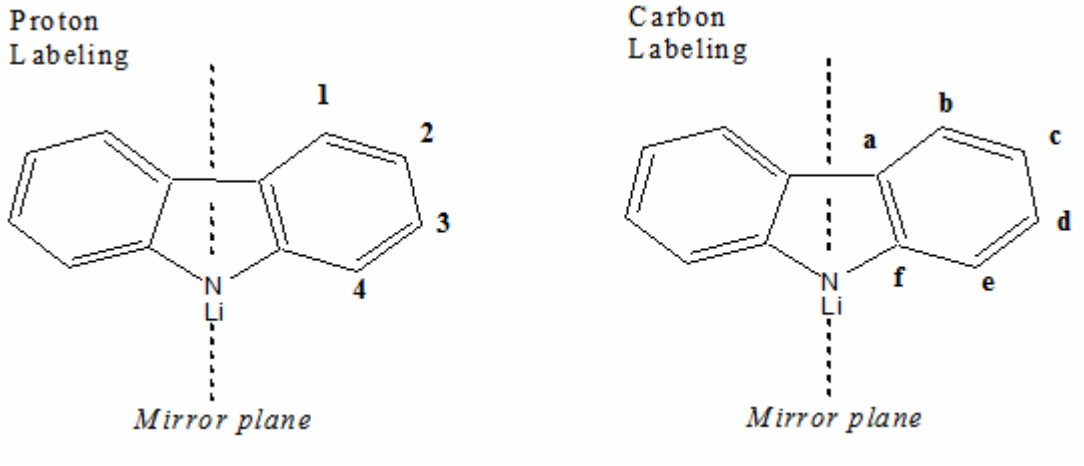

Figure 57: ^{1}H and ^{13}C NMR labeling system for Cb system discussed in this chapter.

Table 19: Tentative ^{1}H NMR spectral assignment for CbLi in d_8-THF.

Proton label	Signal (ppm)	Multiplicity	Coupling Constants
1	7.873	d	J = 7.5 Hz
2	6.682	t	J = 7.5 Hz
3	7	t	J = 7.8 Hz
4	7.288	d	J = 8.1 Hz

Table 20: Tentative ^{13}C NMR spectral assignment for CbLi in d_8-THF

Carbon label	Signal (ppm)
a	125.89
b	119.366
c	114.701
d	113.068
e	125.8
f	153.403

3.3.2 Synthesis of $(Cb)_3TiCl.2THF$ and $(Cb)_2TiCl_2.2THF$

Reaction of three molar equivalents of CbLi with one molar equivalent of $TiCl_4$·2THF affords $(Cb)_3TiCl$, (**6**). The metathesis was carried out in toluene and upon addition of the lithium salt to the titanium-containing solution, turns the mixture a rich blue color. As more of the salt is added, the solution starts to gain darker shades of blue until it is near black in color; this sequence of color changes may indicate that the metatheses are sequential, in part or in full, albeit very rapid as reaction times do not exceed an hour even at -40 °C. Filtration of the mixture from a precipitate, presumed to be lithium chloride, followed by evaporation of the solvent under reduced pressure yields crude $(Cb)_3TiCl$·2THF.

Recrystallization of the crude product from a toluene/hexane solution at low temperature affords dark-blue crystals from the opaque solution. Although the solution is so dark in color, it is difficult to even observe the solid formation in the bottom of the flask.

Compound **6** is an 18 electron complex, assuming that all three amido ligands are acting as LX donors, and the complex shows reasonable resistance to ligand oxidation and hydrolysis in the solid-state. Slow hydrolysis in ambient atmosphere releases free carbazole. The possible structures for this system are illustrated in Figure 58.

The NMR spectrum of this species indicates only one type of THF resonance, meaning that both THF moieties must be in the same chemical environment. This would infer isomer B is the correct structure as both bound THF adducts are in the same environment due to the C_2 rotational axis going through the Cl–Ti–Cb bonds.

Formation of $(Cb)_2TiCl_2 \cdot 2THF$ **7** proceeded in an analogous manner to that of **6**. Reaction of 2 molar equivalents of CbLi with $TiCl_4 \cdot 2THF$ results in metathetical replacement of two chlorides.

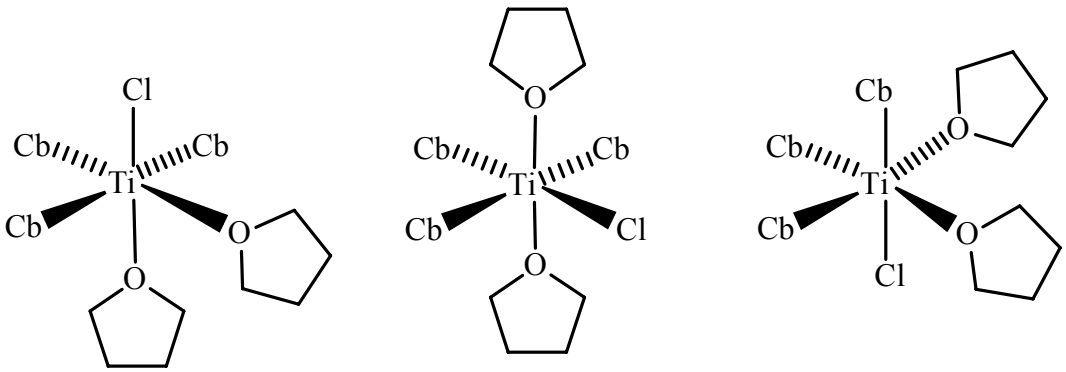

A **B** **C**

Figure 58: The three possible isomers of compound ***6****.*

3.3.3 Spectroscopic studies of $(Cb)_3TiCl.2THF$ and $(Cb)_2TiCl_2.2THF$.

The first thing that was noticed in the spectra of these compounds was the retaining of the THF moiety from the starting material. This seems a little unlikely. Although the synthesis was carried out in pure toluene, recystallization from toluene/hexane solution yielded the *bis*-THF adduct, which is in strong contrast to $(dda)_3TiCl$. In both systems the THF shows a strong shift in the ^1H NMR spectrum, with protons Ha shifting from 1.73 ppm to ~1.16 ppm, possibly due to an inductive effect. Protons Hb do not undergo any significant change. The ^{13}C NMR spectrum shows a strong shift in the carbon bound to proton Hb from 67.51 ppm to 73.255 ppm. No noticeable ppm shift is observed in the carbon bound to Ha.

One could speculate that the reduced π-donation from Cb could leave the titanium more electrophilic. Therefore the requirement of two bound THF moieties would place this system into an octahedral symmetry rather than the observed pseudo-tetrahedral observed in the dda systems. The ^1H NMR spectrum for **6** is shown below in Figure 60, with Tables 21 and 22 assigning the ^1H and ^{13}C NMR resonances for this species, respectively.

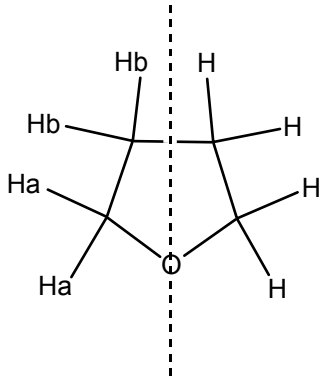

Figure 59: Bound THF moiety in TiCb systems.

In order to correctly assign this species, it was necessary to conduct a series of 2D experiments. Firstly a COSY experiment allowed the assignment of the spin systems within the aromatics of the system (Shown in Figure 61), it can be clearly seen that protons 4 and 3 correlate with each other, as do protons 1 and 2

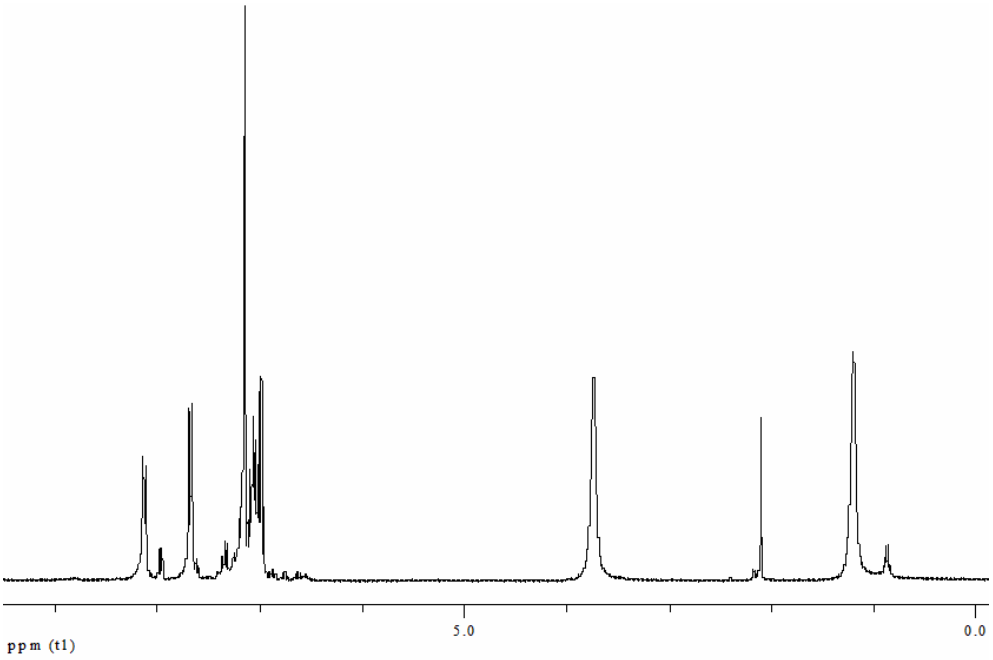

Figure 60: Depicting the ^{1}H NMR spectrum for $TiCb_3Cl{\cdot}2THF$.

Table 21: ^{1}H NMR assignment for $TiCb_3Cl.2THF$ in benzene.

Proton label	Signal (ppm)	Multiplicity	Coupling Constants
THFa	1.165	s	N/A
THFb	3.704	s	N/A
1	7.648	d of d	J = 7.5 Hz J = 1.5 Hz
2	6.967	m	N/A
3	7.039	m	N/A
4	8.109	d	J = 8.4 Hz

Table 22: ^{13}C NMR assignment for $TiCb_3Cl.2THF$ in benzene.

Carbon label	Signal (ppm)
THFa	25.60
THFb	73.26
a	124.287
b	118.707
c	126.438
d	123.793
e	122.439
f	149.263

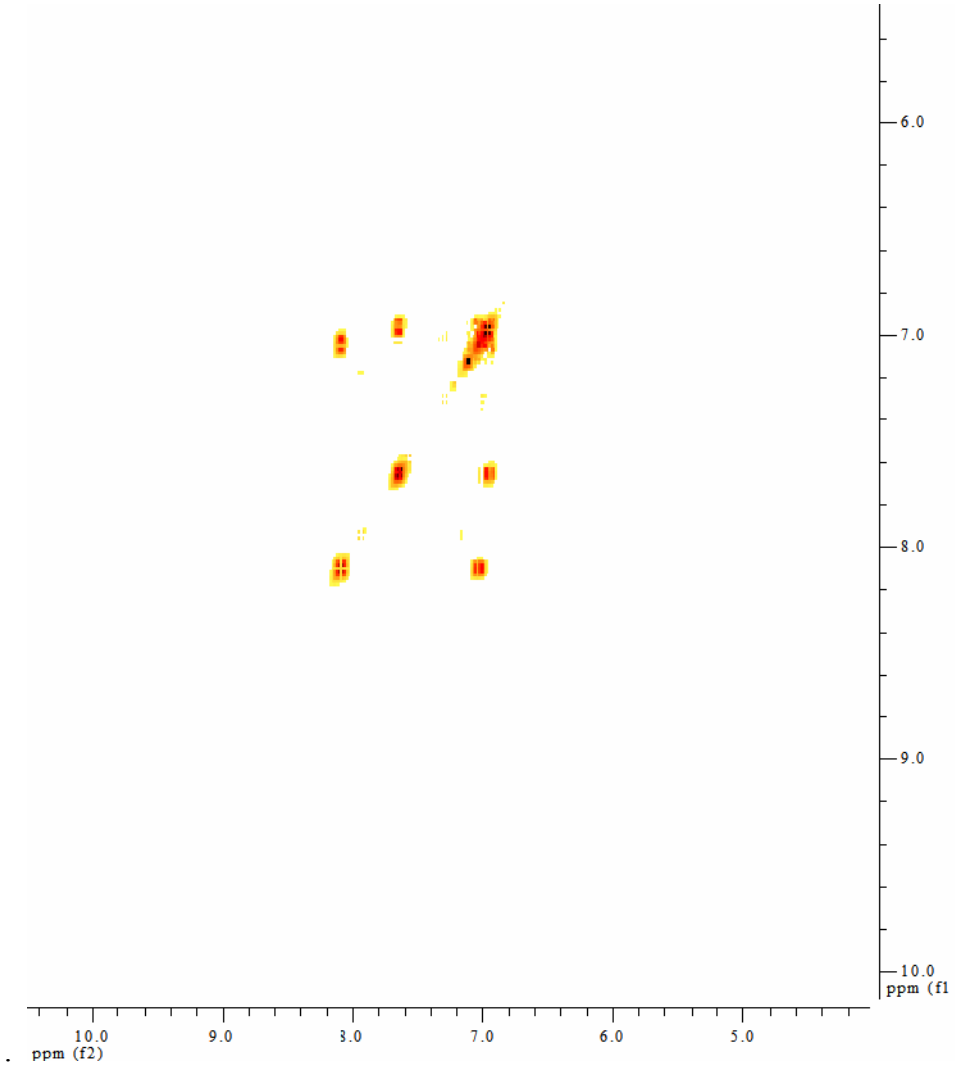

Figure 61: COSY showing H–H correlations in ***6****.*

This was confirmed by the NOESY of this species (which is shown in Figure 62). The NOESY also allowed the confirmation of which proton was *ortho* to the Ti–N bond, through the through-space correlation to the bound THF moieties. This not only helped assign the aromatic region, but also confirmed that these THF moieties were indeed bound to the titanium center. Free THF has a δ of 3.58 ppm of the protons of the CH_2 bound to the ether and 1.73 ppm for the other CH_2 in the system. Once bound to this complex, one observes a large down fieldshift of nearly 0.7 ppm

for the protons that correspond to the signal at 1.73 ppm, shifting to 1.165 ppm. The protons that are bound to the ether, which is directly bound to the titanium, shows only a small shift from 3.58 ppm to 3.704 ppm. Such a significant shift for THF that is coordinated to a titanium(IV) species, differs greatly from related species such as (dda)$TiBH_4$ and $(dda)_2TiCl_2$, as these show marginal shifts. The assignment of the carbons within this system was made easy *via* the use of a TOCSY experiment.

The ^{1}H NMR spectrum for $Ti(Cb)_2Cl_2 \cdot 2THF$ can be seen in Figure 63, using benzene-d_6 as solvent. Again, the THF is strongly bound to the titanium center with a large shift in ppm downfield similar to that observed in **6**. The ^{1}H and ^{13}C NMR spectroscopy assignments of the resonances for this species are shown in Tables 23 and 24, respectively. Comparing the ^{1}H and ^{13}C chemical shifts between the two systems, it can be seen that very little shift can be observed. This indicates that although the electronic makeup of the complex has changed, the electron density upon the ligand remains the same.

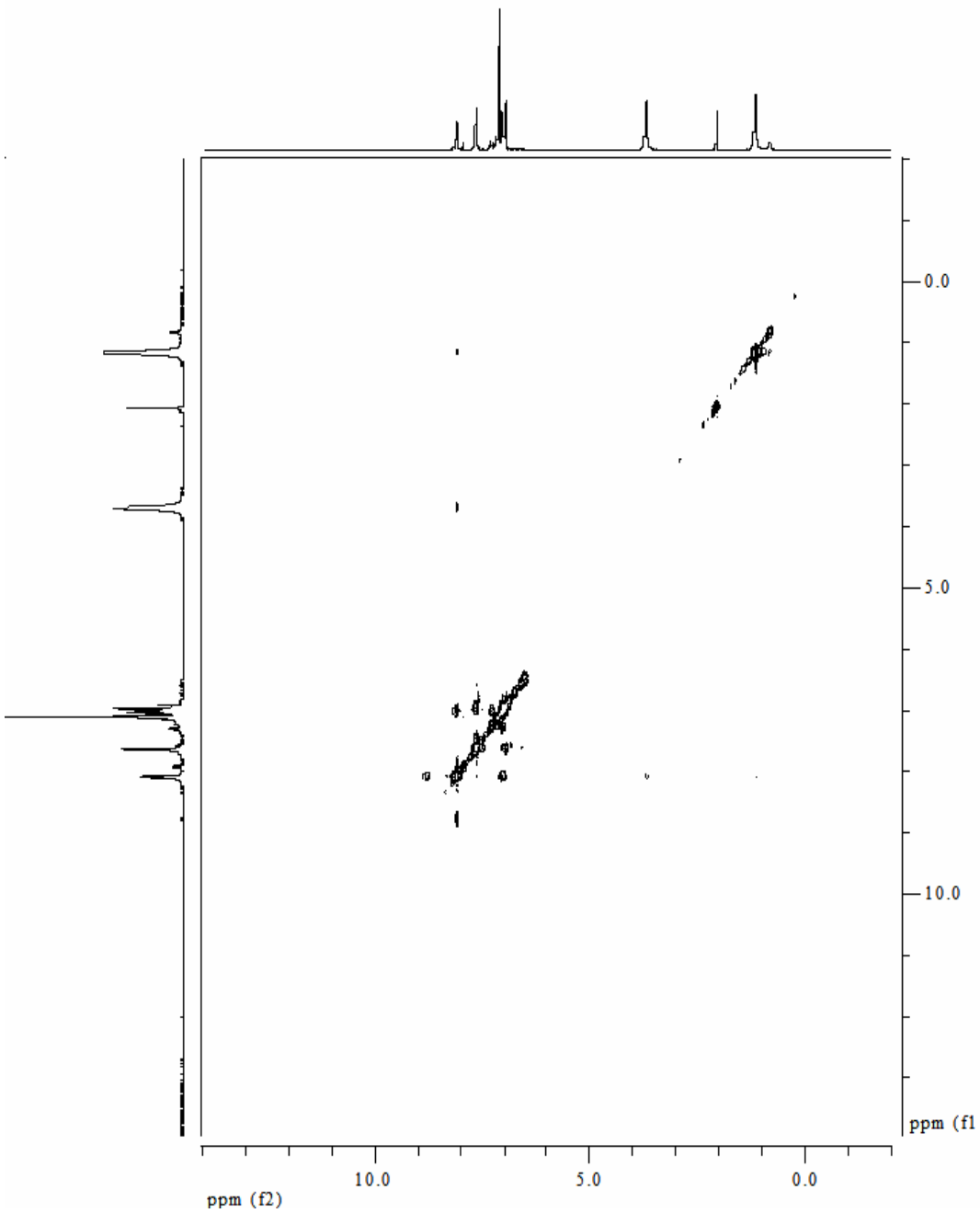

Figure 62: NOESY depicting H–H through-space correlations in ***6****.*

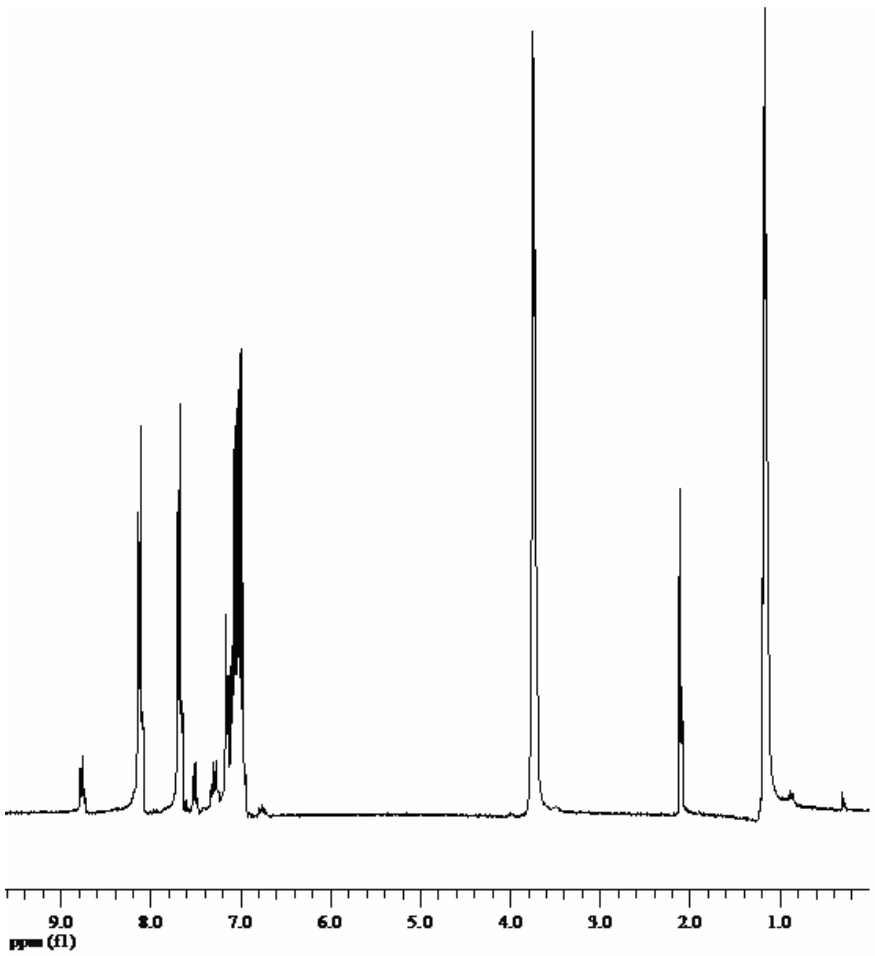

Figure 63: The ^{1}H NMR spectrum of $Ti(Cb)_2Cl_2 \cdot 2THF$ in benzene-d_6, a small amount of residual toluene can also be seen.

Table 23: The ^{1}H NMR assignment of 7 in benzene-d_6.

Proton label	Signal (ppm)	Multiplicity	Coupling Constants
THFa	1.16	s	N/A
THFb	3.74	s	N/A
1	7.686	d	J = 7.5 Hz
2	7.23	m	N/A
3	7.23	m	N/A
4	8.109	d	J = 8.1 Hz

*Table 24: The ^{13}C NMR assignment of **7** THF-d_8.*

Carbon label	Signal (ppm)
a	124.336
b	118.658
c	126.386
d	123.707
e	122.631
f	149.374

3.3.4 Attempted synthesis of $(Cb)_3TiBH_4$

The synthesis of $(dda)_3TiCl$ with $LiBH_4$ yielded the complex $Ti(dda)BH_4$ in very good yields, although this is not the case with $Ti(Cb)_3Cl$. Reaction of **6** with $LiBH_4$ causes presumably metal reduction and the release of carbazole. The reaction mixture is discolored from dark blue to a clear solution with gray colored precipitate. Compound **6** also shows no reactivity with KBH_4, even in THF (which was used to improve solubility of the KBH_4 salt). The formation of this species was unachievable.

3.3.5 Synthesis of $(Cb)_3TiMe$

MeLi dissolved in a THF solution was added dropwise over a period of 3 minutes into a solution of **6** dissolved in toluene at -40 °C. The solution was stirred and allowed to warm to room temperature over a period of 30 minutes. A gradual color change from deep blue to dark red can be observed; the solution is then filtered through a fine frit (washed with pentane) and recrystallized from toluene/hexanes to produce red crystals, in good yield (81%).

3.3.6 Spectroscopic studies of $(Cb)_3TiMe$

The ^1H NMR spectrum for $(Cb)_3TiMe$ varies drastically from its precursor for several reasons: Firstly, the strong singlet at 2.145 ppm that integrates to three protons that has been assigned to the methyl peak of this species. Secondly, the absence of coordinated THF, once the $(Cb)_3TiMe$ has been crystallized out. The NMR spectrum shows no trace of THF. This infers that there has been a drastic change for the electronic requirements for the titanium, which is coupled with a very severe color change. Finally, there is rich splitting that this compound displays in the aromatic region. The full spectrum is given below in Figure 64 alongside a full expansion of the aromatic resonances.

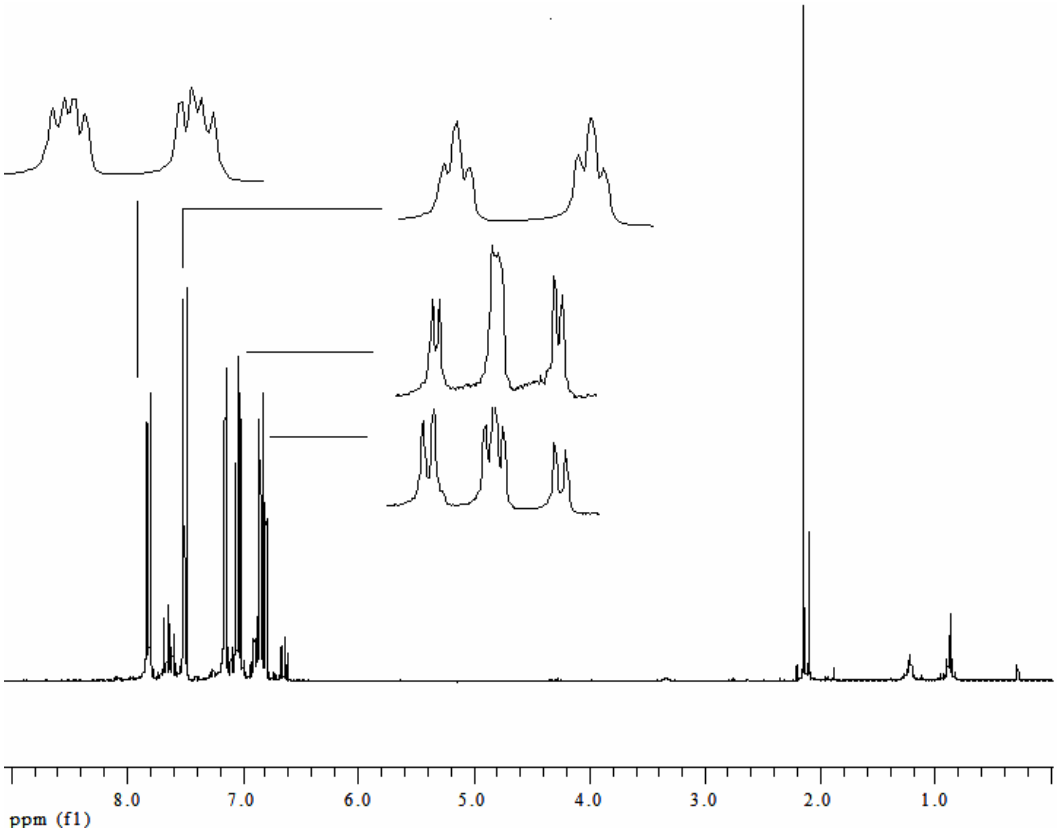

Figure 64: ^1H NMR spectrum of $(Cb)_3TiMe$ with expansions of aromatic splitting.

Table 25 reports to the ^{1}H NMR assignments along with the coupling constants. The splitting is rich and complex. Table 26 reports the tentative carbon assignments, as these have not been fully confirmed using 2D NMR spectroscopy.

3.3.7 Synthesis of $(Cb)_3TiCH_2PMe_2$

Me_2PCH_2Li dissolved in a THF solution was added dropwise over a period of 3 minutes into a solution of **6** dissolved in toluene at -40 °C. The solution was stirred and allowed to warm to room temperature over a period of 30 minutes. A gradual color change from deep blue to dark red was observed over this time. The solution was filtered in order to remove solids (presumably LiCl) and washed with toluene. The filtrate's volume was then lowered under reduced pressure, and the product was precipitated out using pentane. It was then filtered and washed with more pentane. The material assumed to be to be $(Cb)_3TiCH_2PMe_2$ is very oily in nature and was difficult to dry. The NMR spectrum of this species infers that the compound is unstable and readily degrades in the NMR tube over a few hours to form a brown precipitate that is insoluble in the solvent it was once dissolved in, in this case toluene-d_8.

3.4 Discussion and future progress

This chapter has demonstrated that carbozyl can be an effective ligand for the stabilization for titanium complexes. The starkest contrast between the carbozyl and dda ligands is the lowered σ-donor capability from the carbozyl, requiring additional electron density through bound THF moieties. This was very interesting as it provided systems in varied symmetries to what was observed in the dda complexes.

Table 25: ^{1}H NMR assignment of $(Cb)_3TiMe$ in benzene-d_6.

Proton label	Signal (ppm)	Multiplicity	Coupling Constants
1	7.497	d of t	J = 8.1 Hz, J = 0.9 Hz
2	6.827	t of d	J = 8.1 Hz, J = 0.9 Hz
3	7.037	t of d	J = 7.8 Hz, J = 0.9 Hz
4	7.812	d of d of d	J = 8.1 Hz, J = 0.6 Hz J = 0.9 Hz

Table 26: Tentative ^{13}C NMR assignment of $(Cb)_3TiMe$ in benzene-d_6.

Carbon label	Signal (ppm)
a	124.154
b	115.885
c	127.297
d	123.623
e	120.006
f	146.254

Future work would involve solid–state analysis of these complexes to compare them in detail to the solid–state data collected on the dda systems. This would provide more information on the nature of the Ti–N bonds with the carbozyl complexes.

These application of small molecule activation and polymerization as discussed with the dda ligand complexes would be highly interesting with the carbozyl systems also, and will hopefully be explored.

4. Investigation of Tetraamines

4.1 Introduction

Tetrahedral tricyclic tetraamines or adamazines are a variety of compounds that are fundamentally interesting due to the orientation of the four nitrogen lone pairs that are within close proximity to one another. A variety of bowl and cage-adamazanes have been synthesized that differ in their ligating properties due to the spatial arrangement of the lone pairs.

Figure 65 depicts three examples that illustrate the diversity of related molecules. In compound **1**, urotropine, the lone pairs are exohedrally diposed in respect to the framework. Therefore the predicted bonding to metal centers would form polymeric, monodentate structures, which is the basis for many self-assembled transition metal arrays in the solid-state.

Conversely, **2** is thought to display an endohedral arrangement, confining the non-bonding electrons into a small region of space inside the cage. This adds a significant

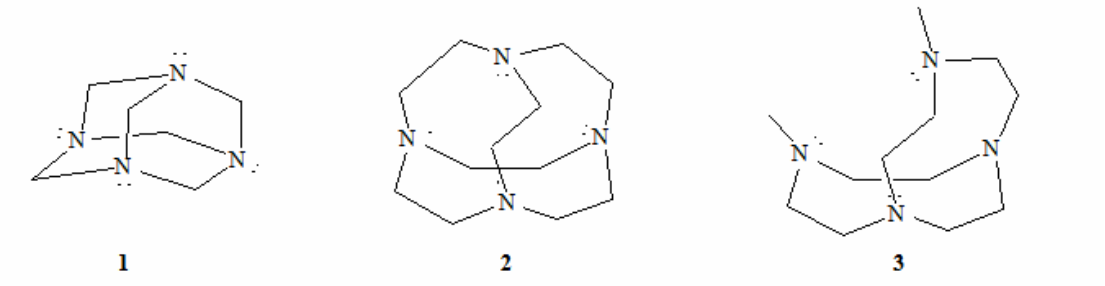

Figure 65: Three related tetraamine species.

columbic contribution to the overall energetics of the molecule. The close proximity of the formal lone pairs causes a heightened concentrated electron density, and the formation of extraordinarily strong hydrogen bonds is observed, to an extent that these species have been labeled as "proton sponges" with pKa$_1$ >24 and pKa$_2$ = 10.8.

Compound **3**, is an example of a bowl-adamanzane as synthesized by Weismann et al.[58] Such compounds are "cross-bridged" tetraamine systems, which are in direct relation to **2**, although the framework has been partially removed on one side to relieve steric constraint and allow the feasibility of transition metal bonding to the available lone pairs.[58] According to modern coordination chemistry principles, ligands that have such rigidity in the framework, assist the formation of a complex with enhanced kinetic stability.[59] Such properties have stimulated increased interest in application to radiopharmaceutical and biomimetic chemistry.[60,61]

The synthesis of macrocyclic chelating agents for metal ions, specifically used by Weissman *et al*., has found application for the delivery of copper radionuclidies, due to the ligand's enhanced chelating ability to help prevent metal loss in *vivo*[62,63]. In particular, the complexes of such chelating ligands with paramagnetic metal ions, especially with gadolinium, are characterized by high stability and can be used in the diagnostic field applications of nuclear magnetic resonance. Two gadolinium complexes, Dotarem® and Prohance®, are at present commercially available. These have chemical structures based on decahydro-2a,4a,6a,8a-tetraazacyclo-

pent[*fg*]acenaphthylene (synthesized in this chapter), alongside some of the other compounds within this chapter.

The primary goal of this project was to synthesize a ligand set that is in a predefined conformation so that it binds to the metal center in a predictable fashion. Work by Weissman *et al.*[64] described the use of cross-bridged cyclams that bind in a *cis-V* (Bosnich–Tobe) nomenclature[65]) with the metal ion binding within the ligand cleft. Securely bound to the four nitrogen lone pairs, this deters other coordination modes and possible decomplexation pathways.

This approach was utilized by Berg and co-workers.[71] Who efficiently applied a related cross-bridged cyclam to stabilize zirconium complexes, which effectively demonstrated the coordination of all four nitrogens in a X_4L_2 mode. This is one of the first examples of a cross-bridged cyclam to be deprotonated and coordinated to a metal center in such a fashion. Work by Weissman *et al*. had only exploited these cyclam systems in purely a L_4 manner, therefore limiting the scope of these versatile ligand sets.

It has been confirmed through the work of Schrock *et al.* that the use of chelating amido ligands sets can effectively stabilize titanium with a bound dinitrogen moiety.[42] The application of the cross-bridged cyclam to a small metal center such as titanium would provide excellent electronic stabilization without the requirement of ancillary ligands, leaving a large cavity for reactivity.

4.2 Synthesis and reactivity of tetraamines

Our route to the variety of tetraamines is shown in Scheme 7. The synthesis follows closely that reported by Athey and Kiefer in 2002,[66] although the synthesis of

these species was performed in a non-classical organic synthetic sense. Given that the nature of these systems investigated is both water and oxygen sensitive, they were handled under a strict nitrogen or argon atmosphere.

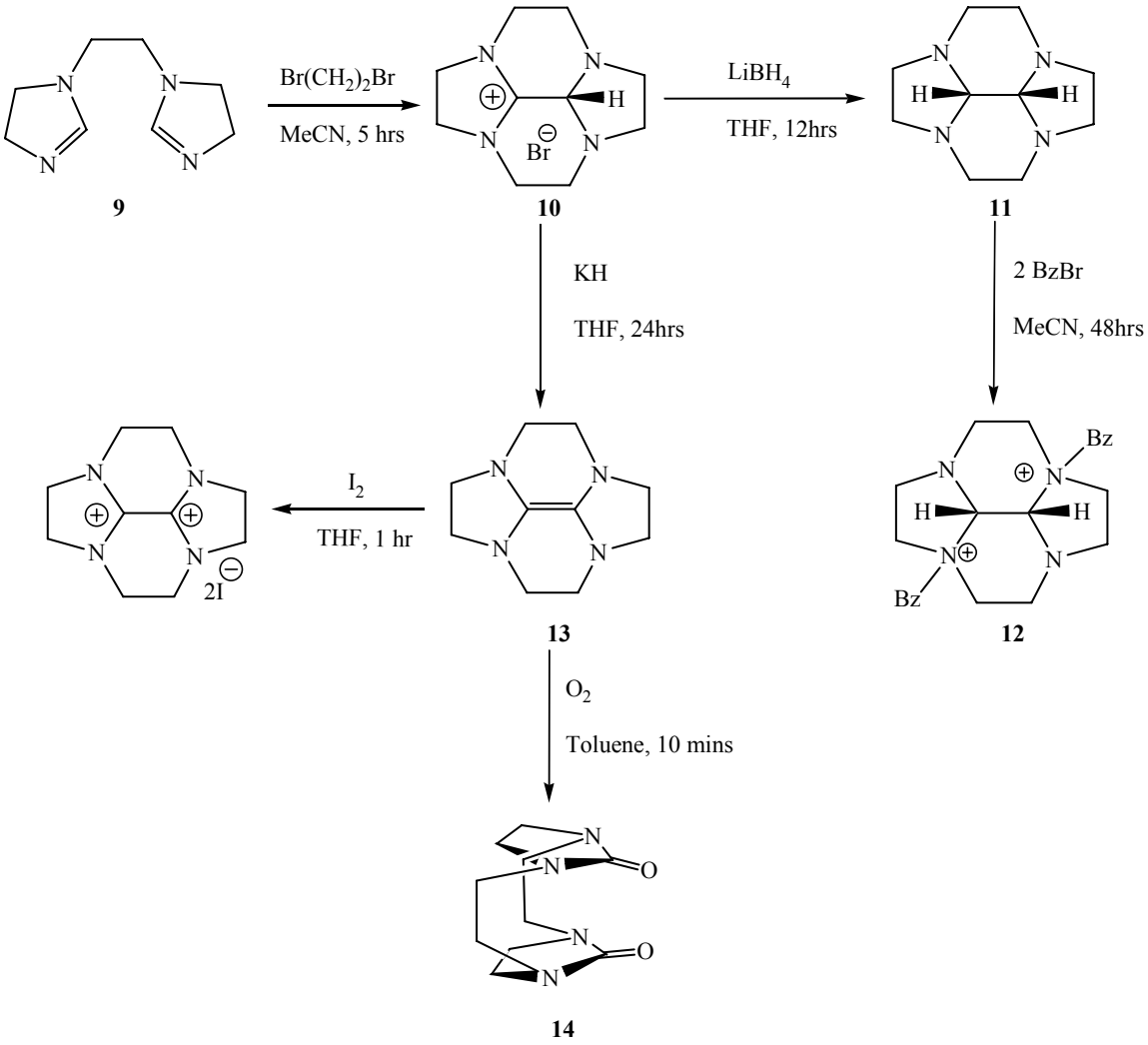

Scheme 4: General reaction scheme for the compounds synthesized in this chapter.

4.2.1 1,1'-Ethylenedi-2-imidazoline (9)

Formation of the diimidazoline, **9** is through the reaction of N,N-dimethylformamide dimethyl acetal with triethyltetraamine (TETA). TETA is exceedingly cheap, although comes as a mixture with its isomer tris(aminoethyl)amine (TREN) in a 65:35 ratio, pure TETA is expensive (one

hundred fold the cost). The two isomers may be separated by acidification using HCl in ethanol at 0 °C. HCl was slowly added to a solution of TETA/TREN, where upon the TREN·3HCl crystallizes out initially as a white crystalline solid, which was filtered and dried under reduced pressure. Continuation of the acidification process results in the formation of the TETA·4HCl as a silky pink colored, sweet smelling compound. Although the acidification process was carried out smoothly, the problem arose in the deprotonation of these species, initial separation from washing the hydrochloride salt with NaOH solution and abstracting organics in either toluene or benzene failed. Saturating the aqueous solution with brine also proved futile, one can only hypothesize that the tetraamine had bound to the cations in solution and prevented abstraction into any organic phase.

To bypass this problem, the reaction was carried out in the crude starting material (65:35), whereupon the N,N-dimethylformamide dimethyl acetal and the TETA/TREN mixture were refluxed under nitrogen for an hour without any added solvent. N,N-dimethylformamide dimethyl acetal is extremely acrid and is best conducted in a fume hood. The reaction mixture is cooled and dried under reduced pressure in order to remove methanol produced in this transformation, prior to being recrystallized in hot THF. If the drying process is not carried out, crystallization will not occur and an oil will separate from the solvent. The crystals are harvested and washed with diethyl ether and dried under reduced pressure, yields were quantitative based upon the amount of TETA in the starting material. Proton and carbon labeling is given in Figure 66, with the proton and carbon NMR spectral assignments given in Table 27.

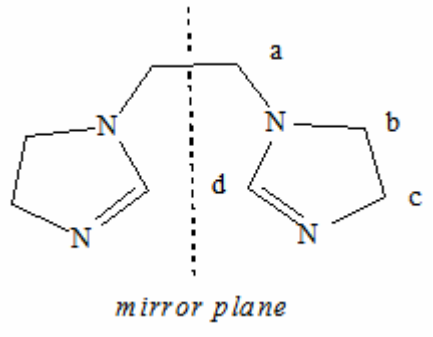

Figure 66: ^{1}H and ^{13}C NMR resonance labeling for 1,1'-Ethylenedi-2-imidazoline.

Table 27: ^{1}H and ^{13}C NMR assignment of 1,1'-Ethylenedi-2-imidazoline

Label	Carbon Signal (ppm)	Proton Signal (ppm)	Multiplicity	Coupling Constants
a	48.8	3.171	T	4.8 Hz
b	46.4	3.751	t of d	J = 9.6 Hz, J = 9.9 Hz
c	55.2	3.154	t of d	J = 9.6 Hz, J = 9.9 Hz
d	157.3	6.698	S	N/A

4.3.2 2,3,4,5,6,7,8,8c-Octahydro-1*H*-4a,6a,8a-triaza-2a-azoniacyclopent[*fg*]acenaphthylene bromide salt (10)

Compound **10** is a highly hygroscopic compound that was synthesized under strictly anhydrous conditions; it readily absorbs water from the air to form orange oil, which is extremely difficult to reverse. When pure, it exists as a bright yellow powder with purity < 98% (NMR), although forms colorless crystals when grown from diethyl ether. The synthesis of **10** was carried out on a Schlenk-line in a 2L flask fitted with a side arm containing compound **9** and potassium carbonate. Reactions were carried out at high dilution in acetonitrile and dibromoethane was added to the solution dropwise over the course of 5 hours at 50 °C. High dilution proved to be necessary to obtain moderate yields (63%), at higher concentration poorer yields of 40 to 45% were obtained. High dilution is predicted to promote cyclization and reduce polymeric side products. The reaction was allowed to proceed for an additional hour where the solution had changed to a characteristic orange color. The mixture was filtered to leave behind a white solid (presumably the potassium carbonate) and dried under reduced pressure. This reaction may also be carried out acetone, where the product crystallizes out of solution and can then be filtered and abstracted from the base with acetonitrile, although yields are lower by 10 to 15%. Recrystallization of the crude material was done so from an acetonitrile/ether solution.

The ^{1}H NMR spectrum of this species (like many of the reported compounds within this chapter) is very difficult to assign due to the fluctionality of these species in solution, combined with the quantity of nonequivalent protons that have

a large amount of peak area overlapping. The 2D NMR investigations used to assign the various protons for each compound were conducted by M. Bragg[67]. The results are summarized in the tables within this chapter.

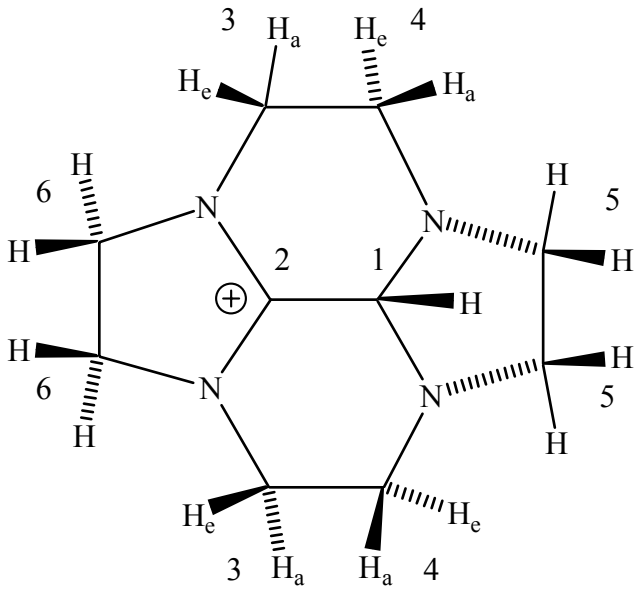

10

*Figure 67: NMR labeling system for compound **10**.*

4.3.3 Decahydro-2a,4a,6a,8a-tetraazacyclo-pent[*fg*]acenaphthylene (11)

Compound **11** is an extremely hygroscopic molecule and readily absorbs water reducing any solid material into an orange oil within 5 minutes. Any bound water within these systems causes the NMR spectra to become increasing broad and difficult to assign.[68] Synthesis was carried out in a similar manner to **10** upon a Schlenk line under nitrogen, in a round bottom flask fitted with a side arm. Compound **10** was dissolved in THF and cooled in an ice bath, whereupon a solution of $LiBH_4$ dissolved in THF was added dropwise over 5 minutes. The reaction was allowed to proceed for approximately 2 hours according to TLC (2:1 THF-MeOH),

the plates being pretreated with a washing of a 2% solution of Et_3N in the mobile phase. Compound **11** is then abstracted from the solution in hot toluene and dried under reduced pressure. Purification was generally carried out *via*

recrystallization in toluene or further through sublimation. Compound **11** is a waxy solid with a yield of 78%. This system was further analyzed through spectroscopy ^{1}H and ^{13}C NMR spectroscopy, alongside 2-D analysis by Bragg, Figure 68 illustrates the labeling scheme for the correlation with Table 29.

Table 28: NMR Assignment of 9.

C# Label	**^{13}C δ/ppm**	**^{1}H δ/ppm HSQC**	**^{2}J (J/Hz)**	**^{3}J(J/Hz)**	**COSY/ TOCSY**	**HMBC (C)**
1	71.98	4.42	na	Na	na	5
2	165.76	na	na	Na	na	na
3e	43.51	3.31	12.2	2.0,. 5.4	3a, 4e, 4a	4,2
3a		3.55	12.2	5.4, 9.8	3e, 4e, 4a	4, 6, 2
4e	44.29	3.19	14	2.0, 5.4	3a, 3e, 4a	3, 5, 1
4a		3.4	14	5.4, 9.8	3a, 3e, 4e	3, 5, 1
5	48.19	3.03	m	M	na	4, 1
6	51.04	3.9	m	M	na	2, 3

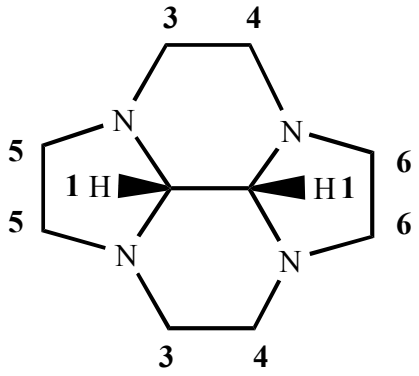

3

Figure 68: Depiction of decahydro-2a,4a,6a,8a-tetraaza-cyclopenta[fg]acenaphthylene (compound 11), the ^{13}C NMR spectrum for this species is particularly simple at room temperature with only five resonances (due to its high symmetry).

Table 29: Complete NMR Assignment of 11.

C# Label	^{13}C δ/ppm	^{1}H δ/ppm HSQC	^{2}J (*J*/Hz)	^{3}J(*J*/Hz)	COSY/TOCSY
1	71.72	na	na	na	na
2a	48.9	2.29	11.1	2.3, 11.1	2b, 3a, 3b
2b		2.79	11.1	2.3, 3.1	2a, 3a, 3b
3a	52.17	3	9.8	3.1, 11.1	3a, 2a, 2b
3b		2.58	9.8	2.3, 2.3	3b, 2a, 2b
4a	52.05	2.4	11.1	7.9, 7.7	4b, 5a, 5b
4b		3	11.1	9.7, 3.4	4a, 5a, 5b
5a	49.74	1.77	7.7	9.7, 7.7	5b, 4a, 4b
5b		2.92	7.7	7.9, 3.4	5a, 4a, 4b

4.3.4 2,3,4,5,6,7,8,8c-Octahydro-1*H*-4a,6a,8a-triaaza-2a-azoniacyclopent[*f*,*g*]acenaphthylene Bromide Salt

The benzylation of **11** was achieved by using an excess of benzyl bromide (2.5 equivalents), which according to literature, reports that best yields were achieved by stirring both **11** with benzyl bromide at room temperature for a period of three weeks,[69] which was a little absurd. Yields within 2% of those reported can be achieved within 24 hours at this reported temperature and concentration. Heating **11** in a solution of methanol and benzylbromide at 40 °C under an atmosphere of nitrogen for 24 hours leaves a brownish-colored solution, which was filtered, leaving a light brown precipitate. The precipitate was washed with diethyl ether and dried under reduced pressure. Recrystallization from hot methanol yielded pale-brown crystals that were analyzed through NMR spectroscopy and X-Ray crystallography. The NMR labeling scheme can clearly be seen in Figure 69 with the correlations from ^{1}H, ^{13}C, HMBC, TOSCY and COSY NMR experiments being given in Table 30.

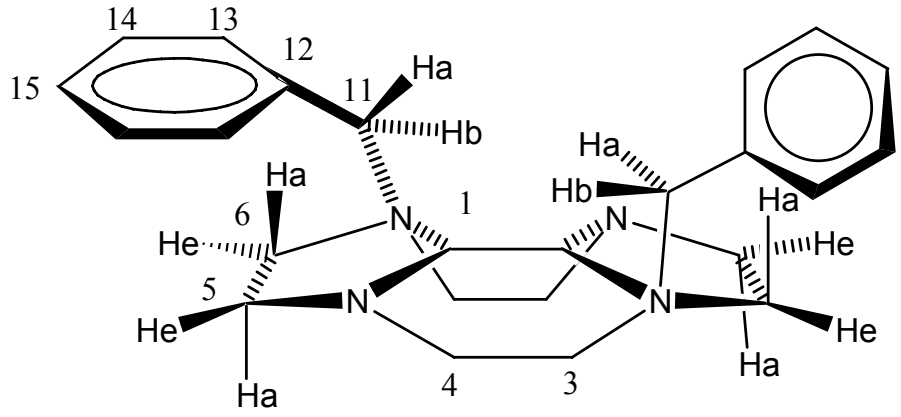

12

Figure 69: Side-view depiction of ***12****, the phenyl hydrogens have been omitted for clarity.*

*Table 30: NMR Assignment of **12**.*

H# Label	^{13}C δ/ppm	^{1}H δ/ppm	m	^{2}J (J/Hz)	^{3}J (J/Hz)	COSY/ TOCSY	^{j}HMBC (C)
1	79.4	3.18	s	N/A	N/A	none	3,4,6,11
3e up	55.98	3.44	ddd	13.2	2.8, 2.0	3e, 4a, 4e	1, 4, 11
3a dn		3.8	ddd	13.2	3.0, 13	3a, 4a, 4e	4, 11
4e dn	44.06	3.34	ddd	13.1	2.8, 3.0	4a, 3a, 3e	1
4a up		3.59	ddd	13.1	13.0, 2.0	4e, 3a, 3e	1, 3, 6
5e dn	62.34	3.54	m	15	5.3, 7.4	5e, 6a, 6e	3, 6, 11
5a up		4.4	ddd	15	5.3, 7.4	5e, 6a, 6e	3, 6, 11
6e up	47.64	3.27	m	-	-	6a, 5a, 5e	4, 5
6a dn		3.55	m	-	-	6b, 5a, 5e	1, 3
11a	62.15	4.94	ddd	13.1	N/A	11a	1, 3, 5, 12, 13
11b		5.15	ddd	13.1	N/A	11b	1, 5, 12, 13
12	128.4	N/A	N/A	N/A	N/A	N/A	N/A
13	133.91	7.68	d	N/A	7	14, 15	11, 15
14	130.97	7.51	m	N/A	N/A	13e	11, 12, 13, 15
15	132.45	7.51	m	N/A	N/A	13e	11, 12, 13, 14

4.3.5 1,2,3,4,5,6,7,8–Octahydro-2a,4a,6a,8a-tetraazacyclopenta[*f*,*g*]acenaphthylene (13)

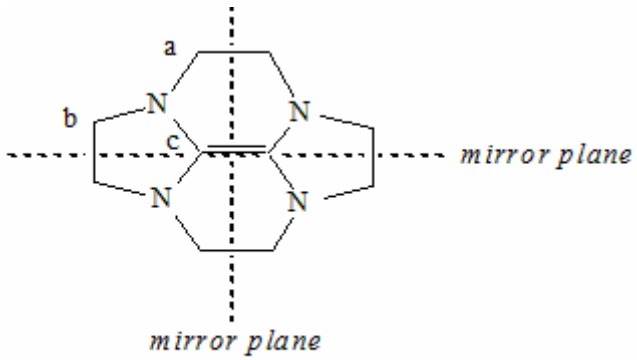

13

Figure 70: 1,2,3,4,5,6,7,8 –Octahydro-2a,4a,6a,8a-tetraazacyclopenta[f,g]acenaphthylene.

Compound **13**, shown in Figure 70**,** was synthesized in a strict inert atmosphere, in our case, an argon atmosphere in a dry box. Reactions were generally carried out in a round bottom flask in THF. Two equivalents of potassium hydride were added to stirring slurry of **10** in THF. The resulting mixture was allowed to react over a period of 24 hours, over this time period the solution paled from orange to pale-yellow. The THF was then removed under reduced pressure and **13** was abstracted using hot hexanes through a filter cannula. Crystallization occurs during filtration and can often block the cannula, although if conducted quickly enough, large crystals can be grown from the hot filtrate. This solution is then cooled to -30 ºC and then filtered cold to leave white crystalline material (**13**) in good yields of 72%. This can be further purified through sublimation, **13** readily sublimes at approximately 60 ºC and under vacuum (1.0 x -10^2 Torr). The crystals yielded from

sublimation are block and colorless. Compound **13** is highly air sensitive and reacts quickly upon exposure to form the diurea **14**.

4.3.6 Spectroscopic analysis and reactivity of 1,2,3,4,5,6,7,8–Octahydro-2a,4a,6a,8a-tetraazacyclopenta[*f,g*]acenaphthylene (13)

The ^{1}H NMR analysis of **13** is unsurprisingly very basic, due to the molecule being planar with two mirror planes crossing perpendicular through the centre of the system and observing D_{2h} symmetry. Figure 71 depicts the ^{1}H NMR spectrum of **13** ran in benzene-d_6, with two signals corresponding to the protons of the five-membered ring at 2.864 ppm and the protons of the six-membered ring at 2.672 ppm.

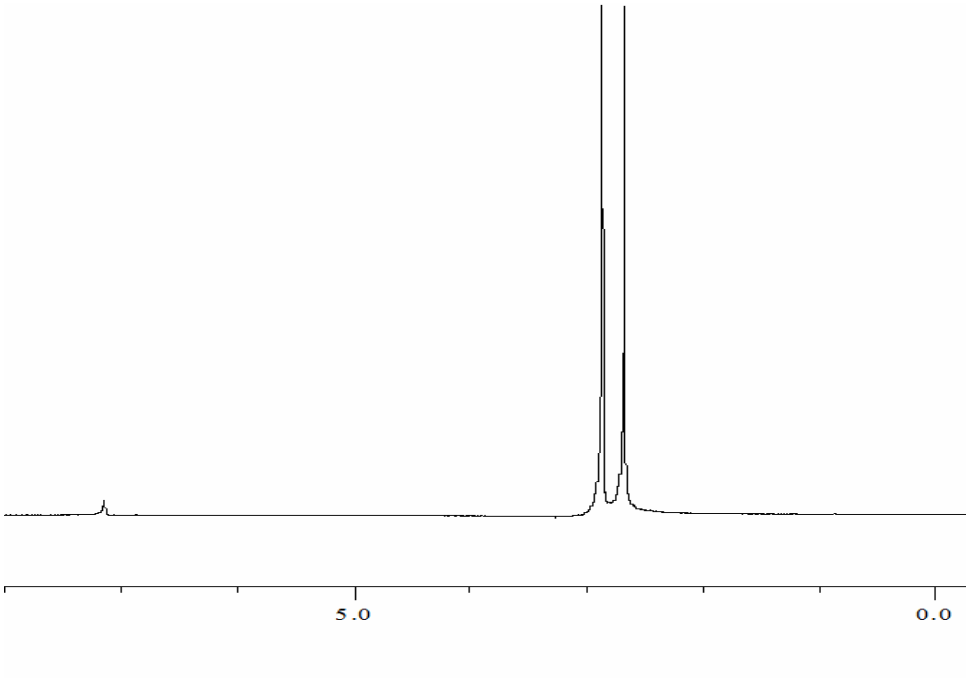

*Figure 71: ^{1}H NMR spectrum of **13** in benzene, clearly showing the two singlets that correlate to the protons in the 5- and 6-membered rings within the molecule.*

The ^{13}C NMR spectrum of this species is equally clear, with three signals correlating to the two different alkyl carbons and the third being the alkene carbon

that is a weak signal at 121.383, just up field of the benzene standard. The signal downfield of benzene is breakthrough. The carbon NMR spectrum is shown below in Figure 72, with the proton and carbon NMR spectral assignments given in Table 31.

4.3.6.1 Alkene oxidation reactivity.

The properties of compound **13** are very similar to Tetrakis(dimethylamino)ethene (TDAE), which has been termed 'organic zinc' due to the reductive power. Compound **13** also demonstrates to be a good reducing agent, in an experiment where HgO and compound **13** were taken up in toluene and refluxed

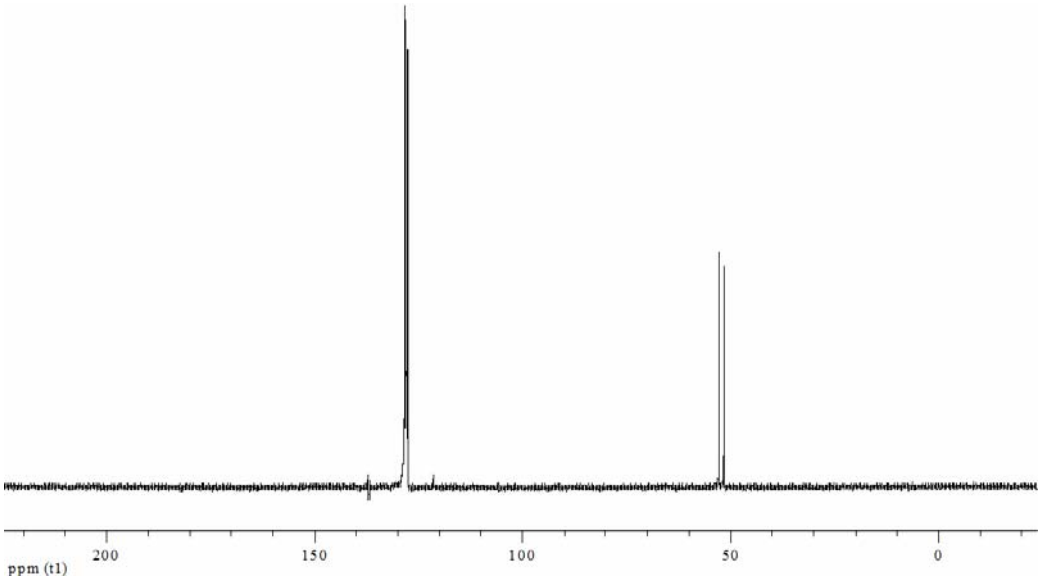

*Figure 72: The ^{13}C NMR spectrum of **13** in benzene-d_6, clearly showing the two resonances that correlate to the carbons in the 5- and 6-membered rings within the molecule.*

for several days under an atmosphere of nitrogen. $Hg_{(l)}$ and the oxidized product of **13** (a diurea discussed as compound **14** in this chapter) were formed.

Similarly, dissolving **13** in a solution of toluene under an atmosphere of dinitrogen in a Schlenk tube and inserting a needle to bubble a stream of dioxygen through this mixture caused an instantaneous reaction and a white precipitate to form. This white precipitate was found to be compound **14**. The mechanism proceeds presumably as presented in Scheme 5 below:

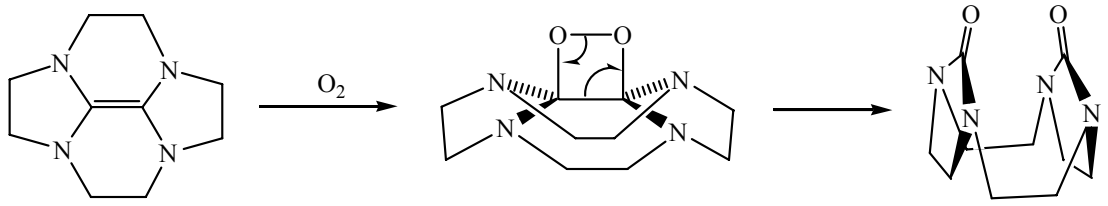

*Scheme 5: A mechanistic scheme of the reaction of **13** with dioxygen.*

*Table 31: The ^{13}C NMR assignment for **13***

Label	Carbon Signal (ppm)	Proton Signal (ppm)	Multiplicity	Coupling Constants
a	51.542	2.672	S	N/A
b	52.797	2.864	S	N/A
c	121.383	N/A	N/A	N/A

Compound **13** also reacts readily with halides to form the dicationic tetraamine shown in Figure 73, this compound was only formed when **13** was slowly added to one equivalent of I_2 in a stirring toluene solution. The bright orange dication readily drops out of solution, the solvent is filtered and the product is washed with diethyl ether and dried under reduced pressure. The dication shows some, although poor, solubility in methanol, which it may be recrystallized from. Adding the I_2 to a stirring solution of **13** in toluene results in what is speculated to be a free radical polymerization of **13** precipitating out all of the starting material as a white insoluble solid.

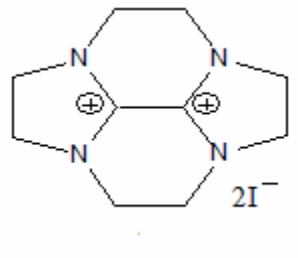

Figure 73: The tetraamine dication iodide.

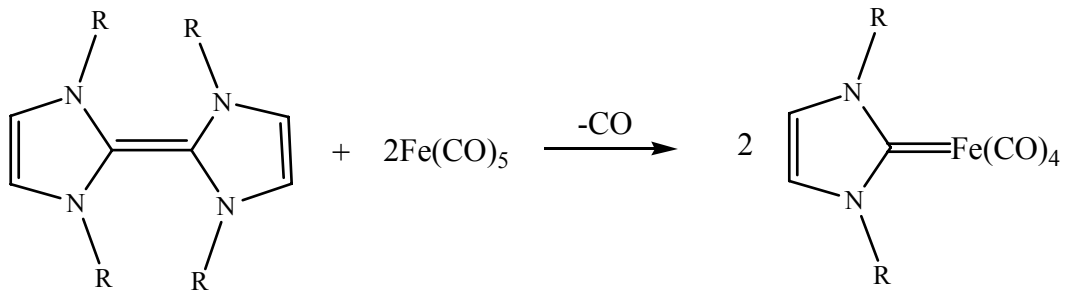

Scheme 6: Lappert's N-Heterocyclic Carbene (NHC) production through olefin insertion.

Compound **13** also exhibits a surprising resistance to olefin insertion by metal ions, it was envisaged that the compound could undergo metal insertion to form the *bis* NHC (N-heterocyclic carbene) ligand (Scheme 6) in a similar fashion to Lappert and co-workers[70] although showed frustrating resilience. For these reactions; compound **13** was refluxed in THF or toluene for 48 hours under nitrogen with 1 equivalent of $Fe(CO)_5$, $FeCl_2$ or $FeCl_3$. Work up and isolation resulted in the recovery of the starting material.

Scheme 7 depicts a reaction where compound **13** was refluxed in a sealed ampoule for 78 hours in toluene. This was carried out in order to observe the formation of the 2+2 cyclo-addition of two of these molecules, although no such product was observed.

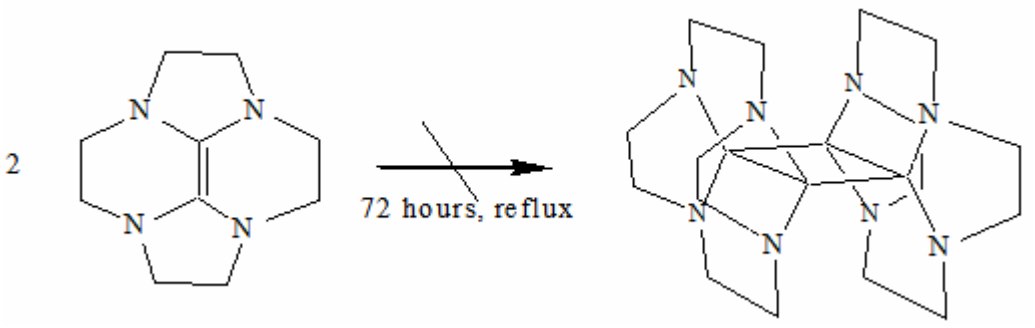

Scheme 7: Attempted [2+2] cycloaddition of ***13***

The dropwise addition of a four equivalents of **13** into a stirring solution of S_8 in toluene hoped to yield the disulfur bridged adduct depicted in Scheme 8, although no such monomer was formed. The reaction quickly formed a black precipitate presumed to be a polymer that was insoluble in all solvents.

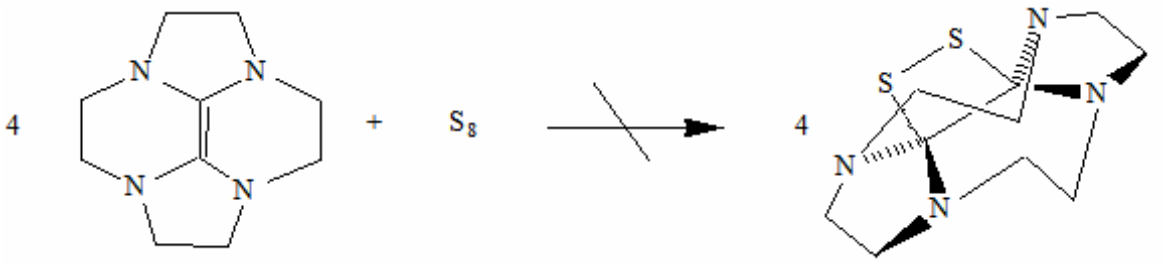

Scheme 8: Attempted reaction of ***13*** *with sulfur and the predicted monomeric product.*

4.3.6.2 Investigation into the Magnetism of 1,2,3,4,5,6,7,8–Octahydro-2a,4a,6a,8a-tetraazacyclopenta[*f*,*g*]acenaphthylene

Most organic materials are diamagnetic, in which all electron spins are paired in an anti-parallel fashion and their magnetic moments cancel, this is depicted in Figure 74, (**A**). Due to the highly reactive nature of unpaired electrons, there are only

a handful of organic materials that contain stable radicals. If the interactions between the molecules are absent or weak, a random orientation of the electron spins occurs, resulting in a paramagnetic material. There is an overall cancellation of the electron magnetic moments if there is no external magnetic field applied (**B**).

If a non-negligible interaction between the unpaired electrons is present, a three dimensional ordering of the electron spins occurs below a critical temperature, *T*c. The ordering can take several different forms; in an antiferromagnetic ordering (**C**) all spins align in an anti-parallel fashion so that the net magnetic moment is zero. In a ferrimagnetic material (**D**) an antiferromagnetic interaction between spins of different strength occurs, however, they do not cancel completely. Ferromagnetism (**E**) is a state in which all spins are aligned in one direction and the critical temperature, *T*c, below which a material becomes ferromagnetic, is called the Curie

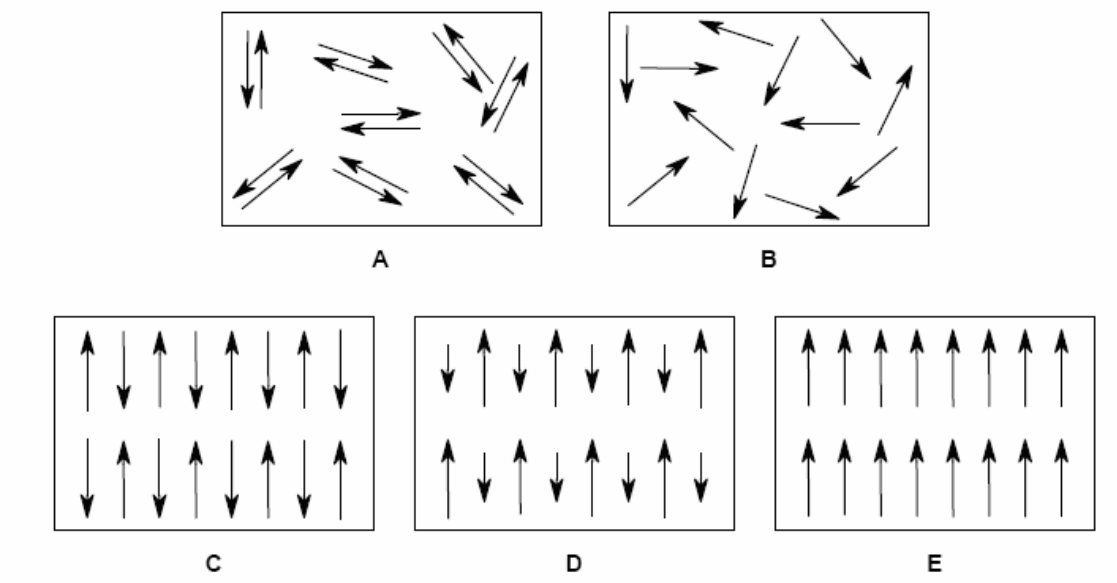

Figure 74: Materials with different types of electron spin orientations; diamagnetic (A),paramagnetic (B), antiferromagnetic (C), ferrimagnetic (D), ferromagnetic (E).

temperature. At this temperature the interaction energy between the spins becomes larger than the thermal energy of the spins and an ordering of unpaired electron spins takes place. Since the interaction energies in most organic compounds are rather small, low *T*c values are commonly observed.

One of the few pure organic ferromagnets was tetrakis(dimethylamino)ethene (TDAE) that was reported to form a reductive intercalate with C_{60}, which has proven to be a weak ferromagnet at temperatures ~ 16 K, which is unusually high for an organic system.

Compound **13** is of obvious interest due to it being a direct analog of TDAE and wanted to observe similar properties once intercalated with C_{60}. In an equal molar ratio C_{60} and **13** were finely ground, mixed and carefully placed within a glass tube which was flame sealed and placed within an oven to be baked over a period of a week at 250ºC. Over this period the mixture turned from black soot to obsidian like material with crystalline regions.

The SQUID data for this sample was collected by Michelle Dolgos at variable temperatures to measure the magnetic susceptibility of **13**, shown in Figure 75. The magnetic ordering below T_C = 22 K which is compares to the TDAE-C_{60} intercalate that observes a T_C of 16 K. The magnetic properties of these species can are due to the organic charge-transfer salt $[\mathbf{13}]^{+\cdot}[C_{60}]^{-\cdot}$, these initial findings indicate that the intercalate of [**13**]-C_{60} has the highest recorded Currie temperature of any known strictly organic species.

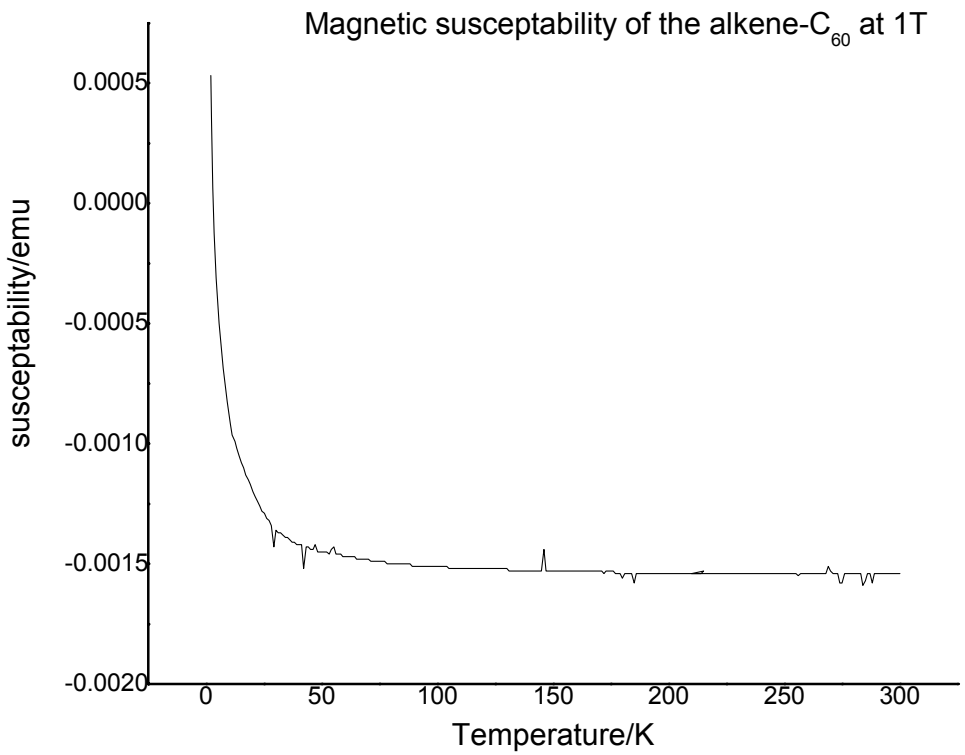

Figure 75: The magnetic susceptibility of the alkene-C_{60} complex clearly showing the critical point where the magnetic susceptibility is theoretically infinite.

4.3.7 1,4,7,10-Tetraaza-tricyclo[8.2.1.14,7]tetradecane-13,14-dione (12)

The diurea shown in Figure 76 is made by taking **13** in a solution of hexane and bubbling O_2 through the solution, this readily oxidizes the alkene bond to form the diurea. Once oxidized the compound is stable and stored on the bench as colorless crystals in a vial.

Compound **14** was synthesized initially from an experiment to test the reducing power of **13** through the reaction of **13** with HgO, the reaction was very slow and after about a week, the NMR was taken of the resulting species to reveal this diurea. The diurea itself is known, although in its *anti* conformer, the species formed through oxidation of **13** is the first example of this species in its *syn* conformation.

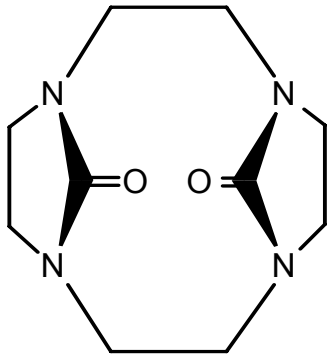

6

*Figure 76: 1,4,7,10-Tetraaza-tricyclo[8.2.1.14,7]tetradecane-13,14-dione (**13**)*

4.3.8 Spectroscopic analysis of 1,4,7,10-Tetraaza-tricyclo[8.2.1.14,7]tetradecane-13,14-dione (14)

The NMR spectral analysis of **14** in D_2O is shown below with the symmetry of **13** clearly broken, along with a substantial shift down field. Figure 77 depicts the ^1H NMR spectrum, with an expansion of the alkyl region to see the splitting on the ring proton signals (marked **a** and **a1**). Integration of these peaks reveals a ration of 4:8:4 which are what would be predicted.

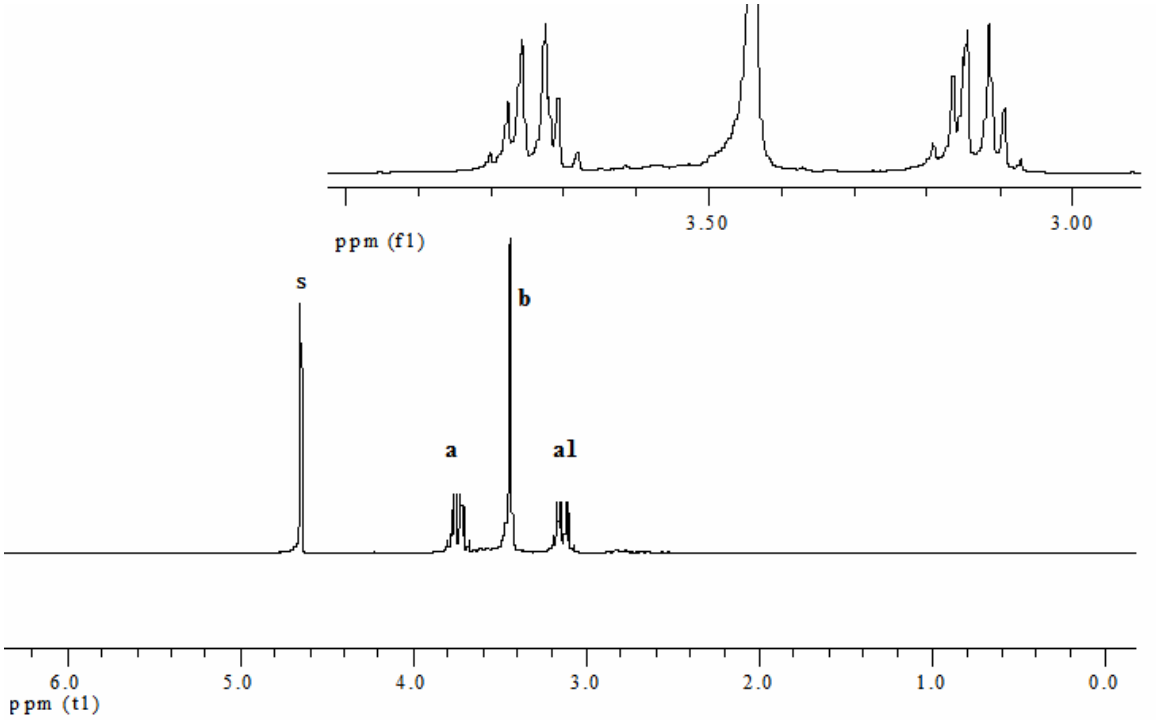

*Figure 77: ^1H NMR spectrum of the diurea **14**, with the expansion of the alkyl resonances superimposed.*

Table 32: ^{1}H and ^{13}C NMR assignment for 14.

Label	Carbon Signal (ppm)	Proton Signal (ppm)	Multiplicity	Coupling Constants
a	39.3	3.741	M	N/A
a1	39.3	3.131	M	N/A
b	48.7	3.437	S	N/A

Crystals for this compound were grown from methanol and crystallized out as the H_2O adduct, probably due to the trace amounts of water that contaminated the methanol.

4.4 Discussion and future work

The original focus of this chapter was to design a versatile ligand for our various titanium systems until publications from Berg and co-workers.[71] Although the ultimate goal of this project was ruined, the project bore forth excellent experimental data that had not been previously resolved or published. It also fashioned the novel compound **13**, this compound was particularly exciting, through its range of unique electronic, steric and reactive properties.

5 Experimental Section

5.1 General Considerations

Unless stated otherwise, all operations were performed in a MBraun dry box under an atmosphere of purified argon or using Schlenk techniques under an argon atmosphere using flamed-dried 316 stainless steel cannulæ and flame-dried Schlenk flasks. All solvents were dried by refluxing in a still over the appropriate drying agent (as indicated in Table 33). Solvents were then harvested from the still collection bulb via canula into an ampule fitted with Teflon screw-cap.

Table 33: The drying methods for various solvents.

Solvent	Drying Agent	Stored Over
Acetonitrile	Calcium Hydride	Molecular Sieves
Benzene	Potassium	Potassium
Chloroform	Calcium Hydride	Molecular Sieves
Dichloromethane	Calcium Hydride	Molecular Sieves
Diethylether	Sodium-Potassium Alloy	Molecular Sieves
Hexanes	Potassium	Potassium
Pentane	Sodium-Potassium Alloy	Potassium
Tetrahydrofuran	Potassium	Molecular Sieves
Toluene	Sodium	Sodium

Hydrocarbons and ethers were taken into the dry box and were tested by taking an aliquot of the solvent and adding a drop of sodium/benzophenone dissolved in tetrahydrofuran (THF), the resulting solution retains the deep blue color of the radical anion. *Bis*(tetrahydrofuran)titanium tetrachloride was prepared by treating a solution of doubly distilled $TiCl_4$ in dichloromethane with a solution of THF in the same solvent at -78 °C; the resultant yellow precipitate was filtered cold, washed with pentane and dried under reduced pressure. Other chemicals were used as supplied. Deuterated solvents were purchased from Cambridge Isotopes and were further dried under the appropriate drying agent and referenced to the residual solvent proton peak, given in Table 34. The chemical shift for ^{31}P is reported with respect to 85% aqueous H_3PO_4 (0 ppm).

^{31}P, ^{1}H and ^{13}C NMR spectra were recorded on Varian Mercury 300 or Bruker INOVA-400 spectrometers at room temperature, unless indicated otherwise. Elemental analysis was carried out at Complete Analysis Laboratories, Inc. Parsippany, New Jersey.

Table 34: Various deuterated solvents used for analysis of compounds discussed within this document.

Solvent	Drying Agent	Stored Over	^{1}H chemical shift (ppm from TMS), (Multiplicity)	^{13}C Chemical Shift (ppm from TMS), (Multiplicity)
Acetonitrile-d_6	Calcium Hydride	Calcium Hydride	1.94 (5)	118.69 (1), 1.39 (7)
Benzene-d_6	Potassium	Potassium mirror	7.16 (1)	128.39 (3)
Chloroform-*d*	Used as received	Molecular Sieves	7.24 (1)	77.23 (3)
Deuterium Oxide	N/A	N/A	4.80 (1)	N/A
Methanol-d_4	Used as received	Molecular Sieves	4.78 (1), 3.31 (5)	49.15 (7)
Methylene Chloride-d_2	Calcium Hydride	Molecular Sieves	5.32 (3)	54.00 (5)
Tetrahydrofuran-d_8	Potassium-Sodium Alloy	Potassium-Sodium Alloy	3.58 (1), 1.73 (1)	67.57 (5), 25.37 (5)
Toluene-d_8	Potassium	Potassium mirror	7.09 (m), 7.00 (1), 6.98 (5), 2.09 (5)	137.86 (1), 129.24 (3), 128.33 (3), 125.49 (3), 20.4 (7)

Single crystal X-ray diffraction data were collected using a Bruker AXS Smart 1000 Diffractometer equipped with a CCD area detector and graphite monochromatized Mo source (Mo $K_{\square}$, 0.71073 Å), with a crystal–to–detector distance of 5.0 cm. Low temperature data collections were completed using a Nicolet LT-2 cooling device, in which the crystals were coated in paratone oil and mounted on a cryoloop. The data were collected using a frame with of ~0.3° and an exposure time of 20 seconds per frame. Data reduction and spherical atom analyses were carried out using Saint. A multi-scan absorption correction was made using SADABS. The spherical atom structures were solved by direct methods (SHELXTL) refined by the full matrix least squares method and completed by a series of difference Fourier syntheses. All non-hydrogen atoms were refined anisotropically, with hydrogen atoms being introduced at idealized positions and refined using a riding model.

5.2 Experimental methodology

5.2.1 Dihydrodibenzoazepinyl lithium

Iminodibenzyl (10 g, 0.05 moles) and toluene (200 mL) were added to a round bottom flask (500mL) within a drybox, the resulting slurry was cooled to -40 °C. To

this stirring suspension was added *t*-butyl lithium in a pentane solution (1.7 M, 100 mL, -40°C), dropwise over the course of 15 minutes. The solution was then allowed to stir and warm to room temperature over a period of 2 hours, whereupon it was cooled to -40 °C in the dry box freezer and then filtered cold through a fine frit, washed twice with hexanes (30 mL), twice with pentane (30 mL) and dried under reduced pressure, which yielded an extremely fine white powder, 8.25g (82% yield, based on iminodibenzyl). Purity was assessed through NMR. ^{1}H NMR (THF-d_8): δ 2.89 (s, 4H), 6.05 (t, J = 7.2 Hz, 2H), 6.48 (d, J = 8.1 Hz, 2H), 6.55 (d, J = 7.2 Hz, 2H), 6.63 (t, J = 7.2 Hz, 2H). ^{13}C NMR (THF-d_8): δ 156.37, 131.46, 129.83, 125.97, 123.35, 111.67, 39.47.

5.2.2 *tris*(Dihydrodibenzoazepinyl)titanium chloride (1)

Finely ground $TiCl_4$·2THF (5 g 0.015 moles) and toluene (200 mL) were added into a round bottom flask (500 mL) and cooled to -40 °C. The resulting yellow slurry was vigorously stirred and to it was added a solution of ddaLi (9.05 g, 0.045 moles) also in a slurry with toluene (100mL, -40°C), dropwise over 15 minutes. Upon the addition of ddaLi**,** the reaction initiates immediately, even at low temperature, with an instant coloration of the solution that can be observed. The solution was allowed to stir and warm to room temperature for 6 hours, where it proceeded to form a dark red colored solution, it was then filtered through a fine frit to remove what is presumed to be the LiCl byproduct and washed 3 times with

toluene (30mL) to ensure complete abstraction of the product. The filtrate was then dried under reduced pressure; recrystallization from toluene/hexane yields an orange crystalline powder, 7.28g (73% yield based from the starting materials). Purity was assessed through NMR. ^{1}H NMR (300 MHz, Toluene-d_8): δ 2.27 (s-broad, 6H), 2.87 (s-broad, 6H), 6.73 (d of d, J = 4.5Hz, J = 5.7Hz, 6H), 6.81 (m, 12H), 7.31 (d of d, J = 4.2Hz, J = 4.8Hz, 6H). ^{13}C NMR (75 MHz Toluene-d_8): δ 151.04, 132.74, 130.54, 126.73, 126.23, 125.98, 31.55.

5.2.3 *bis*(Dihydrodibenzoazepinyl)titanium dichloride (2)

Into a glass round bottom flask (500 mL) was added finely ground $TiCl_4$·2THF (5 g 0.015 moles) and toluene (200 mL), the resulting suspension was then cooled to -40 °C. A solution of ddaLi (6.03 g, 0.030 moles) in a slurry with toluene (100 mL, -40 °C), was added dropwise over the course of 15 minutes. Upon addition of the ddaLi**,** the reaction starts immediately, even at low temperature and the instant dark coloration of the solution can be observed. The solution was allowed to stir and warm to room temperature for 6 hours, over which period the solution turns a dark red color, it was then filtered through a fine frit to remove what is presumed to be the LiCl byproduct and washed 3 times with toluene (30 mL) to ensure maximum yield. The filtrate was then dried under reduced pressure; recrystallization from toluene/hexane yields an orange crystalline powder, 4.54 g

(60% yield). Purity was assessed through NMR. ^{1}H NMR (THF-d_8): δ 2.99 (s, 8H), 7.05 (m, 8H), 7.15 (m, 4H), 7.42 (d, J = 6.0Hz, 4H).

5.2.4 *tris*(Dihydrodibenzoazepinyl)titanium borohydride (3)

Into a glass round bottom flask (500 mL) was added **3** (5 g 7.77 mmoles), toluene (200 mL), to this stirring dark red slurry was added lithium borohydride (195.8 mg, 9.32 mmoles) also in a slurry with toluene (50 mL). The solution was allowed to stir at room temperature for 18 hours, over which period it paled in color to a light orange, it was then filtered through a fine frit, washed 3 times with toluene (30 mL) and then the filtrate was dried under reduced pressure. Recrystallization from toluene/hexane yields a yellow crystalline powder. Purity was assessed through NMR. ^{1}H NMR (THF-d_8): δ 2.27 (d of d, J = 11.7Hz, J = 6.3Hz, 6H), 2.87 (d of d, J = 11.5Hz, J = 6.3Hz, 6H), 6.73 (d, J = 5.4Hz, 6H), 6.81 (t, J = 5.7Hz, 6H), 6.81 (t of d, J = 5.4Hz, J = 1.2Hz, 6H), 7.31 (d, J = 5.7Hz, 6H). ^{13}C NMR (THF-d_8): δ 151.64, 133.50, 131.17, 127.08, 126.88, 126.42, 32.04.

5.2.5 *tris*(Dihydrodibenzoazepinyl)[(dimethylphosphino)-methyl]titanium (4)

Compound **2** (1 g 1.55 mmoles) and toluene (50 mL), were put into a round bottom flask (250 mL), the resulting suspension was cooled to -40 °C and with vigorous

stirring, (dimethylphosphino)-methyl lithium (619.5 mg, 1.55 mmoles), also in a toluene solution (10mL, -40 °C), was added dropwise over 15 minutes. The solution was then allowed to stir and warm to room temperature over a period of 2 hours, whereupon it was filtered through a fine frit, washed 3 times with toluene (20 mL) and then the filtrate was dried under reduced pressure. Recrystallization from toluene/hexane yields bright red crystalline powder, 1.02g (91% yield). Purity was assessed through NMR. ^{1}H NMR (Toluene-d_8): δ 0.72 (d, J = 3.3 Hz, 6H,), 1.94 (s, 2H), 2.45 (s-broad, 6H), 3.27 (s-broad, 6H), 6.83 (m, 12H), 6.94 (m, 6H), 7.43 (d, J = 7.5Hz, 6H). ^{13}C NMR (75 MHz THF-d_8): δ 19.37 (d (C-P), 19.5Hz), 32.47, 32.55 (d (C-P), 12.3Hz), 125.91, 126.77, 126.80, 133.81, 151.25. ^{31}P NMR (300 MHz, THF-d_8): δ -33.09 (s).

5.2.6 *tris*(Dihydrodibenzoazepinyl) titanium methyl (5)

Into a glass round bottom flask (200mL) was added **2** (1 g 1.55 mmoles) in a toluene slurry (50 mL), the solution was cooled to -40 °C and with vigorous stirring, the methyl lithium (34mg, 1.55 mmoles) in a toluene solution (10mL, -40 °C), was added dropwise over 15 minutes. The solution was allowed to stir and warm to room temperature over a period of 1 hour and then filtered through a fine frit, washed 3 times with toluene (20 mL) and then the filtrate was dried under reduced pressure. Recrystallization from toluene/hexane yields bright red crystalline powder, 890mg (89% yield). Purity was confirmed through NMR. ^{1}H NMR (300 MHz, THF-d_8): ^{1}H

NMR (300 MHz, THF-d_8): δ 0.56 (s, 3H), 2.43 (s, 6H), 3.08 (s, 6H), 6.90 (m, 12H), 7.0 (m, 6H), 7.26 (d, J = 5.4Hz, 6H). ^{13}C NMR (75 MHz THF-d_8): δ 150.74, 134.52, 131.25, 127.17, 127.10, 126.16, 61.11, 32.67.

5.2.7 Carbazolyl lithium

Into a glass round bottom flask (500 mL) was added carbazole (10 g, 0.06 moles) and toluene (200 mL) which were then cooled to -40 °C. To this stirring solution was added *t*-butyl lithium in a pentane solution (1.7 M, 110 mL, -40 °C), dropwise over the course of 15 minutes. The solution was then allowed to stir and warm to room temperature for a period of 2 hours, filtered through a fine frit, washed twice with hexanes (30 mL), twice with pentane (30 mL) and dried under reduced pressure. This yielded an extremely fine white/tan powder, 9.57g (93% yield, based from starting carbazole). Purity was assessed through NMR. ^{1}H NMR (THF-d_8): δ 6.72 (t, J = 7.2 Hz, 2H), 7.03 (t, J = 7.2 Hz, 2H), 7.32 (t, J = 8.1 Hz, 2H), 7.91 (t, J = 7.5 Hz, 2H). ^{13}C NMR (THF-d_8): δ 153.49, 125.89, 122.49, 119.46, 114.79, 113.16.

5.2.8 *tris*(Carbazolyl)titanium chloride (6)

Into a glass round bottom flask (500 mL) was added finely ground $TiCl_4$·2THF (5 g 0.015 moles), toluene (200 mL) and cooled to -40 °C, to this

vigorously stirred yellow slurry was added a solution of carbazolyl lithium (7.52 g, 0.045 moles) also in a slurry with toluene (100 mL, -40 °C), dropwise over 15 minutes. Upon addition of the carbazolyl lithium**,** the reaction is assumed to start immediately as an instant dark coloration of solution can be observed. The solution was allowed to stir and warm to room temperature for 12 hours, where it proceeded to form a dark blue colored solution, it was then filtered through a fine frit to remove the LiCl byproduct and washed 3 times with toluene (30 mL). The filtrate was then dried under reduced pressure with recrystallization from a toluene/hexane solution dark blue crystalline powder, 6.20g 57% yield. Purity was assessed through NMR. ^{1}H NMR Benzene-d_6): δ 1.165 (s, 8H), 3.704 (s, 8H), 6.967 (m, 6H), 7.039 (m, 6H), 7.648 (dd, 7.2Hz, 1.5Hz, 6H), 8.109 (d, 8.4Hz). ^{13}C NMR (Benzene-d_6): δ. 124.287, 118.707, 126.438, 123.793, 122.439, 149.263.

5.2.9 *bis*(Carbazolyl)titanium dichloride (7)

Finely ground $TiCl_4 \cdot 2THF$ (5 g 0.015 moles) and toluene (200 mL) were added into a round bottom flask (500 mL) and subsequently cooled to -40 °C, to this vigorously stirred yellow slurry was added a suspension of CbLi (5.01 g, 0.030 moles) also in toluene (100 mL, -40 °C), dropwise over 15 minutes. Upon addition of the lithium salt**,** the reaction starts immediately, with the instant dark coloration of the solution. The solution was then allowed to stir and warm to room temperature for 6 hours, over which period it fashioned a dark blue colored solution. This was then

filtered through a fine frit to remove the LiCl byproduct and washed 3 times with toluene (30 mL) to ensure maximum yield. The filtrate was then dried under reduced pressure; recrystallization from toluene/hexane yields a dark blue crystalline powder, 54% yield. Purity was assessed through NMR. ^{1}H NMR (Benzene-d_6: δ 1.16 (s, 8H), 3.735 (s, 8H), 7.686 (d, 7.5Hz, 4H), 7.23 (m, 8H), 8.109 (d, 8.1Hz, 4H).

5.2.10 *tris*(Carbazolyl) titanium methyl (8)

Compound **6** (1.0 g 1.71 mmoles) was mixed with toluene (50mL), the resulting suspension was then cooled to -40 °C, with vigorous stirring, methyl lithium (38 mg, 1.55 mmoles) in a toluene solution (10 mL, -40 °C), was added dropwise over a period of 15 minutes. The solution was allowed to stir and warm to room temperature over a period of 1 hour and then filtered through a fine frit, washed 3 times with toluene (20 mL) and then the filtrate was dried under reduced pressure. Recrystallization from toluene/hexane yields bright red crystalline powder 81%. Purity was confirmed through NMR. ^{1}H NMR (THF-d_8): ^{1}H NMR (benzene-d_6): δ 7.497 (d of t, J=8.1Hz, J=0.9Hz, 6H), 6.827 (t of d, J=8.1Hz, J=0.9Hz 6H), 7.037 (t of d, J=7.8Hz, J=0.9Hz, 6H), 7.812 (ddd, J=8.1Hz, J=0.6Hz, J=0.9Hz, 6H). ^{13}C NMR (benzene-d_6): δ 124.154, 115.885, 127.297, 123.623, 120.006, 146.254.

5.2.11 1,1'-Ethylenedi-2-imidazoline (9)

Into a round bottom flask (500 mL), was added N, N-dimethylformamide dimethyl acetal (18 g,) and technical grade (60:40 TETA:TREN) tetraamine (10 g, 0.058 moles of TETA), this reaction vessel was purged with nitrogen for 10 minutes and fitted with a reflux condenser. The solution was then heated at reflux for an hour without the addition of solvent, it was then dried upon a rotavaporator at 60ºC for 45 minutes and recrystalized from hot THF, washed with diethylether and pumped to dryness on a vacuum line, yielding white crystals 8.97 g (equivalent yield based on % of TETA used). Purity was assessed through NMR. ^{1}H NMR ($CDCl_3$): δ 6.71 (s, 2H), 3.75 (t, J = 9.9 Hz, 4H), 3.17 (m, 8H) ppm. ^{13}C NMR ($CDCl_3$): δ 157.3, 55.2, 48.8, 46.4 ppm..

5.2.12 2,3,4,5,6,7,8,8c-Octahydro-1*H*-4a,6a,8a-triaaza-2a-azo-niacyclopent[*fg*]acenaphthylene bromide Salt (10)

Potassium carbonate (4.0g, 0.012 moles), **9** (6g, 0.036 moles) and acetonitrile (800 mL) were put into a large round bottom flask (2 L) fitted with a side arm. The solution was purged with nitrogen for 20 minutes and fitted with a reflux condenser. Dibromoethane (9g, 0.049 moles) was then syringed into the solution and it was then heated at reflux for a period of 5 hours, during which time the solution turns an orange color. The Reaction is then filtered (due to hygroscopic nature of the resulting compound all work up is done under a strict nitrogen atmosphere upon a vacuum line and the resulting product was stored in a dry box) and pumped to dryness and then recrystallized from acetonitrile/ether, washed with ether and dried under reduced pressure. Purity was assessed through NMR. ^{1}H NMR (acetonitrile-d_3): δ 4.42 (s,

1H), 3.9 (m, 4H), 3.55 (ddd, J = 5.4 Hz, J = 9.9 Hz, J=12.4 Hz, 2H), 3.4 (ddd, J = 5.3 Hz, J = 9.7 Hz, J = 14.0 Hz, 2H), 3.31 (ddd, J = 2.8 Hz, J = 5.5 Hz, J = 12.1 Hz, 2H), 3.19 (ddd, J = 2.0 Hz, J = 5.4 Hz, 13.9 Hz, 2H), 3.03 (m, 4H) ppm. ^{13}C NMR (acetonitrile-d_3): δ 165.76, 71.98, 51.04, 48.19, 44.29, 43.51 ppm.

5.2.13 Decahydro-2a,4a,6a,8a-tetraazacyclopent[*fg*]acenaphthylene (11)

A round bottom flask fitted with a side arm was taken into the dry box, **10** (5 g, 18.4 mmoles) was added and the flask sealed using a glass stopper and silicon grease. The reaction flask was then taken and attached to a schlenk line, whereupon the reaction solvent (EtOH, 200 mL) was canulated into the flask. The reaction was then cooled using an ice slush bath and a slurry of $LiBH_4$ (2.02g, 92 mmoles) in EtOH (50 mL) was added dropwise over a period of 10 minutes. The reaction was allowed to proceed for approximately 2 hours according to TLC (2 THF: 1 MeOH), the plates being pretreated with a washing of a 2% solution of Et_3N in the mobile phase. The reaction bleaches in color until completion where the solution should be colorless with a white precipitate. The solution is then filtered and the solvent removed under reduced pressure and the product abstracted in toluene (3 x 50mL). The toluene is then removed under reduced pressure and the resulting compound can be further purified via sublimation. The yield of 2.75g (78%) of **11** is based on **10** starting quantities and the purity of the compound was assessed through NMR. ^{1}H NMR (toluene-d_8): δ 3.06 (s, 2H), 2.82 (dq, J = 3.1 Hz, J = 5.3 Hz, 4H), 2.71 (dd, J = 4.8 Hz, J = 9.4 Hz, 4H), 2.42 (dd, J = 5.0 Hz, J = 9.7 Hz, 4H), 2.36 (dq, J = 3.1 Hz, J = 5.4 Hz, 4H) ppm. ^{13}C NMR (toluene-d_8): δ 78.10, 51.42, 50.86 ppm.

5.2.14 1,2,3,4,5,6,7,8–Octahydro-2a,4a,6a,8a-tetraazacyclopenta[*f,g*]acenaphthylene (13)

The resulting compound is very air sensitive and therefore all manipulations of this species are done in a drybox under an atmosphere of argon. Into a round bottom flask (250 mL) containing **10** (5g, 18.4 mmoles) was added THF (200 mL), the resulting slurry was cooled to -35ºC and to it, was added a solution of potassium hydride (1.51g, 36.8mmoles) in THF (50 mL, -35ºC) and the reaction was allowed to go overnight. The solution pales in color, resulting in a colorless solution. The solvent is then removed under reduced pressure and the product abstracted using hot hexanes (3 x 75 mL) and placed into a -78 ºC freezer where the compound crystallizes out. Purification can be carried out through recrystallization in hexanes or through sublimation. The yield on **12** is 2.54g (72%) based upon the amount of starting material (**10)** used, purity was checked using NMR. ^{1}H NMR (300 MHz, C_6D_6) δ 2.86 (s, 8H), 2.67 (s, 8H) ppm. ^{13}C NMR (75 MHz C_6D_6): δ 121.38, 52.80, 51.54 ppm.

5.2.15 Decahydro-2a,4a,6a,8a-tetraazacyclopent[*fg*]acenaphthylene Dibenzyl dibromide Salt (12)

Into a round bottom flask (500 mL) containing **11** (10g, 0.05 moles), was added dry acetonitrile (250 mL) via canula, under an atmosphere of nitrogen. To the resulting orange solution was added benzylbromide (14.03 mL,0.12 moles) via syringe and allowed to react at 40 ºC for 48 hours. The solvent was then removed under reduced pressure, washed with diethyl ether (3 x 50mL) and then recrystallized from hot methanol. This yielded tan colored crystals 24.4g (96% based on starting

quantity of **11**), purity was checked using NMR. ^{1}H NMR (acetonitrile-d_3): δ 3.18 (s, 1H), 3.27 (m, 2H), 3.34 (d of d of d, J = 13.2Hz, J = 3.0Hz, J= 13.0Hz, 2H), 3.44 (d of d of d, J= 13.1Hz, J = 3.0Hz, J = 13.0Hz, 2H), 3.54 (m, 2H), 3.55 (m, 2H), 3.59 (d of d of d, J = 13.1Hz, J = 13.0, J = 2.0, 2H), 3.8 (d of d of d, J = 13.2Hz, J = 2.8Hz, J = 2.0Hz), 4.4 (d of d of d, J = 15.0Hz, J = 5.3Hz, J = 7.4Hz, 2H), 4.94 (m, 2H), 5.15 (m, 2H), 7.54 (m, 4H), 7.68 (d, J = 7.0Hz, 4H) . ^{13}C NMR (acetonitrile-d_3): δ 44.06, 47.64, 55.98, 62.15, 62.34, 79.4, 128.4, 130.97, 132.45, 133.91.

5.2.16 1,4,7,10-Tetraaza-tricyclo[8.2.1.14,7]tetradecane-13,14-dione (14)

A dry schlenk flask was charged with **13** (1g, 5.2 mmoles) and hexanes (50 mL) the solution was stirred at room temperature under a strict argon atmosphere until all of the solid particles had dissolved. The solution was then purged with oxygen through a needle and a white compound immediately precipitated. This solid was washed with THF (2 x 25 mL) and was dried under reduced pressure. Recrystallization from methanol produced colorless crystals, yielding 1.15g (99% conversion of **13**). Purity was assessed through NMR analysis. NMR (D_2O): δ 3.76 (m, 4H), 3.46 (s, 8H), 3.15 (m, 4H) ppm.

References:

(1) Frankland, E.; Dobbin, L. *Journal of the Chemical Society, Transactions* **1878**, *33*, 545-546.

(2) Kealy, T. J.; Pauson, P. L. *Nature* **1951**, *168*, 1039-1040.

(3) Wilkinson, G.; Rosenblum, M.; Whiting, M. C.; Woodward, R. B. *Journal of the American Chemical Society* **1952**, *74*, 2125-2126.

(4) Green, M. L. H. *Journal of Organometallic Chemistry* **1995**, *500*, 127-148.

(5) Cassoux, P.; Crasnier, F.; Labarre, J. F. *Journal of Organometallic Chemistry* **1979**, *165*, 303-318.

(6) Liu, B.; Nitta, T.; Nakatani, H.; Terano, M. *Macromolecular Chemistry and Physics* **2002**, *203*, 2412-2421.

(7) Kashiwa, N. *Journal of Polymer Science, Part A: Polymer Chemistry* **2003**, *42*, 1-8.

(8) Breslow, D. S.; Newburg, N. R. *Journal of the American Chemical Society* **1957**, *79*, 5072-5073.

(9) Natta, G.; Pino, P.; Mazzanti, G.; Giannini, U. *Journal of the American Chemical Society* **1957**, *79*.

(10) Juengling, S.; Muelhaupt, R. *Journal of Organometallic Chemistry* **1995**, *497*, 27-32.

(11) Moehring, P. C.; Coville, N. J. *Journal of Organometallic Chemistry* **1994**, *479*, 1-29.

(12) Coates, G. W.; Waymouth, R. M. *Journal of the American Chemical Society* **1991**, *113*, 6270-6271.

(13) Ivin, K. J.; Rooney, J. J.; Stewart, C. D.; Green, M. L. H.; Mahtab, R. *Journal of the Chemical Society [Section] D: Chemical Communications* **1978**, *14*, 604-606.

(14) Brintzinger, H.; Marvich, R. H. *Journal of the American Chemical Society* **1971**, *93*, 2046-2048.

(15) Piers, W. E.; Bercaw, J. E. *Journal of the American Chemical Society* **1990**, *112*, 9406-9407.

(16) Clentsmith, G. K. B.; Gibson, V. C.; Hitchcock, P. B.; Kimberley, B. S.; Rees, C. W. *Chemical Communications (Cambridge)* **2002**, *14*, 1498-1499.

(17) Johnson, L. K.; Killian, C. M.; Brookhart, M. *Journal of the American Chemical Society* **1995**, *117*, 6414-6415.

(18) Mitchell, J. P.; Hajela, S.; Brookhart, S. K.; Hardcastle, K. I.; Henling, L. M.; Bercaw, J. E. *Journal of the American Chemical Society* **1996**, *118*, 1045-1053.

(19) Mecking, S.; Johnson, L. K.; Wang, L.; Brookhart, M. *Journal of the American Chemical Society* **1998**, *120*, 888-899.

(20) Boehm, L. L. *Angewandte Chemie, International Edition* **2003**, *42*, 5010-5030.

(21) Cundy, C. S.; Eaborn, C.; Lappert, M. F. *Journal of Organometallic Chemistry* **1972**, *44*, 291-297.

(22) Bolton, P. D.; Mountford, P. *Advanced Synthesis & Catalysis* **2005**, *347*, 355-366.

(23) Heatley, F. M.; S., F.; Pritchard, R. G.; Woods, R. J. *Journal of Organometallic Chemistry* **2005**, *690*, 2078-2086.

(24) Kim, Y.; Kapoor, P. N.; Verkade, J. G. *Inorganic chemistry* **2002**, *41*, 4834-4838.

(25) Novak, A.; Blake, A. J.; Wilson, C.; Love, J. B. *Chemical Communications (Cambridge)* **2002**, *23*, 2796-2797.

(26) Bortels, H. *Archiv fuer Mikrobiologie* **1937**, *8*, 13-26.

(27) Schrock, R. R. *Philosophical Transactions of the Royal Society of London, Series A: Mathematical, Physical and Engineering Sciences* **2005**, *363*, 959-969.

(28) Einsle, O.; Tezcan, F. A.; Andrade, S. L. A.; Schmid, B.; Yoshida, M.; Howard, J. B.; Rees, D. C. *Science (Washington, D. C.)* **2002**, *297*, 1696-1700.

(29) Allen, A. D.; Senoff, C. W. *Chemical Communications (London)* **1965**, *24*, 621-622.

(30) Smil, V. *Nature* **1999**, *401*, 429.

(31) Bell, B.; Chatt, J.; Leigh, G. J. *Journal of the Chemical Society [Section] D: Chemical Communications* **1970**, *13*, 842.

(32) Chatt, J.; Heath, G. A.; Richards, R. L. *Journal of the Chemical Society, Dalton Transactions: Inorganic Chemistry* **1974**, *19*, 1972-1999.

(33) Hidai, M.; Tominari, K.; Uchida, Y.; Misono, A. *Journal of the Chemical Society [Section] D: Chemical Communications* **1969**, *23*, 1392.

(34) E., G. G.; R., S. R. *Inorganic chemistry* **2001**, *40*, 3861-3878.

(35) Yandulov, D. V.; Schrock, R. R. *Journal of the American Chemical Society* **2002**, *124*, 6252-6253.

(36) Schrock, R. R. *Philosophical Transactions of the Royal Society of London, Series A: Mathematical, Physical and Engineering Sciences* **2005**, *363*, 959-969.

(37) Schrock, R. R. *Accounts of Chemical Research* **2005**, *38*, 955-962.

(38) Schrock, R. R. *Chemical Communications (Cambridge, United Kingdom)* **2003**, 2389-2391.

(39) Volpin, M. E.; Shur, V. B.; Kudryavtsev, R. V.; Prodaiko, L. A. *Chemical Communications (London)* **1968**, *17*, 1038-1040.

(40) A., P. J.; Emil, L.; J, C. P. *Journal of the American Chemical Society* **2003**, *125*, 2241-2251.

(41) J, C. P. *Dalton transactions (Cambridge, England: 2003)* **2007**, *1*, 16-25.

(42) Baumann, R.; Stumpf, R.; Davis, W. M.; Liang, L.-C.; Schrock, R. R. *Journal of the American Chemical Society* **1999**, *121*, 7822-7836.

(43) Mullins, S. M.; Duncan, A. P.; Bergman, R. G.; Arnold, J. *Inorganic chemistry* **2001**, *40*, 6952-6963.

(44) Fryzuk, M. D.; Johnson, S. A.; Patrick, B. O.; Albinati, A.; Mason, S. A.; Koetzle, T. F. *Journal of the American Chemical Society* **2001**, *123*, 3960-3973.

(45) Schrock, R. R. *Pure and Applied Chemistry* **1997**, *69*, 2197-2203.

(46) Schrock, R. R. *Accounts of Chemical Research* **1997**, *30*, 9-16.

(47) Schrock, R. R. *Chemical Reviews (Washington, D. C.)* **2002**, *102*, 145-179.

(48) Rosenfeld, D. C.; Wolczanski, P. T.; Barakat, K. A.; Buda, C.; Cundari, T. R. *Journal of the American Chemical Society* **2005**, *127*, 8262-8263.

(49) Cundari, T. R. K., Thomas R.; Wolczanski, Peter T *Journal of the American Chemical Society* **2002**, *124*, 1481-1487.

(50) Gray, H. B.; Eisenberg, R.; Stiefel, E. I. *Advances in Chemistry Series* **1967**, *62*, 641-650.

(51) Nygren, C. L.; Bragg, M. E. T.; Turner, J. F. C. *Acta Crystallographica, Section C: Crystal Structure Communications* **2003**, *C59*, 275-276.

(52) Cummins, C. C. *Progress in Inorganic Chemistry* **1998**, *47*, 685-836.

(53) Tanski, J. M.; Parkin, G. *Organometallics* **2002**, *21*, 587-589.

(54) Tanski, J. M.; Parkin, G. *Inorganic Chemistry* **2003**, *42*, 264-266.

(55) Fernandez, A.; Reyes, C.; Ying Lee, T.; Prock, A.; Giering, W. P.; Haar, C. M.; Nolan, S. P. *Perkin 2* **2000**, *7*, 1349-1357.

(56) Pauson, P. L.; Qazi, A. R. *Journal of Organometallic Chemistry* **1967**, *7*, 321-324.

(57) Riley, P. N.; Fanwick, P. E.; Rothwell, I. P. *Journal of the Chemical Society, Dalton Transactions* **2001**, *2*, 181-186.

(58) Niu, W.; Wong, E. H.; Weisman, G. R.; Sommer, R. D.; Rheingold, A. L. *Inorganic Chemistry* **2002**, *5*, 1-4.

(59) Dickinson, R. G.; Raymond, A. L. *Journal of the American Chemical Society* **1923**, *45*, 22-29.

(60) Puckner, W. A.; Hilpert, W. S. *Journal of the American Chemical Society* **1908**, *30*, 1471-1474.

(61) Sprague, J. E.; Peng, Y.; Fiamengo, A. L.; Woodin, K. S.; Southwick, E. A.; Weisman, G. R.; Wong, E. H.; Golen, J. A.; Rheingold, A. L.; Anderson, C. J. *Journal of Medicinal Chemistry* **2007**, *50*, 2527-2535.

(62) Anderson, C. J.; Dehdashti, F.; Cutler, P. D.; Schwarz, S. W.; Laforest, R.; Bass, L. A.; Lewis, J. S.; McCarthy, D. W. *Journal of nuclear medicine: official publication, Society of Nuclear Medicine* **2001**, *42*, 213-221.

(63) Edwards, W. B.; Anderson, C. J.; Fields, G. B.; Welch, M. J. *BioconJugate chemistry* **2001**, *12*, 1057-1065.

(64) Niu, W.; Wong, E. H.; Weisman, G. R.; Hill, D. C.; Tranchemontagne, D. J.; Lam, K.-C.; Sommer, R. D.; Zakharov, L. N.; Rheingold, A. L. *Dalton Transactions* **2004**, *21*, 3536-3547.

(65) Bosnich, B.; Poon, C. K.; Tobe, M. L. *Inorganic Chemistry* **1965**, *4*, 1102-1108.

(66) Athey, P. S.; Kiefer, G. E. *The Journal of organic chemistry* **2002**, *67*, 4081-4085.

(67) Bragg, M. E. T.; Turner, J. F. C. *Unpublished results* **2004**.

(68) Weisman, G. R.; Ho, S. C. H.; Johnson, V. *Tetrahedron Letters* **1980**, *21*, 335-338.

(69) Le Baccon, M.; Chuburu, F.; Toupet, L.; Handel, H.; Soibinet, M.; Dechamps-Olivier, I.; Barbier, J.-P.; Aplincourt, M. *New Journal of Chemistry* **2001**, *25*, 1168-1174.

(70) Cetinkaya, E.; Hitchcock, P. B.; Jasim, H. A.; Lappert, M. F.; Spyropoulos, K. *Journal of the Chemical Society, Perkin Transactions 1: Organic and Bio-Organic Chemistry* **1992**, *5*, 561-567.

(71) O'Connor, P. E., Berg, D. J., Twamley, B. *Organometallics* **2005**, *24*, 28-36

Vita

Andrew James Colvin was born and raised in Worcester, U.K. He attended Bishop Perowne High School, where he graduated in 1994, to pursue his further education at Worcester VI Form College. It was here he developed his interest for chemistry, which influenced his degree selection at the University of Kingston upon Thames, from which he graduated with a BSc. (hons) Chemistry upper second in the summer of 2001. Andrew arrived in Knoxville that fall to study organometallic chemistry at the University of Tennessee, where he will graduate with his doctorate in chemistry in the spring of 2009.